Atmospheric Environment 194 (2018) 58–70

Contents lists available at ScienceDirect

Atmospheric Environment

journal homepage: www.elsevier.com/locate/atmosenv

Use of networks of low cost air quality sensors to quantify air quality in urban settings

Olalekan A.M. Popoola[a,*], David Carruthers[b], Chetan Lad[b], Vivien B. Bright[a], Mohammed I. Mead[a], Marc E.J. Stettler[c], John R. Saffell[d], Roderic L. Jones[a]

[a] Department of Chemistry, University of Cambridge, Lensfield Road, Cambridge, CB2 1EW, UK
[b] Cambridge Environmental Research Consultants Ltd, 3 Kings Parade, Cambridge, CB2 1SJ, UK
[c] Faculty of Engineering, Department of Civil and Environmental Engineering, 614 Skempton Building, South Kensington Campus, Imperial College London, London, SW7 2AZ, UK
[d] Alphasense Ltd., Sensor Technology House, 300 Avenue West, Skyline 120, Great Notley, Essex, CM77 7AA, UK

ARTICLE INFO

Keywords:
Air quality
Low cost sensors
Dense sensor network
Scale separation
Air quality model
Long term measurements

ABSTRACT

Low cost sensors are becoming increasingly available for studying urban air quality. Here we show how such sensors, deployed as a network, provide unprecedented insights into the patterns of pollutant emissions, in this case at London Heathrow Airport (LHR). Measurements from the sensor network were used to unequivocally distinguish airport emissions from long range transport, and then to infer emission indices from the various airport activities. These were used to constrain an air quality model (ADMS-Airport), creating a powerful predictive tool for modelling pollutant concentrations. For nitrogen dioxide (NO_2), the results show that the non-airport component is the dominant fraction (~75%) of annual NO_2 around the airport and that despite a predicted increase in airport related NO_2 with an additional runway, improvements in road traffic fleet emissions are likely to more than offset this increase. This work focusses on London Heathrow Airport, but the sensor network approach we demonstrate has general applicability for a wide range of environmental monitoring studies and air pollution interventions.

1. Introduction

Poor air quality is known to affect human health (Bernstein et al., 2004; Brunekreef and Holgate, 2002; McConnell et al., 2002; Parnia et al., 2002; Pope and Dockery, 2006; Ren et al., 2017; Samoli et al., 2008; WHO, 2009). Urban air quality monitoring, traditionally the remit of expensive and complex reference instruments (Kumar et al., 2015; National Audit Office, 2009) can now be achieved using readily deployable low cost instruments, revolutionising approaches to the study of urban pollution. Over the last few years, low cost sensors have been assessed for their viability in monitoring ambient air quality including measurements of gaseous and particulate matter (PM) pollutants. Whilst some studies show that there are still some challenges with using off the shelf devices (Borrego et al., 2016; Lewis et al., 2016), other studies have demonstrated that some of these limitations can be overcome with careful data processing and network design (Crilley et al., 2018; Kim et al., 2018; Penza et al., 2014; Popoola et al., 2013; Sun et al., 2017; Spinelle et al., 2015; De Vito et al., 2018; Heimann et al., 2015). There have also been attempts at deploying portable sensors as networks to better understand the spatial variability of air pollution (Mead et al., 2013; Miskell et al., 2017; Mueller et al., 2017; Penza et al., 2014; Sun et al., 2016). Schneider et al., 2017 also used a data fusion technique to combine sensor network data with an air quality model which was then used to simulate the spatial pattern of pollutants.

Although there have been several studies on the impact of aviation on ambient air quality (Carslaw et al., 2006; Herndon et al., 2004, 2008; Hu et al., 2009; Masiol and Harrison, 2015; Schürmann et al., 2007), they mainly focused on using sparse array of fixed stations or short term mobile platforms which allowed source apportionment studies within and in the proximity of the airports.

Here we show how low cost air quality instruments, when deployed as a network rather than as individual sensors, provide unprecedented additional insights into the patterns and sources of air pollution.

The case study we have applied this methodology to is London Heathrow Airport and focusses in this paper mainly on NO_X. The limit value for annual average NO_2 of 40 μg/m^3 is not currently being met at some of the areas around London Heathrow airport. The expansion of

* Corresponding author.
E-mail address: oamp2@cam.ac.uk (O.A.M. Popoola).

https://doi.org/10.1016/j.atmosenv.2018.09.030
Received 1 February 2018; Received in revised form 12 September 2018; Accepted 17 September 2018
Available online 18 September 2018

the airport, including a third runway (UK Department for Transport, 2017), has raised concerns that meeting this limit value would be unachievable in the future. The sensor network we deployed at the airport consisted of up to 40 nodes sited across the airport and covering a range of emission environments, each measured a range of species including NO_2, NO, CO and CO_2. The sensor network, together with the novel analysis approach we describe, has allowed pollutant emissions attributable solely to the airport activities to be distinguished from other non-airport related sources. Using the CO_2 measurements made across the network this, in turn, has allowed the direct quantification of NO_X and CO emission indices for a number of different airport related activities.

These measurements, and in particular the direct determination of emission indices, were used to optimize the ADMS-Airport air quality model, creating a powerful predictive tool for pollutant concentrations in and around Heathrow airport.

While this study focuses on the UK's Heathrow Airport, the techniques we describe, that exploit the emerging low-cost air quality sensor technologies and novel analysis approaches, have far wider applicability for environmental monitoring and air pollution interventions.

2. Materials and methods

In this section we briefly describe the low cost sensor network used for the study at LHR, including the state-of-the art modelling air quality model utilised in our study.

2.1. Sensor measurement: SNAQ boxes and network deployment

The sensor nodes were low cost portable air quality devices developed at the Department of Chemistry, the University of Cambridge, UK, as part of NERC (Natural Environmental Research Council) funded Sensor Network for Air Quality (SNAQ) project at London Heathrow airport. Each node measured the parameters summarised in Table 1, made at a 20 s time resolution. In addition, each node was equipped with GPRS and GPS for near real-time data transmission and location/time data respectively (Popoola et al., 2013). Both the particle size and gas species devices were calibrated under laboratory conditions, with the ambient performance of the NO, NO_2 and the CO_2 sensors presented in section 2.2.

Although a network of 40 sensor nodes was ultimately deployed, we are focussing here on a five-week period (4 October-11 November 2012) where only 17 of the sensor network nodes were fully operational, but where additional information on aircraft throttle settings was available (Fig. 1). The sensor network was designed to cover, as far as possible, the different activity zones in and around the airport including the terminals, runways and the main airside roads (Fig. 1). To contextualise the network density, only one routine air quality reference station (LHR2) is located within the deployment zone, with node S47 co-located with this reference station. Two nodes (S47 and S48) were also sited close to each other (~5 m apart), and, were used to study the reproducibility of the SNAQ measurements. All the nodes were mounted at 3 m on lampposts within the airport perimeter. Fig. 2 (and Fig S1) illustrate the high temporal and spatial variability within the airport, influenced by both airport and non-airport related emissions captured by the network.

Table 1
Species measured and techniques for the sensor nodes used for the SNAQ Heathrow study. Only those sensors shown in bold are used in this study.

Species	Methodology	Description of sensor
CO	**Electrochemical**	**Alphasense B4**
NO		
$^{a}NO_2$		
CO_2	**Non-Dispersive Infra-Red**	**Sensair K33**
VOCs (total)	Photo Ionisation Detector	Alphasense PID-AH
Temperature	Pt Resistance Sensor	Pt1000
Relative Humidity	Polymer Capacitive Element	Honeywell HIH4000
Wind Speed/Direction	**Sonic Anemometer**	**Gill WindSonic**
Size Speciated Particulates (ranging 0.38–17.4 μm)	Optical Particle Counter	University of Hertfordshire

[a] The NO_2 sensors used here were 100% cross sensitive to O_3. The data was corrected for this cross interference (see section 2.2), and where it is not the species is presented as O_X (i.e. $NO_2 + O_3$).

2.2. Sensor measurement validation

The performance of the SNAQ units for NO and NO_2 was evaluated by comparing the results from the node co-located with the reference air quality site within the airport (LHR2). Hourly averaged NO_2 data were derived from the hourly O_X reading by correcting for O_3 interference using hourly modelled O_3 data. Comparison of the standard measured gas species (e.g. NO_X) showed that the SNAQ measurements captured variations at the airport with good agreement indicated by the slope (0.9379 ± 0.0081) and coefficient of determination $R^2 \approx 0.95$ (Fig. 3A). This comparison was performed by taking hourly averages of the high temporal resolution (20 s) sensor measurements as the reference data were only reported as hourly averages. As there was no local CO_2 reference instrument available, validation of the SNAQ CO_2 measurements was performed post-study by comparing CO_2 observations made after the deployment with those of a Picarro G2201-I CO_2/CH_4 analyser (Fig. 3B), giving results with a slope of (0.9553 ± 0.0021) and coefficient of determination $R^2 \approx 0.92$. Although, this validation was performed using a single sensor node, we have demonstrated in this study - as with previous studies (Popoola et al., 2016; Mead et al., 2013) - the high level of sensor-sensor repeatability (slopes between 0.9 and 1.0 for all gas species), in this case for two nodes (S47 and S48) which were near co-located for the measurement period (Fig. 4). Errors are standard errors of the ordinary least square estimates.

2.3. Source apportionment

This section describes how we estimate the network baseline (referred to as the non-local signature) which is due to non-local emissions for the measurement period presented in this work (4 October to 11 November 2012).

The major novelty of the sensor network work described here is that local (airport) and non-local (non-local/airport related) fractions of the measured species could be determined independent of wind conditions directly from the network observations without the need for long-term (years) measurements, conditions that limit the extraction of similar information from the traditional sparse routine network measurements. We extracted both the airport fraction and non-airport fraction, as described below, using the local signature to validate the source apportionment of a model, the ADMS-Airport.

Measurements at each sensor node within the network comprise a contribution attributable to emissions local to that sensor – the local signal, and a component advected from outside the network area which will be essentially identical at all sites – the non-local signal.

As emissions of NOx and CO local to each site will always lead to locally elevated concentrations of the pollutants, the concept is then to establish the minimum value of each pollutant across the entire network within a given time window and to equate that to the baseline or non-local signal for that species and period.

To illustrate the process, we will consider for simplicity a three-sensor sub-network with measurements from three nodes (site29, site50 and site19 designated S_1, S_2 and S_3 respectively). In this (arbitrarily chosen) period, S_1 is located at a high pollution site, while S_2 and S_3 are

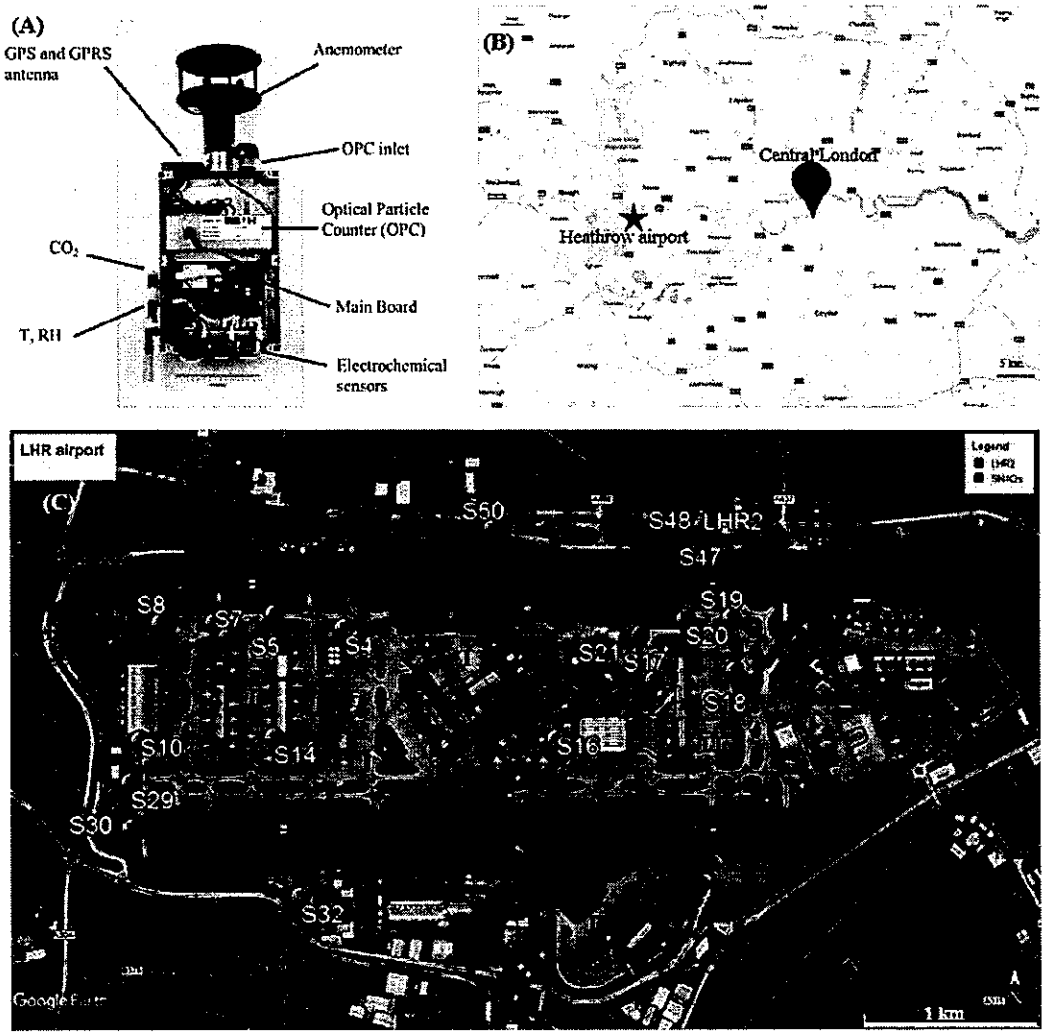

Fig. 1. Instrumentation and deployment: (A) A typical SNAQ sensor node showing the main components, (B) A Google map © showing the location of London Heathrow airport relative to Central London, UK, and (C) the locations (red tags) of the sensor nodes during the study period and the reference monitoring station LHR2 (blue tag) relative to the terminals (1, 3, 4 and 5, all in purple). (For interpretation of the references to colour in this figure legend, the reader is referred to the Web version of this article.)

located at low pollution sites. The data at 20 s resolution, for three hours only in this illustration, are actual measurements used in this study and are shown in Fig. 5 (red, blue, green).

It can be immediately seen that site S_1 has highly variable CO values, significantly elevated above any hemispheric background value (200–300 ppbv) (Lowry et al., 2016). In contrast, sites S_2 and S_3 both show lower variability, and lower absolute CO values. While sites S_2 and S_3 do both show some isolated pollution events, they together define a clear baseline, which in this period is around 400 ppbv and shows a slight upward trend over the three hour period. Fig. 5B, shows a probability histogram for a single hour of the ensemble of measurements shown in Fig. 5A. A clear maximum in probability is seen at ~400 ppbv, associated with measurements from the low pollution sites where the baseline dominates across this sub-network. This reflects the low CO values associated with predominantly the absence of pollution events at sites S_2 and S_3, while site S_1 mainly contributes to the less frequent but more elevated CO values (> 1000 ppbv). The baseline for this period is extracted by taking a percentile (in this case the 10th) of the measurements from the network (in this case just from the three sites) for the defined period, typically one hour. A percentile is chosen rather than the minimum to account for the measurement error for the sensors, with the choice of the 10th percentile reflecting the typical sensor error. The difference between the minimum CO value measured and the 10th percentile in this case is < 10 ppbv (see expanded probability histogram). These differences, which are broadly representative of the entire dataset for CO, are negligible compared to the pollution levels observed (see e.g. Fig. 6). The baseline shown in Fig. 5A is constructed from a linear interpolation between the baselines obtained for individual hour of data (and an additional hour before and after) and, as can be seen, reproduces both the average baseline and trend. A similar approach (Fig. S2) is applied to the other species (except for NO_2, where hourly O_3 corrected data (see section 2 above) was used with the time window of three hours instead of one hour used for the 20 s resolution data). Although three sensors were used in this illustration, the entire network (17 sensor nodes) were used in the baseline determinations presented below.

Applying the above method to the sensor data for each gas species, we successfully extract the network baseline and use this to determine the local signal (Fig. 6 shows results of the source attribution methodology for CO, and Fig. S3-S4 shows results for CO_2 and NO_2).

2.4. Modelling approach

The model used in this work is ADMS-Airport. This model is an

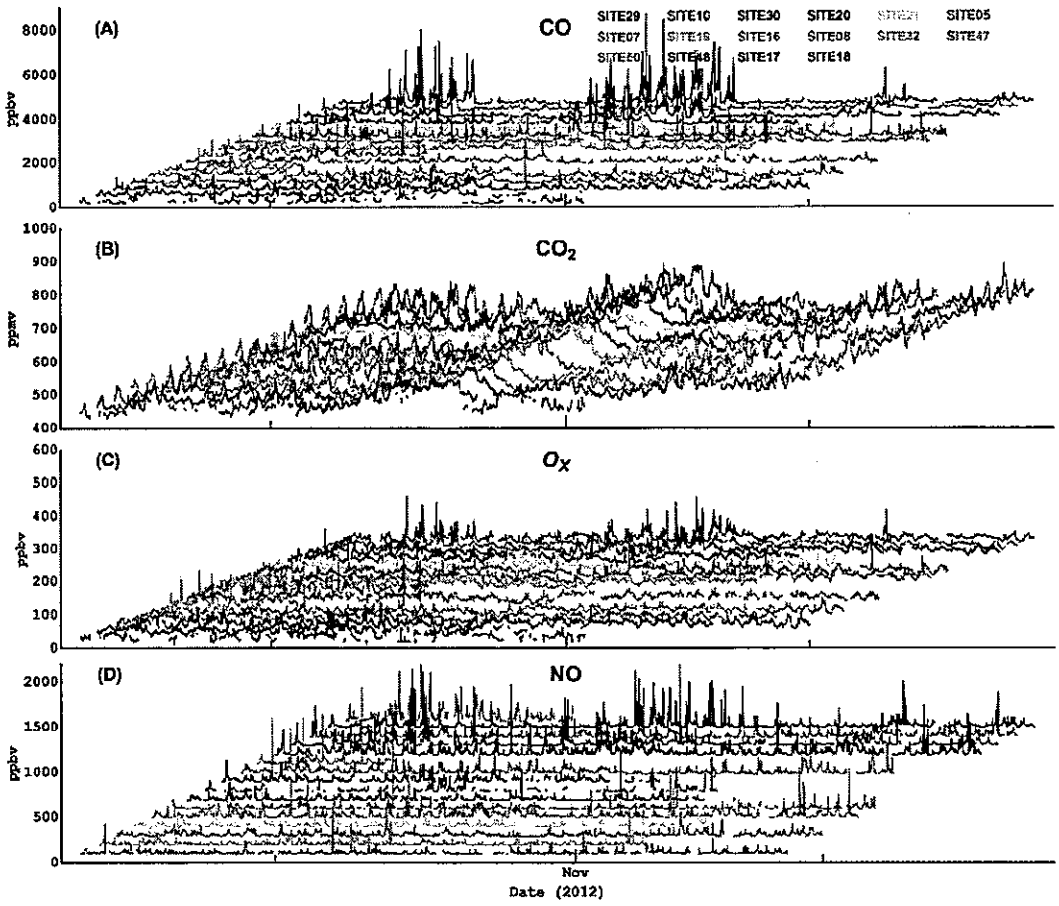

Fig. 2. Time series plots of measurements for the entire five-week study period. From top to bottom are (A) carbon monoxide, (B) carbon dioxide, CO_2, (C) the sum of NO_2 and O_3 (O_X), and (D) nitric oxide, NO.

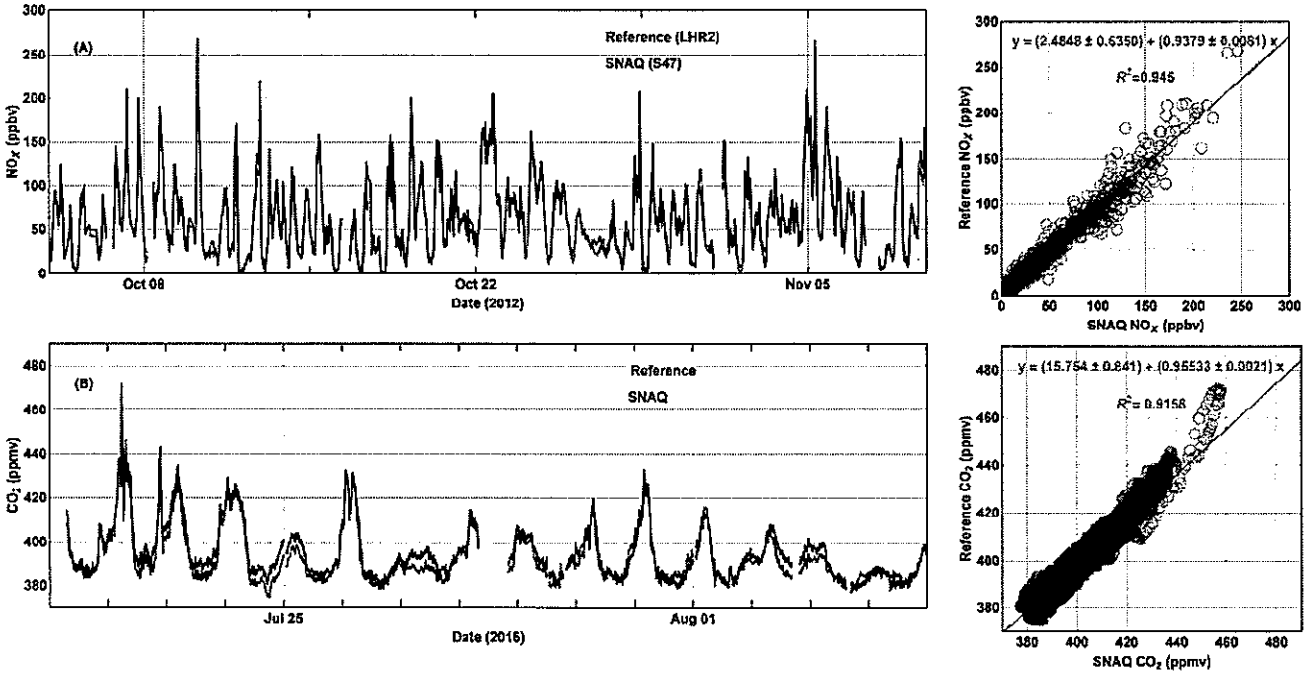

Fig. 3. Comparison between reference method and SNAQ. Temporal variation plots (left panels), and scatter plots (right panels). (A) Hourly average NO_X comparison at LHR2.-(B) Minute average CO_2 comparison. Note there are no comparisons for CO and CO_2 at LHR2 as these species are not part of the species routinely monitored at the reference station. The occasional missing data are due to data transmission issues.

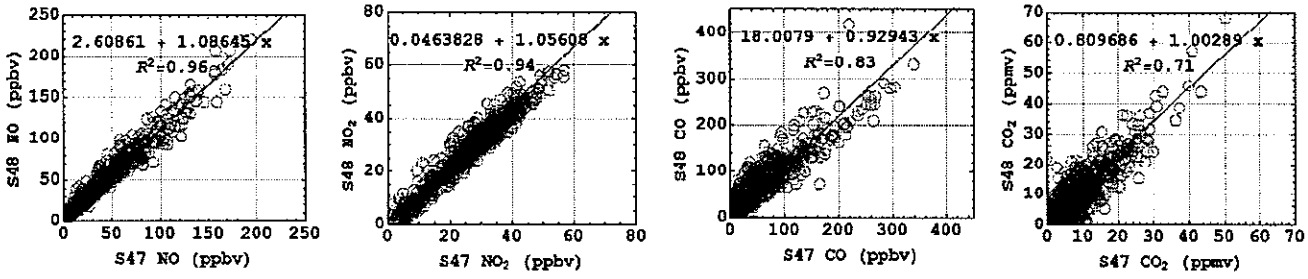

Fig. 4. Correlation plots for SNAQ data for sites 47 and 48. From left to right, hourly mean absolute NO, NO_2, local CO and CO_2.

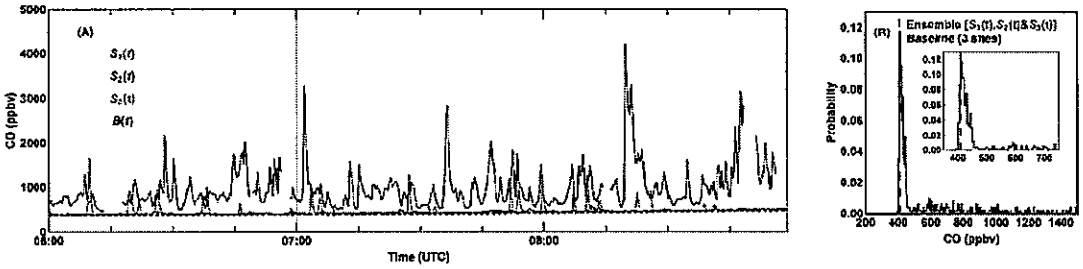

Fig. 5. Time series and probability histogram plot for CO data. (A) time series at 20 s resolution for a three-hour period at three sites in the network (red, green, blue) along with the fitted baseline (dashed black). (B) probability histogram of the combined measurements for the last hour (08:00–09:00) of the three-hour period, with the inset figure showing the same probability histogram on an expanded scale. The 10th percentile of the data is shown in both figures (black dashed). See text for further details. The occasional missing data are due to data transmission issues. For clarity, we have not shown the whole mixing ratio range for both the main and inset images in Fig. 5B. (For interpretation of the references to colour in this figure legend, the reader is referred to the Web version of this article.)

extension of the street scale resolution ADMS-Urban dispersion model (McHugh et al., 1997) for complex urban environments with additional capability for the explicit modelling of aircraft jet engine emissions as jet sources. ADMS-Airport has been recommended by the Project for the Sustainable Development of Heathrow (PSDH) used at Heathrow Airport (UK Department for Transport, 2006) and has been used by the Airports Commission (Module 6 (2015)) as well as the proponents of the three airport expansion schemes considered by the Airports Commission. The overall approach has been to set up an optimised modelling system for a base year of 2012 making extensive use of the sensors, and then to project the airport impact forward to 2030. Model and inventory optimisation for the airport sources was based on the detailed analysis of local fractions of model and monitored data for the sensor locations site 29 and site 30, located north and south of the 09R runway (Fig. 7). Details of model configuration for the hourly and annual predictions are described below.

2.4.1. Hourly average model simulation

Airport emissions were based on a 2012 airport inventory complied by AEA Environment and Energy (AEA, Energy and Environment, 2010) which was then refined using emissions calculated from detailed aircraft activity data for the two-week period 4th November 2012 to 18th November 2012, provided by Heathrow Airport Limited from the Business Objective Search System (BOSS) database, together with CERC's Aircraft Emissions Calculator. This combines European Civil Aviation Conference Report on Standard Method of Computing Noise Contours around Civil Airports performance model (European Civil Aviation Conference, 2005) with Boeing Fuel Flow Method 2 (Doc 9889, 2011). The spatial elements for aircraft emissions and details for all other airside emissions i.e. ground support equipment and auxiliary

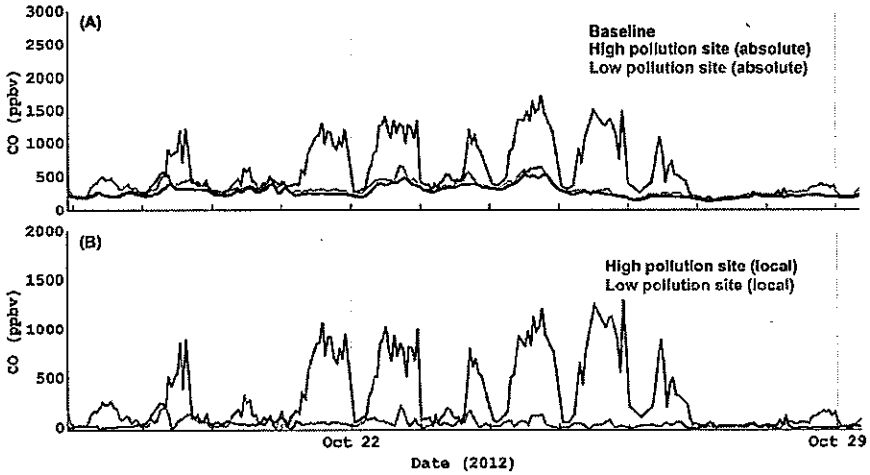

Fig. 6. Time series plot from 18–28 October 2012 for hourly averaged absolute, baseline and local CO data at two sites. (A) Network baseline relative to the absolute mixing ratios, (B) the extracted local mixing ratios.

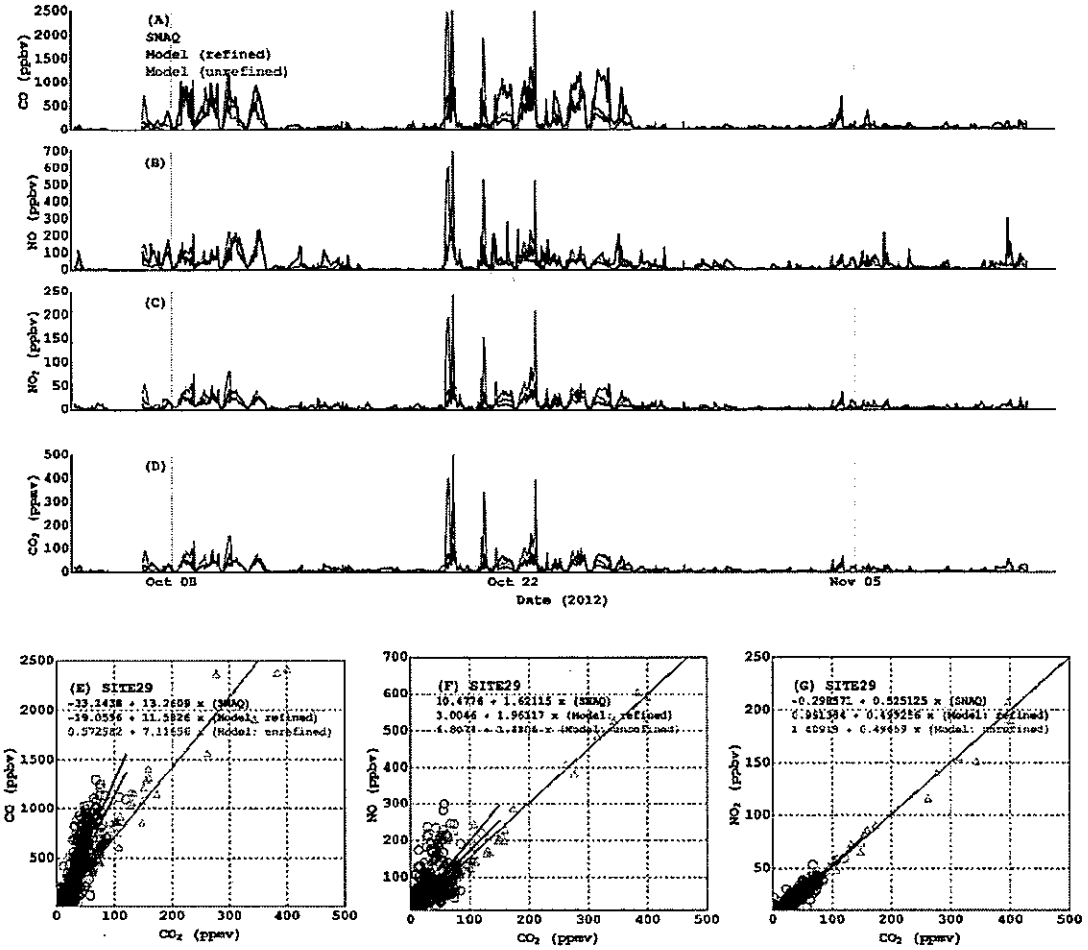

Fig. 7. Comparison of measurement and ADMS model runs. (A–D) time series of CO, NO, NO_2 and CO_2. (E–G) scatter plots of modelled airport CO and NO_2 concentrations (ppbv) against modelled airport CO_2 concentrations (ppmv) for Site 29 sensor location (unrefined model in grey, improved model in red). (For interpretation of the references to colour in this figure legend, the reader is referred to the Web version of this article.)

power units were also obtained from the AEA inventory.

Based on these data the following model/emission improvements were made:

- The dimensions of stand sources were modified to be more representative of the area of emissions;
- The location of take-off sources on runway 09R were moved to better represent the actual start of take-off roll points. For consistency with the new take-off locations, 09R taxi-out and initial climb sources were also moved.
- The treatment of taxiing was refined as follows:
  - a default aircraft speed of 15.4 m/s was previously used for taxiing. There is relatively low model sensitivity to taxiing speeds, but to ensure greater consistency with actual aircraft operations, a speed of 5 m/s was adopted for shorter taxi segments of less than 300 m in length.
  - In addition to engine emissions from the Landing and Take-off (LTO) cycle, taxiing emissions were also modelled as jet sources taking account of the momentum and buoyancy of the source, rather than as ground level volume sources with no initial momentum or buoyancy.
- NO_X and CO taxiing emissions indices were recalculated assuming thrust levels of 4% for short taxi segments and 6.5% for longer segments, together with emission factors for NO and CO which were derived from measured concentration ratios with CO_2 from the sensor network data, rather than the ICAO (International Civil Aviation Organization) default emission factors for 7% thrust. When compared to the ICAO default thrust level of 7% for taxiing, these reduced thrust levels lead to higher CO emission indices and lower NO_x emission indices.

Fig. 7 shows scatter plots of the modelled airport contribution to CO, NO and NO_2 concentrations (ppbv) against the contribution to CO_2 concentrations (ppmv) at the site 29 sensor location, before and after the model refinements. The plots highlight the following effects of the refinements: the large reduction in modelled near ground level concentrations due to the replacement of passive volume sources with buoyant jet sources from taxiing emissions which results in significant plume rise; an increase in the average CO/CO_2 ratios and an increase in the average but greater spread of the $NO_x(NO + NO_2)/CO_2$ ratios, due to the higher CO emission indices and lower NO_x emission ratios, used for the lower thrust settings for taxing, and the increased relative contribution of take-off NO_x emissions to taxiing NO_x emissions at the site.

2.4.2. Annual average model simulation

Non-airport emissions were obtained from the London Atmospheric Emissions Inventory (LAEI) and Slough Emissions Inventory (SEI). 2012 inventories projected from 2008 base year inventories were used; these were the latest versions of the LAEI and SEI available for the study. The road traffic emission factors used to compile these versions of the LAEI and SEI were found to underestimate real world emissions from diesel

vehicles, therefore road emissions were recalculated using modified emission factors for Euro 2 to Euro 5 diesel vehicles. Non-airport emissions within 10 km of the airport were included within the model. Major roads and large industrial sources within 7 km of the airport were modelled explicitly, with all other non-airport emissions modelled as an aggregated source on a 1 km^2 basis.

Monitored concentrations from rural and suburban sites in the Defra's AURN network and the London Air Quality Network (LAQN) were used to estimate the background concentrations due to sources more than 10 km from the airport. Wind-direction dependent background concentrations for the modelled area were calculated using hourly concentrations from Harwell, Southall and Barnes Wetlands monitoring sites. This model set-up allowed use of the Generic Reaction Set chemistry scheme (Venkatram et al., 1994), considering NO_x chemical reactions on an hour-by-hour basis.

Hourly sequential meteorological data from Heathrow Airport was used as input to the model. A surface roughness value of 0.2 m was used for the meteorological measurement site and a value of 0.5 m for the modelling domain (Air Quality Studies for Heathrow, 2007).

Apportionment of the contribution of airport and non-airport emissions to concentrations of NO_x and NO_2 was also carried out. Included within airport emissions is the contribution from all airside emissions and the airport related traffic on surrounding major roads. It is assumed that all traffic on the airport perimeter road along with M4 and M25 spur roads, leading to the airport, is airport related traffic. The traffic flows on these roads is used to apportion an airport traffic contribution on adjacent major roads. To calculate the airport contribution to NO_2 the difference between two model runs was determined: the first including all emissions, the second excluding airport emissions.

The model performance was also verified against Defra and local authority automatic monitors around the airport in 2012, the results showed excellent agreement between modelled and monitored concentrations as summarised Table 2.

2.4.3. Year 2030 and third runway scenarios

The modelling for 2030 considered aircraft fleet changes and airport activity changes, with and without a third runway at Heathrow, equivalent to the 2030 North-West Runway (three runways) and 2030 Do-minimum (two runways) scenarios in the Airports Commission modelling. In addition, a 2012 North-West Runway scenario was modelled i.e. a third runway at Heathrow with the current aircraft emissions technology. Only the airside emissions were modelled for these scenarios due to the uncertainty in road layout with the extended airport.

Scenario aircraft emissions for 2030 were calculated by scaling the 2012 emissions by aircraft movements and fleet-weighted NO_x emissions by aircraft category for 2030 used in the Airports Commission modelling. The location of the new runway and associated taxiways and stands are based on submissions by the scheme proposer to the Airports Commission (Independent report, 2014). Stand emissions are calculated by scaling the baseline 2012 emissions by annual passenger projections.

Runway activity assumed the ending of the Cranford Agreement (LHR Airports Limited, 2016).[1] The scheme design with the third runway proposes rotating runway use between, four modes of operation based on the northern and southern runways alternating between mixed and segregated mode operation, and the central runway operating in segregated mode only. For the modelling, it is assumed that there is, equal use of the four modes during the year, weekly alternation between departure and landing operation on the central runway and intra-day switch between mixed-mode and segregated mode operations on the northern and southern runways.

The airport contribution to total annual average NO_2 concentrations was calculated from modelled annual average NO_x concentrations using primary NO_2 dependent NO_x:NO_2 correlations based on the 2012 baseline modelling including airport and non-airport emissions and using the ADMS chemistry scheme. This was necessary since only sources of NO_x related to the airport were modelled for 2030, which meant that the chemistry scheme within ADMS could not be employed for the 2030 calculations. These NO_2 concentrations, calculated from model derived NO_x:NO_2 correlations, were found to be broadly similar to concentrations obtained using Defra's NO_x to NO_2 Calculator tool (Department for Environment, Food and Rural Affairs, 2016; Jenkin, 2004) for deriving NO_2 concentrations from road NO_x contributions when the primary fraction of NO_2 emissions was typical of road traffic emissions.

[1] http://www.heathrow.com/noise/heathrow-operations/cranford-agreement#, accessed 3rd November 2016.

Table 2
Comparison of monitored (Mon) and modelled (Mod) 2012 annual average concentrations (μg/m^3).

Location	NO_x (μg/m^3)		NO_2 (μg/m^3)		O_3 (μg/m^3)	
	Mon	Mod	Mon	Mod	Mon	Mod
LHR2	106	104.0	48	50.8	–	30.3
Harlington	61	58.7	35	37.1	34	37.5
Heathrow Green Gates	63	60.1	33	36.1	–	39.8
Heathrow Oaks Road	52	53.8	30	31.6	–	42.0

2.4.4. Emission Factor Toolkit (EFT) version 7.0 road traffic NO_x emissions

NO_x emissions by vehicle type from Defra's EFT v7.0 are shown in Table 3 for the average traffic speed on Bath Road (37 km/h), along with total emissions for the typical traffic flow on the road; a decrease of over 80% in NO_x emissions between 2013 and 2030 can be seen. The EFT v7.0 includes emissions factors extracted from COPERT 4 v 11.0; an update of the EFT taking into account revised emission factors for the majority of Euro 5 and Euro 6 light duty diesel vehicles in COPERT 4 v 11.4 is expected to be released by Defra shortly. Emissions of light duty petrol vehicles and all heavy duty vehicles are unchanged between COPERT 4 v 11.0 and COPERT 4 v 11.4. The emissions for all Euro 6 light duty diesel vehicles in EFT 7.0 have emission limit conformity factors in the range 2.6–2.8 (0.208 g/km to 0.224 g/km compared to the type approval limit of 0.08 g/km at 33.6 km/h, in accordance with Defra's definition of conformity factors). The updated emissions in COPERT 4 v 11.4 take into account the legislative stages of the Euro 6 standard, with the introduction of Real Driving Emissions (RDE) regulations from 2017 (Euro 6c and Euro 6d); for 2017–2019 vehicles (Euro 6c), the updated emissions have conformity factors in the range 3.94–5.05 (0.315 g/km to 0.404 g/km) and for post-2020 vehicles (Euro 6d) conformity factors in the range 1.97–2.45 (0.158 g/km to 0.196 g/km); this is expected to lead to a reduction in road transport emissions along Bath Road for 2030 when compared with emissions calculated using COPERT 4 v 11.0 (Updated Air Quality Re-analysis, 2017).

3. Results

3.1. Air quality network measurements

To illustrate the type of information available using the low cost sensor technique, Fig. 8 shows time series of 20 s average carbon monoxide (CO) across the network on varying timescales: for the entire period in this study, for a week and for a single day. For clarity, the data are ordered from low to highly polluted sites in each panel. Several of the sensors have incomplete time series because of power supply and data transmission issues, however an overall pattern is clear. Firstly, there is a diurnal periodicity evident, with some sensor locations, generally those close to direct aircraft emissions (e.g. S10, S29, S30), showing high levels of CO in contrast to other locations at which much

Table 3
EFT 7.0 NO_x emission factors by vehicle type (g/km) and total emissions for Bath Road traffic flow (g/km/s), 2013 and 2030 fleet assumptions.

NOx emission factors at 37 km/h (g/km/vehicle)	2013	2030	Emissions reduction 2013 to 2030	EFT fleet assumptions for 2030 (for road type: Outer London Urban)
Petrol Cars (includes hybrids)	0.182	0.048	73.5%	97% Euro 6
Diesel Cars (includes hybrids)	0.624	0.233	62.6%	95% Euro 6
Taxis	0.868	0.052	94.0%	11% Euro 6; 87% zero emission vehicles
Petrol LGVs	0.009	0.004	56.9%	86% Euro 6
Diesel LGVs	0.749	0.209	72.1%	98% Euro 6
Rigid HGVs	3.846	0.316	91.8%	99% Euro VI
Artic HGVs	6.360	0.422	93.4%	98% Euro VI
Buses/Coaches (includes hybrids)	5.511	0.319	94.2%	> 98% Euro VI
Motorcycles	0.119	0.037	69.1%	> 70% Euro 5 (highest motorcycle standard)
NOx emissions (g/km/s) for Bath Road traffic	**2013**	**2030**	**Emissions reduction 2013 to 2030**	**Traffic breakdown**
All vehicles (32,989 vehicles/day)	0.296	0.051	82.7%	76.4% cars; 8.7% taxis; 6.4% LGVs; 5.2% Buses & coaches; 2.0% Rigid HGVs; 0.4% Articulated HGVs; 1.0% Motorcycles

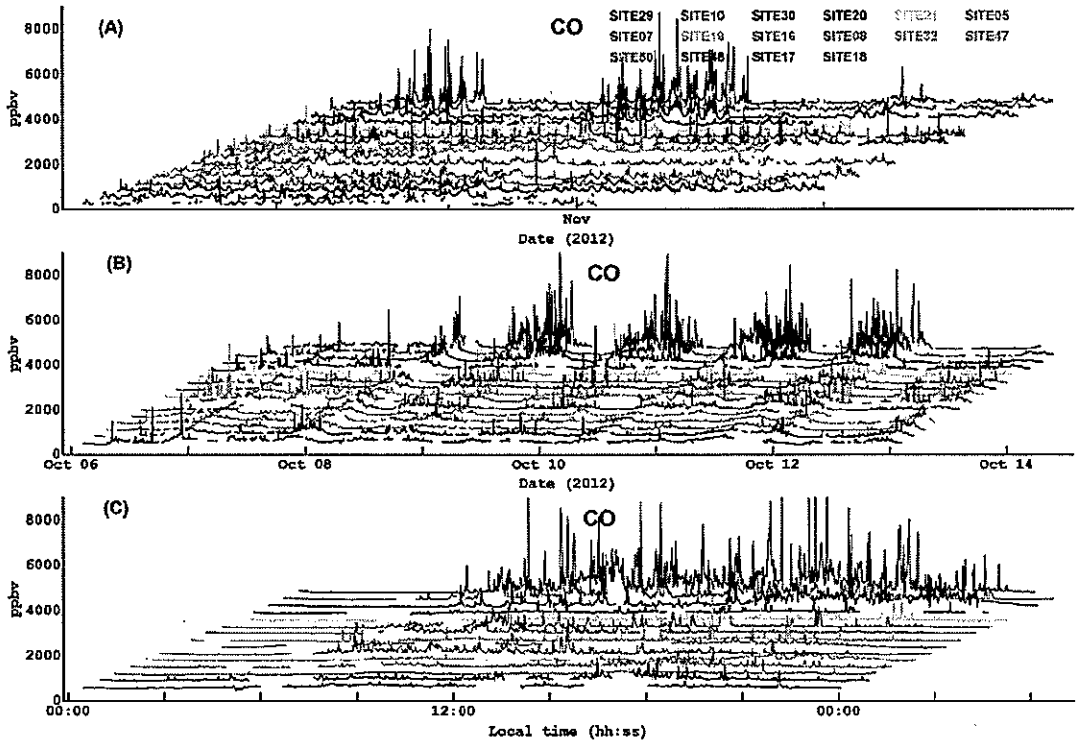

Fig. 8. Time series plots of carbon monoxide measurements across the network nodes operating during the study period: five-week study period (A), one week (6–12 October 2012 - B) and the one day (8 October 2012 -C). Equivalent plots for other species are shown in Fig. S2.

lower levels are seen (e.g. S17, S48). For the overall data set (Fig. 8A), the coarse pattern is that there are two periods of several days of highly polluted conditions separated by less polluted periods. These differences are associated with changing general meteorological conditions, mainly wind direction, which influences runway usage (direction of take-off) and background pollutant concentrations as well as the dispersion of pollutants. Viewing a week of data (Fig. 8B) the strong diurnal pattern associated with the daily airport operation becomes clearer, and finally, looking at a single day (Fig. 8C), individual pollution events can be seen associated with single aircraft movements. Similar patterns are observed across the network for the other species (see Fig. 2).

The main novelty of this deployment was that there were multiple sensors positioned as components of a network of sensor nodes across the airport. Individual sensors in the network measure pollutant levels which are a combination of emissions local to that site and those from further afield. The critical point is that while individual sensors have pollutant signatures unique to the emission sources close to each site, sources which are external to the network itself (as a whole) produce a near identical response across every node of the network. The methods used to distinguish individual sensor responses (local signatures) from the network signature (non-local signature) are presented in section 2.3. The method was applied to all the sensor nodes in the network, and examples of such a separation for NO_2 and CO_2 are shown for a single site (S29) in Fig. 9.

For both NO_2 and CO_2 the observations at this site (which we term absolute) show periods of significant diurnal variation (in excess of 50 ppmv and 50 ppbv for CO_2 and NO_2 respectively), interspersed with periods where diurnal patterns are less evident. In contrast, the network measurements (which we term non-local or baseline) show less diurnal variation but do show longer periods of elevated pollutant concentrations, for example around October 9th and October 24th. Both types of

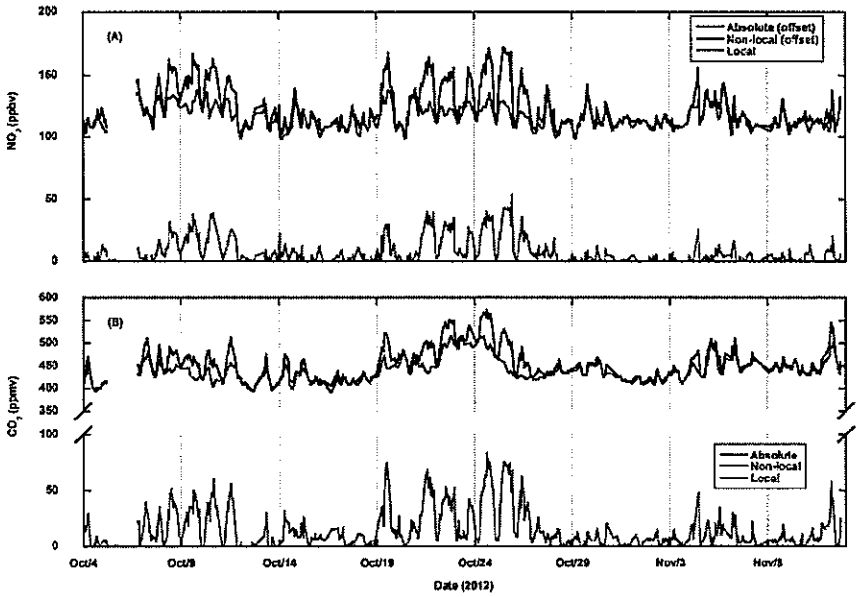

Fig. 9. Time series depicting elements of the source separation for site 29 over the five-week study period. The upper panel (A) observed (absolute) values, together with local and non-local signatures (see text for definitions) for NO_2 and with the equivalent plot for CO_2 (B). Observations obtained at the site are shown in black (with offset of 100 ppbv for absolute and non-local NO_2 applied for clarity), with the network (non-local) signature in red. The derived local measurements are shown in each case in blue. (For interpretation of the references to colour in this figure legend, the reader is referred to the Web version of this article.)

features are characteristic of meteorological impacts on dispersion of pollutants, runway usage, and, as will be seen below, longer range transport of pollutants. Finally, for both CO_2 and NO_2 the site specific (local) signatures retain the diurnal patterns, with the underlying longer-term variations removed.

Polar bivariate plots (Carslaw and Ropkins, 2012), where pollutant concentrations for a time series are shown as functions of wind speed and wind direction, are powerful tools for source attribution studies, both for source location and for providing the basis for the determination of emission indices. Fig. 10A–D shows polar bivariate plots for the hourly average local signatures (i.e. absolute measurements with the network baseline signature removed) for CO, NO, NO_2 and CO_2 for the site discussed above (site 29). The meteorological data (wind speed and direction) for these analyses are taken from the anemometer on the sensor node itself (see panel (E)). The main features in Fig. 10A–D are two distinct regions of elevated concentrations to the NE and SE of the measurement site, both associated with aircraft activities near site 29. The NE lobe shows lower levels of both NO_x ($NO + NO_2$) and the ratio of NO_x to CO_2 and higher levels of CO than the SE lobe, signifying aircraft taxiing to the NE and aircraft taking off to the SE. This is consistent with the location of a taxiway and the runway relative to site 29 (Fig. 1C). NO_2 is comparable for both lobes, consistent with the lower NO but much higher ratio of NO_2 to NO_x for taxiing emissions than for take-off emissions (Herndon et al., 2004). CO_2 in the NE lobe is also higher than in the SE lobe, which considering that the emissions rate of CO_2 is higher for take-off, suggests poorer initial dispersion of taxiing emissions relative to take-off emissions. The figures thus illustrate the additional benefits of multi-species measurements in characterising sources in detail as well as combining them with meteorological information. Note also that the higher concentrations in the local measurements are generally associated with higher wind speeds from the source direction reflecting the buoyant nature of ground level aircraft jet engine plumes (Bennett et al., 2010).

As is discussed in section 2.3, once the local pollutant signatures for each node are obtained (i.e. the background signature removed), emission indices (the amount of pollutant emitted per unit of CO_2) can now be calculated for the different sites. Fig. 4 shows how concentrations of local NO, NO_2 and CO vary with the local CO_2 at site 29. The ratio of the measurements (the graph gradient) is then used to estimate the emissions index (Table S1) for that pollutant which, in this case, correspond to 26.7 ± 0.56 g/kg for CO, 3.50 ± 0.16 g/kg for NO_2, and 1.70 ± 0.04 g/kg for NO. Note that as these are ratios of co-emitting species, they are not dependent on the degree to which any plume is intersected.

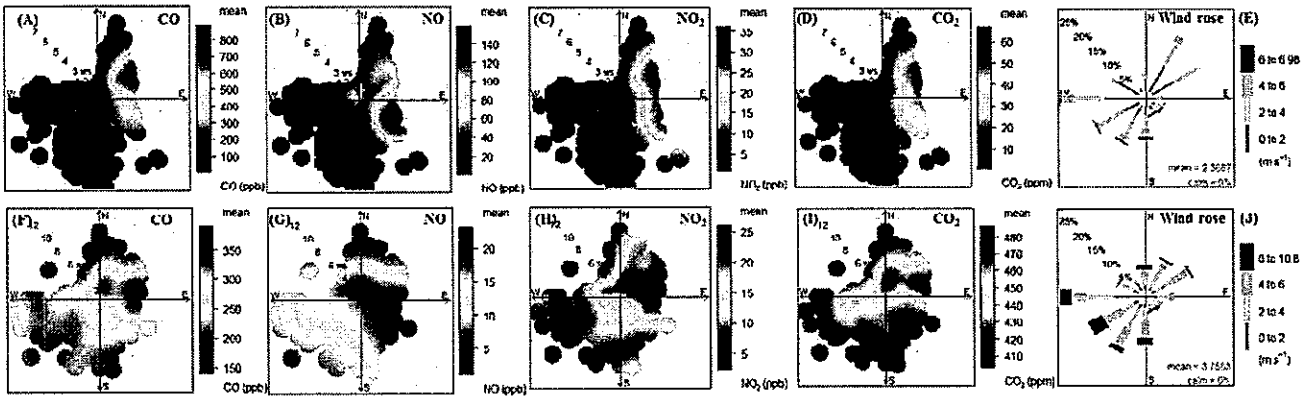

Fig. 10. Polar bivariate and wind rose plots for hourly average data at site 29 for the five-week study period. (A–E) local CO, NO, NO_2, CO_2 and wind rose, plots make use of measured wind data at site. (F–J) non-local (network baseline) CO, NO, NO_2, CO_2 and wind rose, plots make use of wind data obtained from the Met Office (Met Office, 2012) site at LHR2 and are thus representative of the large-scale flow.

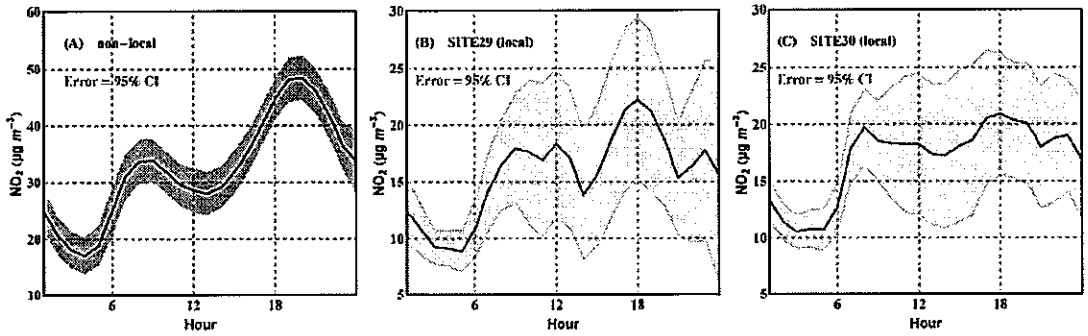

Fig. 11. Average diurnal profiles of NO_2 for the 5 week study period. (A) Non-local signature, (B) local signature at site 29 and (C) local signature at site 30. Shaded areas are 95% confidence intervals about the mean. Note NO_2 are expressed in μg m^{-3}.

Fig. 10F–I also show polar bivariate plots for CO, NO, NO_2 and CO_2, except in this case for the non-local (non-airport) component, with the meteorological measurements now taken from the Met Office site at Heathrow airport (Met Office, 2012) which can be taken to represent the large-scale wind field (Fig. 10J). Note that as these plots are derived from the entire sensor network and not from any one sensor, unlike the local site-specific signatures there is only one per species for the entire network. Firstly, we observe that, in contrast to the local pollutant signatures (Fig. 10A–D), elevated concentrations are observed at lower wind speeds when dispersion of pollutants would be expected to be reduced, but secondly there are also elevated pollutant levels when the wind is from the easterly sector, consistent with high pollutant concentrations being advected across the airport from central London (Fig. 1B).

A key feature of the non-local NO_2 signature is that its diurnal pattern (Fig. 11A), with morning and evening peaks, matches that typically seen from road traffic emissions (Vardoulakis et al., 2007). This contrasts with the diurnal profiles from the local signatures at the airport (Fig. 11B and C), which show flatter signatures during the day with a night time baseline associated with the more uniform level of daytime airport activities and the night time airport closure.

3.2. ADMS airport model and measurement comparison

This comparison uses data from the local pollution signatures extracted from the sensor network and modelled equivalent emissions for the ADMS-Airport model. The emissions and model set-up have been optimised using the sensors data, as described in section 2.4, and using known average thrust settings for British Airways (BA) aircraft at Heathrow for the period. The sensor data were averaged to hourly means to match the timescale of the ADMS-Airport model outputs. Overall, there was good agreement between the model output and the measurements for all the gas species of interest across the network, as shown in the example for site 29 close to the west end of the southern runway (Fig. 7) which compares, for each of CO, NO, NO_2 and CO_2, the local signature from the sensor with the both the refined and unrefined model prediction taking account only of the airport emissions. Both measurement (blue) and refined model (red) are consistent in showing periods of high and low daily concentrations associated different modes of runway usage as meteorological conditions vary. The peak concentrations observed in early October and the week beginning 19 October are from the southern runway under the so-called easterly runway operational mode when aircraft take-off and land into the easterly wind. Heathrow airport most frequently operates under westerly mode (take-off and landing in this direction) consistent with the prevailing wind, however if the wind is from the east, an easterly operational mode is initiated (LHR, 2017).

Fig. 12 shows a comparison of modelled and measured local NO_2 concentrations for all the active sensor sites, averaged over the five-week measurement period. Also shown are comparisons of the average

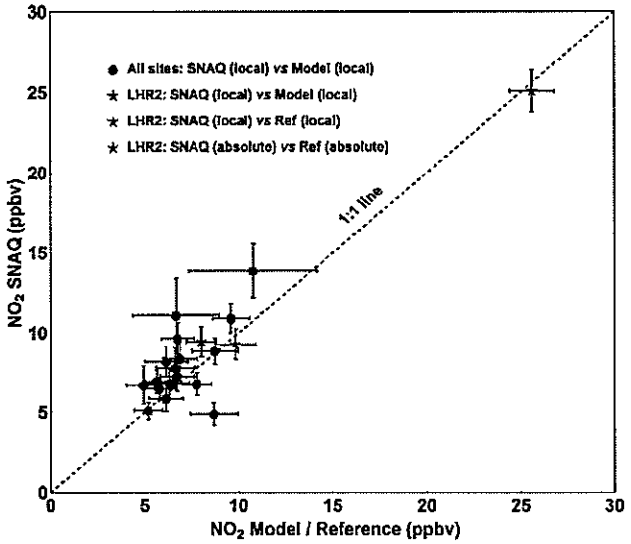

Fig. 12. Comparison of measured local NO_2 amounts for all the active sensor sites with the ADMS model averaged over the five-week measurement period (solid red circles). Also shown are the average local and total NO_2 mixing ratios at the one airport reference site (green and blue solid stars respectively) as well as the measured and modelled local NO_2 at the reference site (black). The error bars on y and x axes are ± 3σ. (For interpretation of the references to colour in this figure legend, the reader is referred to the Web version of this article.)

NO_2 local and total mixing ratios at the one reference site at the airport (LHR2). Firstly, there is broadly good correspondence between modelled and measured local NO_2 across the entire network confirming the high level of ADMS model performance. Secondly, the co-located SNAQ and reference instrument show excellent agreement both in local and absolute terms confirming the performance of the low cost NO_2 sensor.

An average absolute NO_2 concentration of 25 ppbv (~50 μg/m^3) was observed at the airport reference site (site 47), compared to local airport contribution of 9 ppbv (~18 μg/m^3). This demonstrates that local airport emissions account for only ~36% of the total NO_2 observed at that site and confirming that non-airport emissions dominate for the measurement period even at this airside location. A previous study (Carslaw et al., 2006), based on hourly NO_x and NO_2 data for 8 measurement sites in the broad neighbourhood of the airport, reported a lower bound for the airport contribution of 27%. In contrast to the current study however, in that work the background contribution was estimated from one site only so that the effect of any emission sources between that site and the airport could not be accounted for.

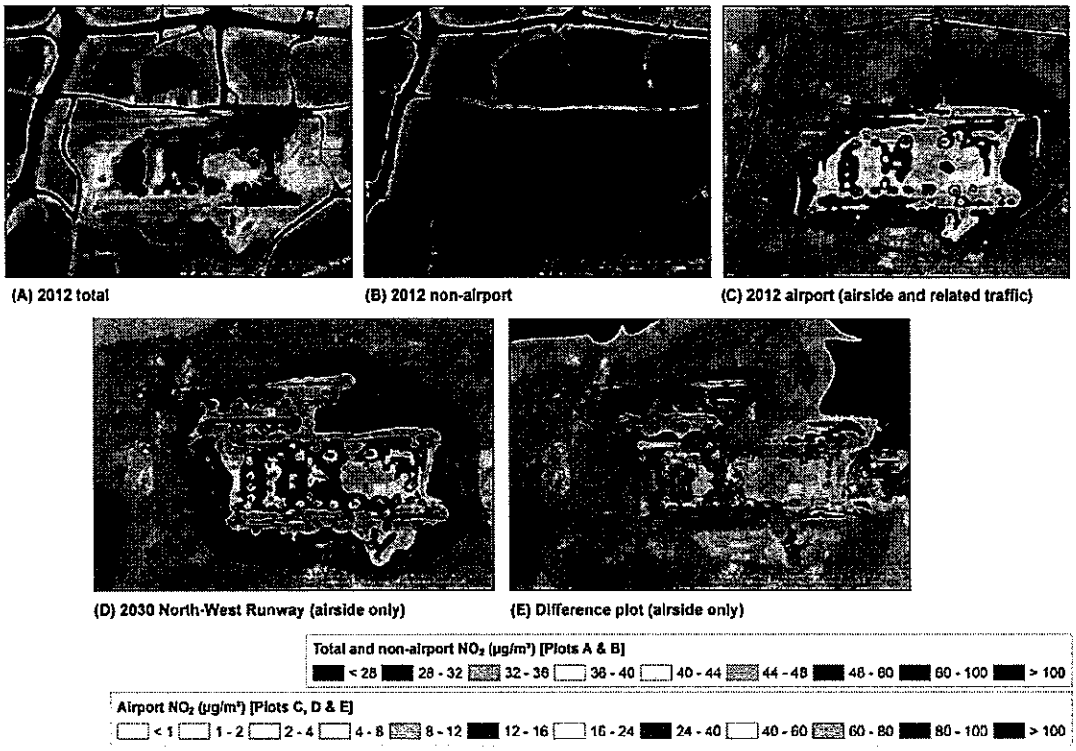

Fig. 13. Annual average modelled NO_2 concentrations (µg/m^3). (A) total NO_2 concentrations for 2012 (B) non-airport excluding airside and airport related traffic for 2012, (C) airside and airport related traffic emissions for 2012, (D) airside NO_2 concentrations for 2030 North-West Runway scenario, and (E) difference plot of the predicted contributions of the 2030 North-West Runway and 2012 baseline.

3.3. Model annual average predictions using the ADMS-Airport model

In order to identify regions where the NO_2 annual mean limit value is exceeded, we used the ADMS-Airport model, as refined by the sensor network measurements, to predict annual mean NO_2 concentration in and around Heathrow Airport. A contour plot of modelled annual average NO_2 concentrations for 2012 obtained by averaging the model output for each hour of the year is shown in Fig. 13A. This shows exceedence (yellow, orange and red) of the NO_2 limit value within and close to the airport and close to major roads. Source apportioned model calculations are depicted in Fig. 13B and C, detailing the annual average contributions of airport and non-airport emissions; the airport emissions include road traffic emissions associated with the airport.

4. Discussion and conclusion

We have used the network of sensor nodes to distinguish between and quantify local and non-local contributions to the different pollutant measurements. From this we have been able to independently derive emission ratios for the airport activities at the different node sites.

The non-airport mean NO_2 concentration contribution derived from the observations of ~16 ppbv (~32 µg/m^3) shown in Fig. 11A indicates that most of the NO_2 observed in the proximity of the airport arises from emissions which are unrelated to the airport activities. The polar bivariate plot analysis of this non-airport contribution also unequivocally indicates that the predominant non-airport emission sources are in the ENE/E direction, i.e. from the Greater London region. Importantly, the diurnal profile of this signal is characteristic of road traffic related emissions as the morning and evening rush hour peak events are clearly evident in the figure and thus it can be concluded that these sources are largely associated with road traffic emissions from Greater London.

The ADMS-Airport model, with emission indices validated and refined by comparison with the equivalent airport emissions derived directly from the sensor network measurements, shows that within the airport perimeter annual average NO_2 levels, at typically 50 µg/m^3 (Fig. 13A), are above the EU annual average limit of 40 µg/m^3. However, beyond the airport perimeter, annual average NO_2 levels only marginally exceed this limit except near major roads (40–44µg/m^3 up to 1 km to the north of the airport and lower further away). However, the model results show that in the area immediately outside the airport where the NO_2 annual average limit value is exceeded, only 12–16 µg/m^3 (~6–8 ppbv) of NO_2 (Fig. 13C) can be attributed to airport activities, ~30–36% of the total NO_2.

Model evaluations of the potential impact of an airport expansion (the addition of a third runway with its increased aircraft movements) suggest that the airport contribution to the north east of the airport will rise to ~20 µg/m^3 (~10 ppbv) with the addition of a third runway (Fig. 13D–E).

This work demonstrates a technique for source apportionment in complex environments, in this case a major international airport, using a low cost air quality sensor network. The wider impact of such work is that is can lead to an improved understanding of the impacts of policy decisions and interventions. For Heathrow airport, there is an expectation (Airports Commission July 2015) that on the timescale of the airport expansion, changes to the road traffic fleet, particularly the introduction of cleaner (Euro 6) and zero emission vehicles, NOx levels in the London plume reaching the airport will fall significantly. As an example of the likely magnitude of this effect, projections from 2013 to 2030 using the Emission Factor Toolkit (EFT) 7 published by Defra (2016) suggest a reduction of more than 80% in road NO_x emissions just to the north of the airport (see section 2.4.4). If this projection is correct, then even with a third runway and the associated roadside activities, NO_2 levels would be expected to fall below the current NO_2 annual average limit, meaning that the area would then be compliant for NO_2. Clearly crucial to achieving compliance with the NO_2 annual

average limit value by 2030 would be the extent to which vehicle engine technologies do indeed reduce NO_x emissions across the vehicle fleet.

The critical components of this study are the explicit separation of local and non-local emissions and the direct determination of emission indices using the sensor network coupled to appropriate analysis methods, and together are important demonstrations of the potential of this emerging low-cost air quality sensor technology.

Heathrow airport represents in some senses a special case, particularly in that on the spatial scale of the airport the pollutant baselines at any time can be represented by single values. Extending the technique across wider domains such as across an entire mega-city, while conceptually very similar to the approach we have taken, would be expected to require baselines which could vary spatially.

The measurement and analysis methodology we have demonstrated in this case study has wide applicability in many complex air quality environments including developing megacities, and has the clear potential to inform in a cost-effective manner policies and interventions which would mitigate potential health impacts of air quality and other environmental issues including the monitoring of greenhouse gas emissions.

Acknowledgment

The authors would like to thank NERC, United Kingdom NE/I007490/1 for funding the SNAQ London Heathrow project. We would also like to acknowledge David Vowles, Spencer Thomas and Luke Cox of Heathrow Airport Limited for helping with the logistics at Heathrow Airport.

Appendix A. Supplementary data

Supplementary data to this article can be found online at https://doi.org/10.1016/j.atmosenv.2018.09.030.

References

AEA, Energy & Environment, 2010. Heathrow airport emission inventory 2008/9, AEAT/ENV/R/2906 issue 2. Document 04 app H emissions inventory in background information volume 1 submitted by heathrow airports limited to the airports commission. https://www.gov.uk/government/uploads/system/uploads/attachment_data/file/368785/reports-04to39.zip.

Air Quality Studies for Heathrow, 2007. Base Case, Segregated Mode, Mixed Mode and Third Runway Scenarios Modelled Using ADMS-airport, Cambridge Environmental Research Consultants. Report Ref FM699/R23_Final/07. http://cerc.co.uk/environmental-software/assets/data/doc_validation/ADMS-Airport_Adding%20Capacity_Air%20Quality.pdf.

Airports Commission July, 2015. Airports Commission: Final Report. ISBN: 978-1-84864-158-7. https://www.gov.uk/government/uploads/system/uploads/attachment_data/file/440316/airports-commission-final-report.pdf.

Bennett, M., Christie, S., Graham, A., Raper, D., 2010. Lidar observations of aircraft exhaust plumes. J. Atmos. Ocean. Technol. 27, 1638–1651. https://doi.org/10.1175/2010jtecha1412.1.

Bernstein, J.A., Alexis, N., Barnes, C., Bernstein, I.L., Nel, A., Peden, D., Diaz-Sanchez, D., Tarlo, S.M., Williams, P.B., 2004. Health effects of air pollution. J. Allergy Clin. Immunol. 114, 1116–1123. https://doi.org/10.1016/j.jaci.2004.08.030.

Borrego, C., Costa, A.M., Ginja, J., Amorim, M., Coutinho, M., Karatzas, K., Sioumis, T., Katsifarakis, N., Konstantinidis, K., De Vito, S., Esposito, E., Smith, P., André, N., Gérard, P., Francis, L.A., Castell, N., Schneider, P., Viana, M., Minguillón, M.C., Reimringer, W., Otjes, R.P., von Sicard, O., Pohle, R., Elen, B., Suriano, D., Pfister, V., Prato, M., Dipinto, S., Penza, M., 2016. Assessment of air quality microsensors versus reference methods: the EuNetAir joint exercise. Atmos. Environ. 147, 246–263. https://doi.org/10.1016/j.atmosenv.2016.09.050.

Brunekreef, B., Holgate, S., 2002. Air pollution and health. Lancet 360, 1233–1242. https://doi.org/10.1016/s0140-6736(02)11274-8.

Carslaw, D.C., Beevers, S.D., Ropkins, K., Bell, M.C., 2006. Detecting and quantifying aircraft and other on-airport contributions to ambient nitrogen oxides in the vicinity of a large international airport. Atmos. Environ. 40, 5424–5434. https://doi.org/10.1016/j.atmosenv.2006.04.062.

Carslaw, D.C., Ropkins, K., 2012. Openair — an R package for air quality data analysis. Environ. Model. Software 27–28, 52–61. https://doi.org/10.1016/j.envsoft.2011.09.008.

Crilley, L.R., Shaw, M., Pound, R., Kramer, L.J., Price, R., Young, S., Lewis, A.C., Pope, F.D., 2018. Evaluation of a low-cost optical particle counter (Alphasense OPC-N2) for ambient air monitoring. Atmos. Meas. Tech. Discuss. 11, 709–720. https://doi.org/10.5194/amt-11-709-2018.

Defra, 2016. UK department for environment Food and rural Affairs, emission factor Toolkit v7.0. https://laqm.defra.gov.uk/review-and-assessment/tools/emissions-factors-toolkit.html.

Department for Environment, Food and Rural Affairs, 2016. Local air quality management, NO_X to NO_2 calculator. https://laqm.defra.gov.uk/review-and-assessment/tools/background-maps.html#NOxNO2calc.

De Vito, S., Esposito, E., Salvato, M., Popoola, O., Formisano, F., Jones, R., Di Francia, G., 2018. Calibrating chemical multisensory devices for real world applications: an in-depth comparison of quantitative machine learning approaches. Sensor. Actuator. B Chem. 255, 1191–1210. https://doi.org/10.1016/j.snb.2017.07.155.

Doc 9889, 2011. Airport Air Quality Manual. International Civil Aviation Organization ISBN 978-92-9231-862-8.

European Civil Aviation Conference, 2005. Report on Standard Method of Computing Noise Contours Around Civil Airports. third ed. ECAC Document 29.

Heimann, I., Bright, V.B., McLeod, M.W., Mead, M.I., Popoola, O.A.M., Stewart, G.B., Jones, R.L., 2015. Source attribution of air pollution by spatial scale separation using high spatial density networks of low cost air quality sensors. Atmos. Environ. 113, 10–19. https://doi.org/10.1016/j.atmosenv.2015.04.057.

Herndon, S.C., Jayne, J.T., Lobo, P., Onasch, T.B., Fleming, G., Hagen, D.E., Whitefield, P.D., Miake-Lye, R.C., 2008. Commercial aircraft engine emissions characterization of in-use aircraft at hartsfield-jackson atlanta international airport. ES T (Environ. Sci. Technol.) 42, 1877–1883. https://doi.org/10.1021/es072029+.

Herndon, S.C., Shorter, J.H., Zahniser, M.S., Nelson, D.D., Jayne, J., Brown, R.C., Miake-Lye, R.C., Waitz, I., Silva, P., Lanni, T., Demerjian, K., Kolb, C.E., 2004. NO and NO2 emission ratios measured from in-use commercial aircraft during taxi and takeoff. ES T (Environ. Sci. Technol.) 38, 6078–6084. https://doi.org/10.1021/es049701c.

Hu, S., Fruin, S., Kozawa, K., Mara, S., Winer, A.M., Paulson, S.E., 2009. Aircraft emission impacts in a neighborhood adjacent to a general aviation airport in southern California. ES T (Environ. Sci. Technol.) 43, 8039–8045. https://doi.org/10.1021/es900975f.

Independent report, 2014. Additional Airport Capacity: Heathrow Airport North West Runway. Heathrow Airports Limited.

Jenkin, M.E., 2004. Analysis of sources and partitioning of oxidant in the UK—Part 1: the NO_X-dependence of annual mean concentrations of nitrogen dioxide and ozone. Atmos. Environ. 38, 5117–5129. https://doi.org/10.1016/j.atmosenv.2004.05.056.

Kim, J., Shusterman, A.A., Lieschke, K.J., Newman, C., Cohen, R.C., 2018. The BErkeley atmospheric CO2 observation network: field calibration and evaluation of low-cost air quality sensors. Atmos. Meas. Tech. Discuss. 11, 1937–1946. https://doi.org/10.5194/amt-11-1937-2018.

Kumar, P., Morawska, L., Martani, C., Biskos, G., Neophytou, M., Di Sabatino, S., Bell, M., Norford, L., Britter, R., 2015. The rise of low-cost sensing for managing air pollution in cities. Environ. Int. 75, 199–205. https://doi.org/10.1016/j.envint.2014.11.019.

Lewis, A.C., Lee, J.D., Edwards, P.M., Shaw, M.D., Evans, M.J., Moller, S.J., Smith, K.R., Buckley, J.W., Ellis, M., Gillot, S.R., White, A., 2016. Evaluating the performance of low cost chemical sensors for air pollution research. Faraday Discuss 189, 85–103. https://doi.org/10.1039/c5fd00201j.

LHR Airport Limited. http://www.heathrow.com/noise/heathrow-operations/cranford-agreement#, Accessed date: 3 November 2016.

LHR, 2017. Heathrow Operations: Wind Direction. LHR Airports Limited. http://www.heathrow.com/noise/heathrow-operations/wind-direction.

Lowry, D., Lanoisellé, M.E., Fisher, R.E., Martin, M., Fowler, C.M.R., France, J.L., Hernández-Paniagua, I.Y., Novelli, P.C., Sriskantharajah, S., O'Brien, P., Rata, N.D., Holmes, C.W., Fleming, Z.L., Clemitshaw, K.C., Zazzeri, G., Pommier, M., McLinden, C.A., Nisbet, E.G., 2016. Marked long-term decline in ambient CO mixing ratio in SE England, 1997–2014: evidence of policy success in improving air quality. Sci. Rep. 6, 25661. https://doi.org/10.1038/srep25661.

Masiol, M., Harrison, R.M., 2015. Quantification of air quality impacts of London heathrow airport (UK) from 2005 to 2012. Atmos. Environ. 116, 308–319. https://doi.org/10.1016/j.atmosenv.2015.06.048.

McConnell, R., Berhane, K., Gilliland, F., London, S.J., Islam, T., Gauderman, W.J., Avol, E., Margolis, H.G., Peters, J.M., 2002. Asthma in exercising children exposed to ozone: a cohort study. Lancet 359, 386–391. https://doi.org/10.1016/S0140-6736(02)07597-9.

McHugh, C.A., Carruthers, D.J., Edmunds, H.A., 1997. ADMS–Urban: an air quality management system for traffic, domestic and industrial pollution. Int. J. Environ. Pollut. 8, 666–674. https://doi.org/10.1504/ijep.1997.028218.

Mead, M.I., Popoola, O.A.M., Stewart, G.B., Landshoff, P., Calleja, M., Hayes, M., Baldovi, J.J., McLeod, M.W., Hodgson, T.F., Dicks, J., Lewis, A., Cohen, J., Baron, R., Saffell, J.R., Jones, R.L., 2013. The use of electrochemical sensors for monitoring urban air quality in low-cost, high-density networks. Atmos. Environ. 70, 186–203. https://doi.org/10.1016/j.atmosenv.2012.11.060.

Met Office, 2012. Met Office Integrated Data Archive System (MIDAS) Land and Marine Surface Stations Data (1853-current). NCAS British Atmospheric Data Centre [cited: 6 August, 2013].

Miskell, G., Salmond, J., Williams, D.E., 2017. Low-cost sensors and crowd-sourced data: observations of siting impacts on a network of air-quality instruments. Sci. Total Environ. 575, 1119–1129. https://doi.org/10.1016/j.scitotenv.2016.09.177.

Module 6, 2015. Air Quality Local Assessment Detailed Emissions Inventory and Dispersion Modelling. Jacobs UK Limited.

Mueller, M., Meyer, J., Hueglin, C., 2017. Design of an ozone and nitrogen dioxide sensor unit and its long-term operation within a sensor network in the city of Zurich. Atmos. Meas. Tech. 10, 3783–3799. https://doi.org/10.5194/amt-10-3783-2017.

National Audit Office, 2009. Air quality, briefing for the house of commons environmental Audit committtee. https://www.nao.org.uk/wp-content/uploads/2010/01/

Air_Quality.pdf.
Parnia, S., Brown, J.L., Frew, A.J., 2002. The role of pollutants in allergic sensitization and the development of asthma. Allergy 57, 1111–1117. https://doi.org/10.1034/j.1398-9995.2002.02167.x.
Penza, M., Suriano, D., Villani, M.G., Spinelle, L., Gerboles, M., 2014. Towards air quality indices in smart cities by calibrated low-cost sensors applied to networks. In: IEEE SENSORS 2014 Proceedings, pp. 2012–2017. https://doi.org/10.1109/icsens.2014.6985429.
Pope, C.A., Dockery, D.W., 2006. Health effects of fine particulate air pollution: lines that connect. J Air Waste Manage 56, 709–742. https://doi.org/10.1080/10473289.2006.10464485.
Popoola, O., Mead, I., Bright, V., Baron, R., Saffell, J., Stewart, G., Kaye, P., Jones, R., 2013. A portable low-cost high density sensor network for air quality at London Heathrow airport. In: AGU 2013 Fall Meeting, San Francisco, California.
Popoola, O.A.M., Stewart, G.B., Mead, M.I., Jones, R.L., 2016. Development of a baseline-temperature correction methodology for electrochemical sensors and its implications for long-term stability. Atmos. Environ. 147, 330–343. https://doi.org/10.1016/j.atmosenv.2016.10.024.
Ren, M., Li, N., Wang, Z., Liu, Y., Chen, X., Chu, Y., Li, X., Zhu, Z., Tian, L., Xiang, H., 2017. The short-term effects of air pollutants on respiratory disease mortality in Wuhan, China: comparison of time-series and case-crossover analyses. Sci. Rep. 7, 40482. https://doi.org/10.1038/srep40482.
Samoli, E., Peng, R., Ramsay, T., Pipikou, M., Touloumi, G., Dominici, F., Burnett, R., Cohen, A., Krewski, D., Samet, J., Katsouyanni, K., 2008. Acute effects of ambient particulate matter on mortality in europe and north America: results from the APHENA study. Environ. Health Perspect. 116, 1480–1486. https://doi.org/10.1289/ehp.11345.
Schneider, P., Castell, N., Vogt, M., Dauge, F.R., Lahoz, W.A., Bartonova, A., 2017. Mapping urban air quality in near real-time using observations from low-cost sensors and model information. Environ. Int. 106, 234–247. https://doi.org/10.1016/j.envint.2017.05.005.
Schürmann, G., Schäfer, K., Jahn, C., Hoffmann, H., Bauerfeind, M., Fleuti, E., Rappenglück, B., 2007. The impact of NOx, CO and VOC emissions on the air quality of Zurich airport. Atmos. Environ. 41, 103–118. https://doi.org/10.1016/j.atmosenv.2006.07.030.
Spinelle, L., Gerboles, M., Villani, M.G., Aleixandre, M., Bonavitacola, F., 2015. Field calibration of a cluster of low-cost available sensors for air quality monitoring. Part A: ozone and nitrogen dioxide. Sensor. Actuator. B Chem. 215, 249–257. https://doi.org/10.1016/j.snb.2015.03.031.
Sun, L., Westerdahl, D., Ning, Z., 2017. Development and evaluation of A novel and cost-effective approach for low-cost NO(2) sensor drift correction. Sensors 17, 1916. https://doi.org/10.3390/s17081916.
Sun, L., Wong, K.C., Wei, P., Ye, S., Huang, H., Yang, F., Westerdahl, D., Louie, P.K.K., Luk, C.W.Y., Ning, Z., 2016. Development and application of a next generation air sensor network for the Hong Kong marathon 2015 air quality monitoring. Sensors 16, 211. https://doi.org/10.3390/s16020211.
Updated Air Quality Re-analysis, 2017. Impact of New Copert Emission Factors and Associated New Pollution Climate Mapping Sensitivity Testing. WSP Parsons Brinckerhoff Report No. 62103867-041. https://www.gov.uk/government/uploads/system/uploads/attachment_data/file/588752/updated-air-quality-re-analysis.pdf.
UK Department for Transport, 2006. Project for the Sustainable Development of Heathrow – Report of the Air Quality Technical Panel Chapter 4 – Dispersion Modelling. . http://webarchive.nationalarchives.gov.uk/20071209143920/http://www.dft.gov.uk/pgr/aviation/environmentalissues/heathrowsustain/chapter4dispersionmodelling.
UK Department for Transport, 2017. Consultation on Draft Airports National Policy Statement: New Runway Capacity and Infrastructure at Airports in the South East of England. ISBN:978-1-84864-189-1. https://www.gov.uk/government/uploads/system/uploads/attachment_data/file/589082/consultation-on-draft-airports-nps.pdf.
Vardoulakis, S., Valiantis, M., Milner, J., ApSimon, H., 2007. Operational air pollution modelling in the UK—street canyon applications and challenges. Atmos. Environ. 41, 4622–4637. https://doi.org/10.1016/j.atmosenv.2007.03.039.
Venkatram, A., Karamchandani, P., Pai, P., Goldstein, R., 1994. The development and application of a simplified ozone modeling system (SOMS). Atmos. Environ. 28, 3665–3678. https://doi.org/10.1016/1352-2310(94)00190-V.
WHO, 2009. Ambient air pollution: a global assessment of exposure and burden of disease, geneva. http://apps.who.int/iris/bitstream/10665/250141/1/9789241511353-eng.pdf.

Atmospheric Environment 171 (2017) 82–90

Contents lists available at ScienceDirect

Atmospheric Environment

journal homepage: www.elsevier.com/locate/atmosenv

Development of an environmental chamber for evaluating the performance of low-cost air quality sensors under controlled conditions

Vasileios Papapostolou, Hang Zhang, Brandon J. Feenstra, Andrea Polidori*

South Coast Air Quality Management District, Diamond Bar, CA 91765, USA

HIGHLIGHTS

- A state-of-the-art laboratory chamber was developed to evaluate air quality sensors.
- This chamber generates stable and reproducible environmental conditions.
- Sensors should be tested under a wide range of T and RH conditions.
- A rigorous sensor testing method was also developed.
- As technology improves a more standardized testing protocol should be developed.

GRAPHICAL ABSTRACT

ARTICLE INFO

Article history:
Received 24 March 2017
Received in revised form
23 September 2017
Accepted 1 October 2017
Available online 4 October 2017

Keywords:
Low-cost sensors
Sensor evaluation
Environmental chamber
Testing protocol
Particle pollutants
Gaseous pollutants

ABSTRACT

A state-of-the-art integrated chamber system has been developed for evaluating the performance of low-cost air quality sensors. The system contains two professional grade chamber enclosures. A 1.3 m^3 stainless-steel outer chamber and a 0.11 m^3 Teflon-coated stainless-steel inner chamber are used to create controlled aerosol and gaseous atmospheres, respectively. Both chambers are temperature and relative humidity controlled with capability to generate a wide range of environmental conditions. The system is equipped with an integrated zero-air system, an ozone and two aerosol generation systems, a dynamic dilution calibrator, certified gas cylinders, an array of Federal Reference Method (FRM), Federal Equivalent Method (FEM), and Best Available Technology (BAT) reference instruments and an automated control and sequencing software. Our experiments have demonstrated that the chamber system is capable of generating stable and reproducible aerosol and gas concentrations at low, medium, and high levels. This paper discusses the development of the chamber system along with the methods used to quantitatively evaluate sensor performance. Considering that a significant number of academic and research institutions, government agencies, public and private institutions, and individuals are becoming interested in developing and using low-cost air quality sensors, it is important to standardize the procedures used to evaluate their performance. The information discussed herein provides a roadmap for entities who are interested in characterizing air quality sensors in a rigorous, systematic and reproducible manner.

Published by Elsevier Ltd.

* Corresponding author.
E-mail address: apolidori@aqmd.gov (A. Polidori).

https://doi.org/10.1016/j.atmosenv.2017.10.003
1352-2310/Published by Elsevier Ltd.

1. Introduction

Studies have shown that air pollutants, such as fine particulate matter ($PM_{2.5}$), ozone (O_3), volatile organic compounds (VOC), and nitric oxides (NO_x), can cause serious respiratory diseases, cardiovascular disorders, and other adverse health effects (Heck et al., 2013; Weichenthal et al., 2011). Conventionally, air quality and pollutant concentrations are monitored by the federal government as well as state and local regulatory agencies using sophisticated and expensive fixed-site instruments (Snyder et al., 2013). The number of monitoring sites is thus limited by the cost of instrumentation and availability of trained personnel to operate and maintain such equipment. Because of their relatively low spatial density, available fixed air monitoring sites are mostly designed to characterize air quality over a wide geographical area. However, they do not typically provide the granularity that is often necessary to fully understand local air quality conditions. Due to recent technological advancements in micro-sensors, embedded systems, and wireless networks, manufacturers have begun marketing low-cost and relatively easy-to-use air quality sensors. These devices, provided they produce reliable data, can significantly augment and improve current ambient air monitoring capabilities. A wide range of sensor applications is now changing the paradigm of air pollution monitoring (Snyder et al., 2013). In its 2014–2018 Strategic Plan, the United States Environmental Protection Agency (U.S. EPA) has recognized the need to extend the existing air pollution monitoring to lower cost measurements (EPA, 2014). Herein, a sensor is considered low-cost if its market cost is less than $2000. If a device is presented as a multi-pollutant sensor device, then the cost per pollutant type should be less than $2000. With the recent commercialization of low-cost and easy-to-use devices, susceptible groups and individuals such as children, seniors, asthmatics, pregnant women, and people interested in measuring air pollution in their communities can monitor air quality and assess potential personal exposure. Citizen scientists and community groups have now access to a wealth of information to better understand how air pollution may impact their neighborhoods (Deville Cavellin et al., 2016; Jiao et al., 2015). Air quality sensors deployed near industrial facilities, such as those for fence-line monitoring applications, can provide empirical data to supplement existing ambient air monitoring infrastructure (Pikelnaya et al., 2013). Portable sensor mounted on a mobile vehicle can also be used to monitor urban air quality and map the spatial variation of traffic related emissions (Hagler et al., 2010; Van den Bossche et al., 2015).

The development of reliable low-cost air quality sensors is complex. These devices have to detect one or more specific target pollutants while being inert to interferent species and meteorological parameters. They also have to be calibrated to give accurate readings, which often requires the need of specialized and expensive reference instrument. Furthermore, various algorithms and processing procedures are used to convert the sensor's signal to air pollution concentrations. Therefore, not all low-cost sensors are reliable or able to provide meaningful air quality information (Williams et al., 2014). Consequently, their performance needs to be fully characterized under various pollutant levels and different environmental conditions to assure data quality.

Environmental chambers have been an indispensable tool in studying gas-phase atmospheric chemistry (Cocker et al., 2001) and pollutant exposure (Papapostolou et al., 2013) because they can provide controlled environments. Over the past years, there have been several studies on sensor performance evaluation that involved environmental chambers. At EPA, a glass exposure chamber was constructed to evaluate the performance of O_3, nitrogen dioxide (NO_2) and VOC sensors (Williams et al., 2014, 2015). Temperature and relative humidity (RH) were controlled by an air conditioning system, supplemented with heating pads, dry ice, and a water bubbler. Important parameters such as linear correlation coefficient, detection limit, concentration resolution, response time, and temperature and RH influences were examined. Yet, due to the chamber size limitations and restricted resources, the intra-model variability, the effect of interferents and weather conditions were not tested in those studies. Joint Research Center (JRC) has published a series of technical reports and papers describing its efforts in evaluating and calibrating gaseous sensors (Spinelle et al., 2014). In the JRC laboratory testing approach, an "O"-shaped ring-tube exposure chamber was developed to evaluate an ozone sensor (model B4-O3, Alphasense, UK) under controlled temperature, RH, wind velocity, and gaseous interferent concentrations. The sensor reported highly linear output, good precision, and little baseline drift, but it was sensitive to NO_2 and was affected by hysteresis due to RH variations. Although this work was conducted for an ozone sensor, it provided important guidelines for other gas sensors evaluation. In another study, three particle sensors, including Shinyei PPD42NS, Samyoung DSM501A and the Sharp GP2Y1010AU0F, were evaluated in a customized acrylic chamber where particulate atmosphere was created by burning incense (Wang et al., 2015). The method was limited in scope, as the system could not generate stable and reproducible particulate environment, thus was not appropriate for systematic evaluation of PM sensors of different types. Additionally, a Shinyei PPD42NS particulate sensor was also evaluated in a chamber, but only under ambient temperature and RH conditions (Austin et al., 2015). Similar studies (Northcross et al., 2013; Sousan et al., 2016a, 2016b) have definitely expanded our understanding on the potential and limitations of low-cost air monitoring devices. Nonetheless, there has not been any effort to develop methods, protocols, and procedures to systematically evaluate the performance of low-cost particle and gaseous sensors under a wide range of environmental conditions.

Herein, we describe the development of a state-of-the-art chamber system for the performance evaluation of low-cost air quality sensors. To the best of our knowledge, this integrated chamber system is the first that can generate stable and reproducible environmental conditions with diverse temperature, RH, and known PM and gas concentration profiles. The chamber system is coupled with an array of FRM, FEM, and BAT reference instruments for comparison purposes. In this paper, we focus on the development of methods and the validation of the chamber's ability to generate a wide range of environmental conditions. Indicative laboratory experiments are presented to exemplify the practical application of the chamber system and the testing methods. A summary of all available laboratory testing results conducted within Air Quality – Sensor Performance Evaluation Center (AQ-SPEC) can be found on a dedicated website (www.aqmd.gov/aq-spec). Our sensor evaluation results indicate that sensor performance can be better characterized when parameters such as accuracy, precision, detection limit, climate susceptibility, and the effect of interferents are investigated systematically.

2. Methodology

2.1. Chamber system overview

A chamber system, designed by the AQ-SPEC team, hardware developed and integrated by AmbiLabs (Warren, RI), has been installed inside the South Coast Air Quality Management District's Chemistry Laboratory (Fig. 1 and Figure S-1).

The chamber system consists of:

i) A professional grade environmental test chamber (G-Series Elite, model GD-32-3-AC, Russells, Holland, MI) capable of

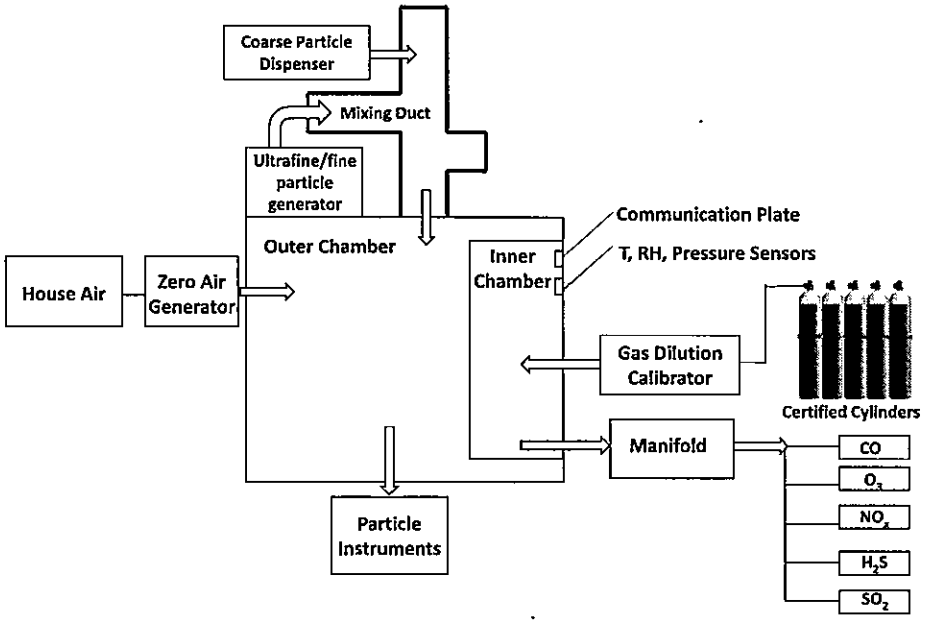

Fig. 1. Schematic of chamber system.

creating a wide range of temperature and relative humidity. This includes a stainless steel rectangular-shaped enclosure (1.3 m^3, here referred to as "outer chamber"), a heating/cooling system for controlling the test temperature, a humidifier/de-humidifier for varying the relative humidity;

ii) A custom-made Teflon-coated stainless steel cylindrical-shaped enclosure (0.11 m^3, here referred to as "inner chamber"), installed inside the "outer chamber";

iii) A dry, gas- and particle-free "zero-air" generation system (described in details in Supporting Information);

iv) An aerosol generator (model AGK, 2000; PALAS, Germany) to generate ultrafine/fine particles;

v) A particle dispenser (model SAG 410/U, TOPAS, Germany) to dispense fine/coarse particles;

vi) A dynamic dilution calibrator with an internal ozone generator (model T700U by Teledyne API, San Diego, CA);

vii) An array of FRM, FEM and BAT reference instruments (Table 1), whose sampling inlets are in-line with the chamber and about 20 cm from the sensor trays (see Figure S-1);

viii) An integrated computer software that controls the various operating/experimental parameters, T/RH set-points and reference instrument data logging.

Specifically, the integrated computer software (Polidori et al., 2016) allows for the design of extensive sensor testing experiments using programmed sequences, and consists of three main integrated components: a custom program sequence runner for setting chamber T/RH and for controlling PM concentrations in aerosol experiments (Figure S-2), a Teledyne APIcom software for controlling concentrations in gas experiments (Figure S-3), and a WinAQMS Data Acquisition and Control System (Figure S-4) (WinAQMS Air Quality Monitoring Software, Ecotech, RI). The software provides full control over the chamber system, enabling measurements to be recorded, automatic calibrations to be performed and system errors to be monitored. WinAQMS allows collection of data directly from the gas and particle instruments in digital format, thus eliminating digital to analog and analog to digital conversion errors.

Table 1
Reference instruments used in the laboratory low-cost sensor evaluation.

Manufacturer	Model	Measures	Range	LDL	Measurement technique	Method	Flow rate (LPM)
GRIMM	EC180	PM_{10}, $PM_{2.5}$, and PM_1 environmental dust monitor	0.1–1500 μg/m^3	0.1 μg/m^3	light scattering	FEM	5
TSI	Model 3321	aerodynamic particle sizer, 0.5–20 μm aerodynamic sizing	0-10,000 particles/m^3	0.001 particle/m^3	double-crest optical	BAT	5
TSI	Model 3091	fast mobility particle sizer, 5.6–560 nm	N/A	N/A	electrical mobility	BAT	10
Ecotech	Serinus 55	hydrogen sulfide	0-20 ppm	0.4 ppb	UV fluorescent radiation, external thermal converter	FRM	0.675
Ecotech	Serinus 10	ozone	0-20 ppm	0.5 ppb	nondispersive UV photometer	FEM	0.5
Ecotech	Serinus 40	nitric oxide, nitrogen dioxide, and nitrogen oxides	0-20 ppm	0.4 ppb	gas-phase chemilluminescence detection	FRM	0.6
Ecotech	EC 9850T	sulfur dioxide trace analyzer	0-20 ppm	0.3 ppb	fluorescence spectroscopy	FRM	0.75
Ecotech	EC 9830T	carbon monoxide trace analyzer	0-20 ppm	200 ppb	infrared photometric detection and gas filter correlation	FRM	1

2.2. Aerosol and gaseous test environments

Controlled aerosol environments are generated in the rectangular-shaped outer chamber to conduct PM sensor evaluations. As previously mentioned, the system is equipped with two particle generators, an ultrafine/fine particle generation system PALAS AGK 2000 and a fine/coarse particle dispenser TOPAS SAG 410/U. In the PALAS particle generator, test aerosol is generated in a consistent and systematic manner in terms of particle count/mass concentrations and particle size distribution. A specially developed nozzle prevents salt crystallization at the nozzle outlet. The liquid suspension is dried in a vertical dryer (model TR2000, PALAS, Germany) that has a smooth 90° elbow shape. The dried aerosol is then diluted with dry "zero-air" into a mixing duct, and directed into the outer chamber. The particle concentration and size distribution can be adjusted by changing the salt type and concentration as well as by varying the aerosol injection frequency and duration in the chamber using the integrated custom software (see Section 2.1). The TOPAS dust dispenser is used to introduce fine/coarse particles in the outer chamber. Standard dry dust (e.g., Arizona test dust ISO 12103 A4 Coarse Grade or dolomite powder) is dispensed into the chamber through a two-step process: first, dust is continuously supplied from a dust reservoir onto the rotating belt, and subsequently, the dust material is injected into the mixing duct and then the outer chamber with compressed "zero-air". The first step is key to achieve a stable and reproducible particulate concentration, but is quite challenging, especially when the target concentration is very low. Key dispenser components such as the toothed belt and the scraper ensure the delivery of consistent amounts of dust.

In a typical fine particle ($PM_{2.5}$) experiment testing a PM sensor, the outer chamber is first conditioned to a target temperature and RH. Aqueous potassium chloride solution (KCl, 17% by weight) is nebulized in the aerosol generator and is subsequently dried in the PALAS dryer. Dry particles are then directed into the chamber. The chamber operates in a dynamic mode at a flowrate of about 23 L/min. On average, 2–3 h are needed to achieve a stable particle concentration and size distribution in the chamber, which is between 2 and 3 chamber mean residence times for a chamber volume of 1.3 m^3.

Controlled gaseous atmospheres are generated in the cylindrical-shaped inner chamber where gas sensors are installed for testing. The relatively low inner chamber volume of 0.11 m^3 (about 1/12th of the outer chamber) allows to decrease the time needed to reach a stable gas concentration in the chamber and, consequently, to reduce the consumption of certified standard gases used for experiments. The inner chamber is coated with polytetrafluoroethylene (PTFE) to provide an inert surface for reactive gases (e.g., O_3 and H_2S).

In a typical experiment of testing a gas sensor, the inner chamber is first conditioned to the target temperature and RH. The targeted gas pollutant(s) from a certified compressed gas cylinder (or in the case of ozone, generated by the dilution calibrator) is first passed through a gas dilution calibrator where the appropriate test flow is adjusted and mixed with pre-conditioned zero-air inside the inner chamber. The dynamic dilution calibrator is capable of producing a broad range of gas pollutant concentrations.

2.3. Chamber preparation and sensor evaluation

Prior to a laboratory testing experiment, the chamber wall surfaces are wiped off with isopropyl alcohol and the sensors to be tested are mounted on the supporting Teflon-made trays. All sensors are pre-treated with routine set-up procedures, such as filter replacement (when necessary), zero calibration, flow rate check, date/time synchronization, and battery charge. Power and software control cables are connected through the communication plate located on the right-hand side of the outer chamber. The chamber door is then closed and dry, particle- and gas-free air is flushed through the system to provide a clean background for a new experiment.

The general evaluation procedure is based on a side-by-side comparison between the sensor(s) to be tested and the reference FRM, FEM and BAT instrument(s) measuring the same pollutant(s). During a typical experiment, the concentration of the target pollutant is increased from zero-air baseline to the first concentration level. The target pollutant concentration is then kept stable for a set period of time at the steady-state stage. This procedure is repeated multiple times over multiple pollutant concentrations spanning from very low (e.g., below typical ambient conditions or less than 50% of the U.S EPA National Ambient Air Quality Standards (NAAQS)) to very high (e.g., well above ambient conditions or more than 200% of the U.S. EPA NAAQS), and under different temperature (e.g., 5–35 °C) and RH levels (e.g., 20–80%). Performance-related parameters, similar to those established by EPA, JRC and other organizations that have conducted similar sensor testing experiments (Spinelle et al., 2013, 2014; Williams et al., 2014; Williams et al., 2015) are quantitatively defined and include intra-model variability, accuracy, precision, lower detection limit, linear correlation coefficient (R^2), effect of interferent species, climate susceptibility, and data recovery (Polidori et al., 2016). Most of these parameters, except for the linear correlation coefficient, are evaluated based on data acquired from the steady-state stages.

3. Results and discussion

3.1. Chamber temperature and relative humidity control

Studies have shown that temperature and relative humidity can have a negative impact on sensor performance and, consequently, affect the reported pollutant concentration. Commercially available metal oxide gas sensors are mainly made of tin dioxide (SnO_2) deposited on porous alumina or silica. At high humidity level, adsorption of water vapor and potential moisture condensation decrease the SnO_2 baseline resistance, resulting into reduced sensitivity. The effective surface area available for sensing the target pollutant also drops in time due to moisture adsorption (Sohn et al., 2008). In addition, prolonged exposure to high humidity levels leads to the formation of stable chemisorbed hydroxide ions (OH^-), causing sensitivity degradation or drifted baseline values (Wang et al., 2010). For optical particle sensors, relative humidity is known to affect their performance due to the condensational growth of the particles' hygroscopic components. The enlargement of the particle size contributes to the overestimation of the particle mass concentration (Chakrabarti et al., 2004; Fischer and Koshland, 2007).

Temperature, on the other hand, does not generally influence sensor performance as much as relative humidity. However, in some particle sensors, the air sample is conveyed by a current generated using a built-in heater. At extreme temperatures, the flow rate of the current could be altered, and consequently affect the resulting laser or infrared particle count readings (Wang et al., 2015). Manufacturers use proprietary algorithms to convert particle count into particle mass concentration. In some cases, the algorithm takes into account not only the particle density and shape, but also the operating temperature and humidity.

For the above reasons, it is imperative that the sensors are evaluated under representative environmental conditions. As suggested by the specification, our chamber system is capable of reaching a broad range of temperature and relative humidity

conditions (T range: −32 °C to +177 °C; RH range: 10%–95%). The chamber's capability to create stable and reproducible temperature and relative humidity conditions was demonstrated in two separate experiments. In the first experiment, the temperature set point was increased by 5 °C every 30 min from 5 to 35 °C, while maintaining relative humidity constant at 40%. As shown in Fig. 2 (a), the chamber was capable of delivering accurate temperature control. At each step, the temperature reached the target value within 3 min from the previous set point and remained stable throughout the 30 min period. Previous studies have also demonstrated that testing chambers are capable of controlling temperature conditions within ±2 °C (Zhao et al., 2015).

Regarding humidity control, two different chamber dehumidification processes are available and may be used. If the temperature and humidity combination falls in the shaded area in Figure S-5 T-RH performance envelop, dehumidification is accomplished by eliminating excess of water at the cooling coils. For conditions that lie outside the shaded area in T-RH performance envelope (Figure S-5), the dehumidification of the chamber can be achieved by purging the system with dry zero air. In an experiment to validate chamber's humidity control, the chamber was held at a constant temperature of 20 °C, and RH was ramped from 20% to 80% at 10% intervals. Each RH level was maintained for 60 min. In Fig. 2 (b), at the lowest set point of 20%, RH fluctuated between 20% and 23%. This was somewhat expected because this T-RH combination is outside the shaded T-RH performance envelop, and therefore RH could not be maintained at such low level without purging dry zero-air. At higher RH set points, the measured RH fluctuations around the target values were between ±0.8% and ±3.9% and were considered very small and within the acceptable range. It should be noted that in previous chamber studies, RH conditions were not accounted for (Austin et al., 2015; Sousan et al., 2016a; Zhao et al., 2015). In other cases where water bubblers were used to generate certain RH levels, gas flows were split based on calculations, and only the theoretical RH level was reported. Actual RH variations in the chamber were not monitored nor discussed (Wang et al., 2015; Wei et al., 2013). Here, the two experiments clearly demonstrated the chamber's capability to produce a broad range of environmental conditions that can be used to appropriately test sensors' climate susceptibility.

3.2. Generation of stable testing atmospheres

The chamber's ability to generate stable aerosol and gas atmospheres is crucial for performing sensor evaluation, as many testing parameters are calculated based on the data acquired under steady-state conditions. Thus, a set of experiments was conducted to fully evaluate the chamber's ability to produce stable concentrations of laboratory generated particles, CO (an unreactive gas), and O_3 (a reactive gas). Stability for each pollutant was evaluated at five indicative concentration levels from "very low" to "very high". The "very low" level is chosen to represent a pollutant concentration below the U.S. EPA NAAQS requirement. It is also close to the lowest concentration the chamber system could generate or the reference analyzers could detect. The "low" and "medium" pollutant levels are similar to the average ambient pollutant concentration level and 50% above the average ambient pollutant concentration level, respectively. The "high" pollutant level is at least 100% higher than the average NAAQS standard level. The "very high" pollutant level is close to the maximum concentration the chamber could generate or the reference analyzers could accurately detect. Table S−1 shows some indicative concentration set-points of different pollutant types.

3.2.1. Stability of aerosol experiments

During an aerosol atmosphere experiment, the chamber was first allowed to reach the target concentration (in about 2 h), then the experiment was continued for another 3 h to evaluate chamber's ability to maintain the stable concentration. Stability is evaluated by estimating the relative percentage of standard deviation (% RSD) based on the measured concentration variations at each steady-state. All experiments were carried at 20 °C and 40%.As shown in Fig. 3 (a), five target aerosol concentrations, from "very low" to "very high" were generated by the ultrafine/fine particle generator. The steady-state concentrations were reached within 2 h, and were measured to be 6.4, 25.7, 36.4, 125.7, and 229.7 μg/m^3. Stability, expressed by one SD of the concentration variations during the steady-state, was found to be 0.2, 0.5, 0.5, 3.2 and 4.3 μg/m^3 for the five concentration mentioned above, respectively. Larger variations were observed at higher pollutant concentrations. The % relative SDs were between 1.4% and 3.1% over the entire duration of steady-state for each experiment (last 3 h), suggesting that the chamber is capable of maintaining excellent stability over a wide concentration range. To achieve steady-state conditions, the rate of aerosol injection in the chamber must equal the rate of the amount of aerosol removed from the chamber. The observed stability is achieved mainly due to i) the particle generator's ability to provide precise and consistent amount of aerosol during each injection ii) efficient particle mixing inside the chamber using a set of two fans installed on the back wall of the outer chamber that ensure a homogenous and uniform environment. The FEM GRIMM reference dust monitor sampled at a constant flowrate of 5 L/min.

Particle decay and settling was also investigated. An aerosol decay experiment, described in the Supporting Information, showed that the particle decay process in the chamber tracked well with the first order kinetics, which was also consistent with previous study (Cocker et al., 2001). The modelled decay process has a reaction rate constant of 0.004 min^{-1} and a half-life of 173 min (shown in Figure S-6). In addition, the mixing fan speed had an effect on the ultimate particle concentrations, mainly on the portion lost onto the chamber wall. Intuitively, the higher the fan speed, the higher the chance of a particle hitting the chamber walls,

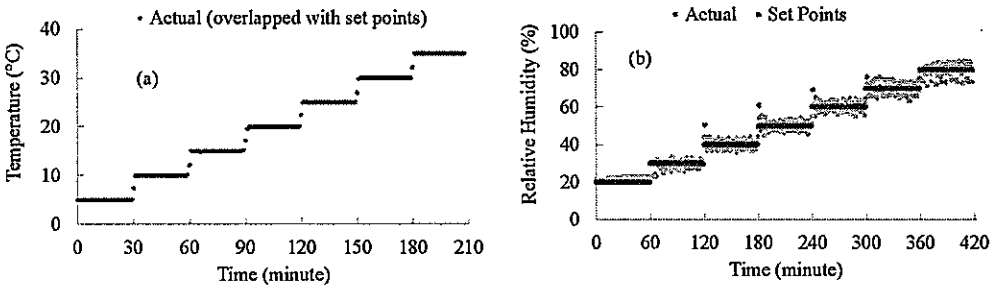

Fig. 2. Chamber's response with (a) 5 °C increment temperature ramping (at constant 40% RH); (b) 10% increment RH ramping (at constant 20 °C).

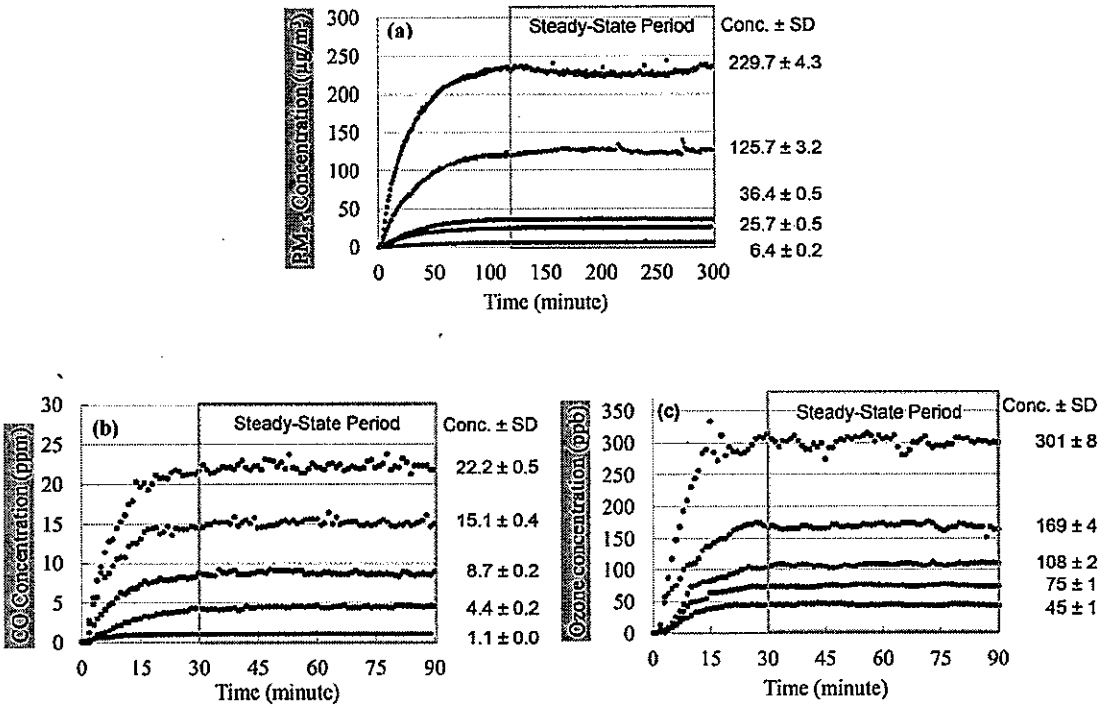

Fig. 3. (a) Stability of various particle concentration levels, (b–c) Stability of various gaseous concentration levels.

and the lower the eventual test aerosol mass concentration. Figure S-7 shows the distinct decrease in aerosol concentration as the mixing fan frequency increased from 20 to 40 Hz, and from 40 to 60 Hz resulting into a higher speed and a distortion in the uniform mixing of particles inside the chamber. Thus, the mixing fan speed was kept at a constant frequency of 25 Hz in all experiments.

3.2.2. Stability of gas experiments

To evaluate the stability of the gas atmospheres, experiments with CO and O_3 were conducted in the inner chamber. The chamber was allowed to ramp up to the target concentration (in about 30 min), then the experiment was continued for another 60 min. For CO, the steady-state concentrations were reached in about 30 min. At the "very low" target concentration of 1 ppm, the variation at steady-state was negligible. At the highest target concentration of 22.2 ppm, the variation was 0.5 ppm, or 2.3% RSD. For O_3, despite of its reactive nature, the system maintained stable O_3 concentrations at all levels, ranging from 45 to 301 ppb. The variation at the 45 ppb target concentration was only 1 ppb, while the variation at the 301 ppb target concentration was only 8 ppb, which represented 2.2% and 2.7% RSD, respectively. Previous calibration study of CO, NO, and NO_2 sensors in an acrylic glass chamber also showed relatively stable gas concentrations over a 1 h period (Mead et al., 2013). Similar to the aerosol atmosphere, the gas atmosphere steady-state condition in the chamber was achieved by balancing the input and output of the pollutant gas. Certified gas and "zero-air" dilution flow were regulated by a mass flow controller. As shown in Fig. 3 (b) and (c), regardless of the reactivity of the gas pollutant, the chamber system was able to maintain a stable gas concentration needed for sensor evaluation.

3.3. Reproducibility of stable aerosol and gaseous atmospheres

As discussed in the previous sections, the temperature and relative humidity can be accurately controlled over a wide range (Section 3.1). The chamber is capable of maintaining stable aerosol and gaseous atmospheres (Section 3.2). To compare different types of sensors, each characteristic parameter needs to be evaluated under similar testing atmospheres. The chamber system is expected to generate similar pollutant concentrations in repeated experiments. Therefore, following stability tests, the reproducibility of chamber performance was demonstrated in several experiments.

3.3.1. Reproducibility of aerosol experiments

For aerosol atmosphere, the reproducibility of experiments were evaluated for low, medium, and high PM concentrations (relative to U.S. EPA NAAQS). For each concentration, three repeated runs were used to determine the reproducibility of the chamber system. As shown in Fig. 4 (a), the average pollutant concentrations from three repeated experiments were plotted. At the steady-state stage, error bars (one SD of three concentrations reported in the repeated experiments) were used to represent the variation in pollutant concentrations among the three experiments. At low PM level, the steady-state concentrations for three repeated runs were 15.9, 15.8, and 19.6 μg/m^3, respectively. It represented 12.6% variation (calculated using one SD divided by average concentration of three repeated runs) of the average value at low concentration. At medium PM level, the steady-state concentrations for the runs were 36.4, 41.4, and 44.6 μg/m^3, which represented 10.0% variation. At high PM level, the steady-state concentrations for the runs were 229.2, 219.3, and 233.6 μg/m^3, and the variation was only 3.2%. Considering the large volume of the chamber, the system demonstrated the ability of generating highly reproducible PM concentrations.

3.3.2. Reproducibility of gas experiments

To evaluate the chamber's ability to generate reproducible gaseous atmospheres, experiments in the inner chamber were run using an unreactive gas CO and a reactive gas O_3. Similar to the

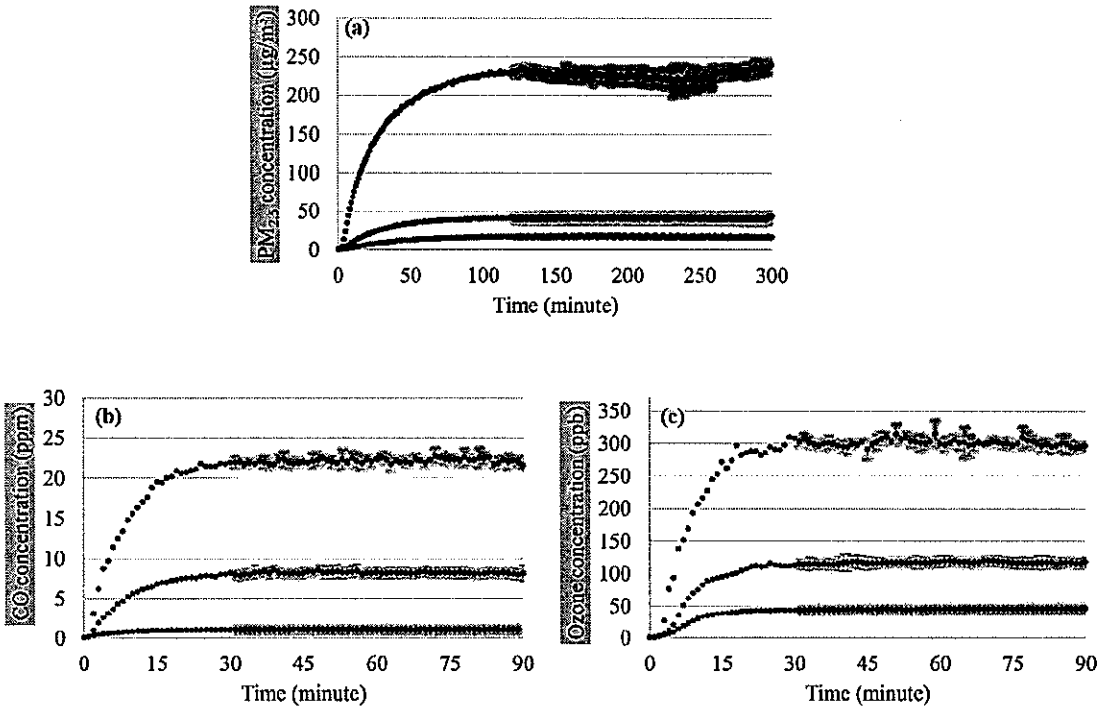

Fig. 4. (a) Reproducibility of various particle concentration levels, (b–c) Reproducibility of various gaseous concentration levels.

aerosol experiments, representative concentrations at low, medium, and high pollutant levels were tested.

The CO concentration reproducibility was tested at 1, 8, and 22 ppm, showed in Fig. 4 (a). For each concentration, the variation between three runs was under 7.5%. The O_3 concentrations reproducibility was tested at 45, 120, and 300 ppb, showed in Fig. 4 (b). For each concentration, the variation between three runs was under 7.0%.

In summary, our results indicate that the chamber system has excellent reproducibility in creating similar conditions. It is suitable for evaluating air quality sensors of different types, as they can be compared against each other.

3.4. Laboratory sensor evaluation and testing design

The laboratory testing procedures are described in AQ-SPEC's Laboratory Evaluation of Low-Cost Air Quality Sensors – Laboratory Setup and Testing Protocol (Polidori et al., 2016). In general, the laboratory testing consists of two phases: (I) concentration ramping at average ambient conditions; (II) sensor climate susceptibility evaluation. In Phase I, the chamber is first conditioned to 20 °C and 40% RH, and a concentration ramping experiment begins. A total of 5 concentration steps are selected to simulate a diverse pollutant concentration profile from "very low" to "very high" (relative to the U.S. EPA NAAQS). Every concentration step change occurs only after a stable pollutant concentration has been reached in the chamber and a sufficient time is allowed in the steady-state period. Each step is held for 150 min during an aerosol test and 40 min during a gas test. Sample experiments are presented in Fig. 5. Data is analyzed to quantitatively evaluate sensor's accuracy, lower detection limit, and linear correlation coefficient. In Phase II, pollutant concentration, temperature and RH are each varied at three different levels (low, medium, and high) for a total of 27 different combinations. Specifically, low, medium, and high pollutant concentrations are selected based on Tables S–1. Temperature is varied between low (5 °C), medium (20 °C), and high (35 °C). RH is varied between low (15%), medium (40%), and high (65%). A complete list of the conditions used is listed in the Supplemental Information. Data acquired from this phase are used to derive information on sensor's climate susceptibility and precision. For gaseous sensors, the effect of interferents is also examined. Depending on the sensor's target pollutant type and its detecting technology, the interferents and their concentrations are chosen as recommended by 40 CFR Part 53 Table B-320 or from information provided in other studies (Austin et al., 2006; Mead et al., 2013). For example, for an electrochemical ozone sensor, NO_2 and sulfur dioxide (SO_2) are considered interferents, and sensor's response towards either of these compounds is investigated separately.

4. Conclusion

This state-of-the-art laboratory chamber is the first of its kind designed and developed to systematically evaluate the performance of commercially available air quality sensors. A series of experiments were conducted to demonstrate the system's capability of generating stable and reproducible aerosol and gaseous atmospheres, as well as its capability of simulating a wide range of temperature (T) and relative humidity (RH) conditions. An environmental chamber system of this type is capable of engaging in comprehensive characterizations, validations and calibrations of air quality sensors. Preliminary testing results have shown important information regarding sensor accuracy, precision, detection limit, correlation coefficient, interferents, and climate susceptibility. Information from both the field and laboratory testing should be taken into consideration to better understand sensor performance under baseline, ambient, and extreme T/RH conditions and pollutant levels.

Institutions and organizations interested in evaluating the performance of low cost air quality sensors should work together to develop standardized field and laboratory testing procedures. This

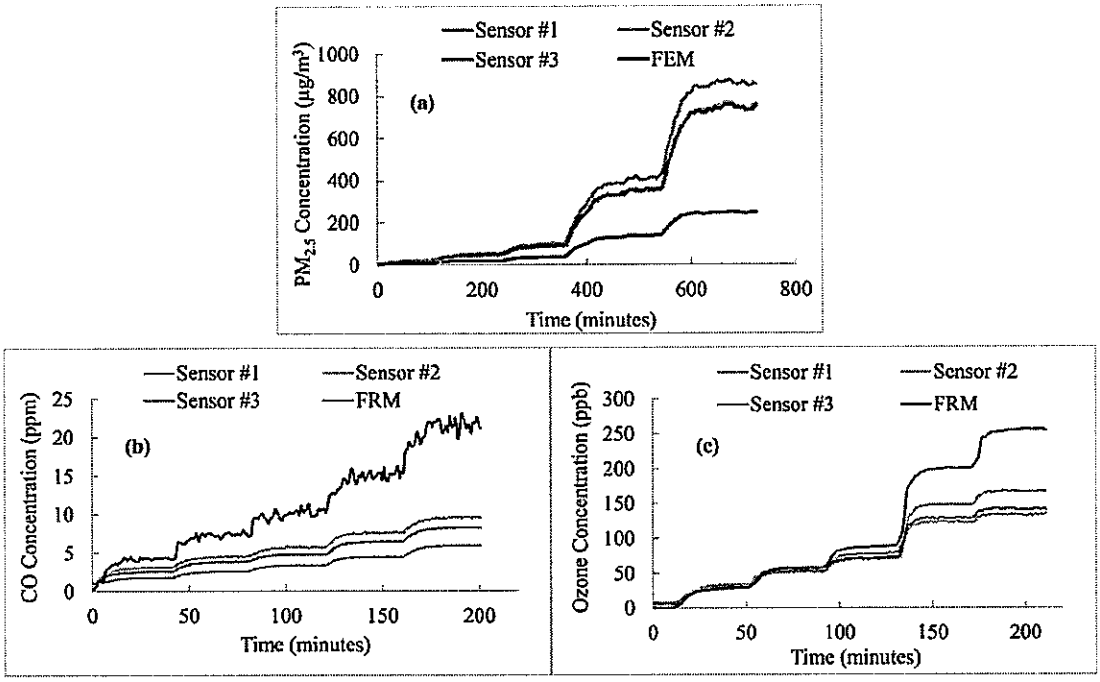

Fig. 5. Examples of sensor evaluation experiments: (a) aerosol, (b) CO, and (c) O_3 atmospheres.

paper provides other researchers with a well proven method to fully characterize the performance of different sensor types. Low-cost sensors can already be used for augmenting ambient air monitoring networks, community based monitoring, screening for hot spots, science education, and qualitative personal monitoring. Thus, it is important for the scientific community to fully understand the capabilities and limitations of this emerging technology.

Disclaimer

Mention of trade names or commercial products does not constitute endorsement or recommendation for use. Potential consumers are welcome to review the completed field and laboratory evaluation reports at www.aqmd.gov/aq-spec.

Acknowledgements

This work in the AQ-SPEC program was supported by internal funds of the South Coast Air Quality Management District. A detailed description of the AQ-SPEC program is included in the Supporting Information. The authors would like to thank AmbiLabs for the collaborative effort in developing and integrating chamber hardware and software components.

Appendix A. Supplementary data

Supplementary data related to this article can be found at https://doi.org/10.1016/j.atmosenv.2017.10.003.

References

Austin, C.C., Roberge, B., Goyer, N., 2006. Cross-sensitivities of electrochemical detectors used to monitor worker exposures to airborne contaminants: false positive responses in the absence of target analytes. J. Environ. Monit. 8, 161–166.

Austin, E., Novosselov, I., Seto, E., Yost, M.G., 2015. Laboratory evaluation of the Shinyei PPD42NS low-cost particulate matter sensor. PLoS One 10, e0137789.

Chakrabarti, B., Fine, P.M., Delfino, R., Sioutas, C., 2004. Performance evaluation of the active-flow personal DataRAM $PM_{2.5}$ mass monitor (Thermo Anderson pDR-1200) designed for continuous personal exposure measurements. Atmos. Environ. 38, 3329–3340.

Cocker, D.R., Flagan, R.C., Seinfeld, J.H., 2001. State-of-the-art chamber facility for studying atmospheric aerosol chemistry. Environ. Sci. Technol. 35, 2594–2601.

Deville Cavellin, L., Weichenthal, S., Tack, R., Ragettli, M.S., Smargiassi, A., Hatzopoulou, M., 2016. Investigating the use of portable air pollution sensors to capture the spatial variability of traffic-related air pollution. Environ. Sci. Technol. 50, 313–320.

EPA, 2014. Fiscal Year 2014-2018 EPA Strategic Plan (Washington D.C).

Fischer, S.L., Koshland, C.P., 2007. Field Performance of a Nephelometer in Rural Kitchens: Effects of High Humidity Excursions and Correlations to Gravimetric Analyses.

Hagler, G.S.W., Thoma, E.D., Baldauf, R.W., 2010. High-resolution mobile monitoring of carbon monoxide and ultrafine particle concentrations in a near-road environment. J. Air & Waste Manag. Assoc. 60, 328–336.

Heck, J.E., Wu, J., Lombardi, C., Qiu, J., Meyers, T.J., Wilhelm, M., et al., 2013. Childhood cancer and traffic-related air pollution exposure in pregnancy and early life. Environ. Health Perspect. 121, 1385–1391.

Jiao, W., Hagler, G.S.W., Williams, R.W., Sharpe, R.N., Weinstock, L., Rice, J., 2015. Field assessment of the village green project: an autonomous community air quality monitoring system. Environ. Sci. Technol. 49, 6085–6092.

Mead, M.I., Popoola, O.A.M., Stewart, G.B., Landshoff, P., Calleja, M., Hayes, M., et al., 2013. The use of electrochemical sensors for monitoring urban air quality in low-cost, high-density networks. Atmos. Environ. 70, 186–203.

Northcross, A.L., Edwards, R.J., Johnson, M.A., Wang, Z.-M., Zhu, K., Allen, T., et al., 2013. A low-cost particle counter as a realtime fine-particle mass monitor. Environ. Sci. Process. Impacts 15, 433–439.

Papapostolou, V., Lawrence, J.E., Ferguson, S.T., Wolfson, J.M., Diaz, E.A., Godleski, J.J., et al., 2013. Development and characterization of an exposure generation system to investigate the health effects of particles from fresh and aged traffic emissions. Air Qual. Atmos. Health 6, 419–429.

Pikelnaya, O., Flynn, J.H., Tsai, C., Stutz, J., 2013. Imaging doas detection of primary formaldehyde and sulfur dioxide emissions from petrochemical flares. J. Geophys. Res. Atmos. 118, 8716–8728.

Polidori, A., Papapostolou, V., Zhang, H., 2016. Laboratory Evaluation of Low-cost Air Quality Sensors - Laboratory Setup and Testing Protocol (Diamond Bar, CA).

Snyder, E.G., Watkins, T.H., Solomon, P.A., Thoma, E.D., Williams, R.W., Hagler, G.S.W., et al., 2013. The changing paradigm of air pollution monitoring. Environ. Sci. Technol. 47, 11369–11377.

Sohn, J.H., Atzeni, M., Zeller, L., Pioggia, G., 2008. Characterisation of humidity dependence of a metal oxide semiconductor sensor array using partial least squares. Sensors Actuators B Chem. 131, 230–235.

Sousan, S., Koehler, K., Hallett, L., Peters, T.M., 2016a. Evaluation of the alphasense optical particle counter (OPC-N2) and the grimm portable aerosol spectrometer (PAS-1.108). Aerosol. Sci. Technol. 50, 1352–1365.

Sousan, S., Koehler, K., Thomas, G., Park, J.H., Hillman, M., Halterman, A., et al.,

2016b. Inter-comparison of low-cost sensors for measuring the mass concentration of occupational aerosols. Aerosol. Sci. Technol. 50, 462–473.
Spinelle, L., Aleixandre, M., Gerboles, M., 2013. Protocol of Evaluation and Calibration of Low-cost Gas Sensors for the Monitoring of Air Pollution (Luxembourg).
Spinelle, L., Gerboles, M., Aleixandre, M., 2014. Report of Laboratory and In-situ Validation of Micro-sensor for Monitoring Ambient Air: Ozone Micro-sensor Alphasense. model B4–O3 sensor.
Van den Bossche, J., Peters, J., Verwaeren, J., Botteldooren, D., Theunis, J., De Baets, B., 2015. Mobile monitoring for mapping spatial variation in urban air quality: development and validation of a methodology based on an extensive dataset. Atmos. Environ. 105, 148–161.
Wang, C., Yin, L., Zhang, L., Xiang, D., Gao, R., 2010. Metal oxide gas sensors: sensitivity and influencing factors. Sensors 10, 2088–2106.
Wang, Y., Li, J., Jing, H., Zhang, Q., Jiang, J., Biswas, P., 2015. Laboratory evaluation and calibration of three low-cost particle sensors for particulate matter measurement. Aerosol. Sci. Technol. 49, 1063–1077.
Wei, W., Howard-Reed, C., Persily, A., Zhang, Y., 2013. Standard formaldehyde source for chamber testing of material emissions: model development, experimental evaluation, and impacts of environmental factors. Environ. Sci. Technol. 47, 7848–7854.
Weichenthal, S., Kulka, R., Dubeau, A., Martin, C., Wang, D., Dales, R., 2011. Traffic-related air pollution and acute changes in heart rate variability and respiratory function in urban cyclists. Environ. Health Perspect. 119, 1373–1378.
Williams, R., Long, R., Beaver, M., 2014. Sensor Evaluation Report.
Williams, R., Kaufman, A., Garvey, S., 2015. Next Generation Air Monitor (NGAM) VOC Sensor Evaluation Report.
Zhao, Y., Wang, F., Zhao, J., 2015. Size-resolved ultrafine particle deposition and brownian coagulation from gasoline vehicle exhaust in an environmental test chamber. Environ. Sci. Technol. 49, 12153–12160.

Atmospheric Environment 70 (2013) 186–203

Contents lists available at SciVerse ScienceDirect

Atmospheric Environment

journal homepage: www.elsevier.com/locate/atmosenv

The use of electrochemical sensors for monitoring urban air quality in low-cost, high-density networks

M.I. Mead [a,*], O.A.M. Popoola [a], G.B. Stewart [a], P. Landshoff [c], M. Calleja [d], M. Hayes [b], J.J. Baldovi [a], M.W. McLeod [a], T.F. Hodgson [a], J. Dicks [e], A. Lewis [e], J. Cohen [f], R. Baron [g], J.R. Saffell [g], R.L. Jones [a,*]

[a] University Chemical Laboratory, University of Cambridge, Lensfield Road, Cambridge CB2 1EW, UK
[b] Cambridge eScience Centre, Cavendish Laboratory, J.J. Thomson Avenue, Cambridge CB3 0HE, UK
[c] Centre for Mathematical Sciences, University of Cambridge, Wilberforce Road, Cambridge CB3 0WA, UK
[d] University Computing Service, University of Cambridge, New Museums Site, Pembroke Street, Cambridge CB2 3QH, UK
[e] Environmental Services, Cambridge City Council, Mandela House, Cambridge CB2 1BY, UK
[f] Centre for Transport Studies, Imperial College London, Imperial College Road, London SW7 2BU, UK
[g] Alphasense Ltd, Sensor Technology House, 300 Avenue West, Skyline 120, Great Notley, Essex CM77 7AA, UK

HIGHLIGHTS

- Suitably configured electrochemical sensors can be used for air quality studies.
- Evidence of performance of electrochemical sensors at parts-per-billion levels.
- Sensors are sensitive, low noise, highly linear and generally highly selective.
- Measurement density (space and time) unachievable using current methods.
- Show low-cost air quality sensor networks are now feasible for widespread use.

ARTICLE INFO

Article history:
Received 14 August 2012
Received in revised form
12 November 2012
Accepted 16 November 2012

Keywords:
Urban air quality
Real-time measurements
Sensor networks
Air quality
Carbon monoxide (CO)
Nitric oxide (NO)
Nitrogen dioxide (NO_2)
Nitrogen oxides (NO_x)
Electrochemical sensors

ABSTRACT

Measurements at appropriate spatial and temporal scales are essential for understanding and monitoring spatially heterogeneous environments with complex and highly variable emission sources, such as in urban areas. However, the costs and complexity of conventional air quality measurement methods means that measurement networks are generally extremely sparse. In this paper we show that miniature, low-cost electrochemical gas sensors, traditionally used for sensing at parts-per-million (ppm) mixing ratios can, when suitably configured and operated, be used for parts-per-billion (ppb) level studies for gases relevant to urban air quality. Sensor nodes, in this case consisting of multiple individual electrochemical sensors, can be low-cost and highly portable, thus allowing the deployment of scalable high-density air quality sensor networks at fine spatial and temporal scales, and in both static and mobile configurations.

In this paper we provide evidence for the performance of electrochemical sensors at the parts-per-billion level, and then outline results obtained from deployments of networks of sensor nodes in both an autonomous, high-density, static network in the wider Cambridge (UK) area, and as mobile networks for quantification of personal exposure. Examples are presented of measurements obtained with both highly portable devices held by pedestrians and cyclists, and static devices attached to street furniture. The widely varying mixing ratios reported by this study confirm that the urban environment cannot be fully characterised using sparse, static networks, and that measurement networks with higher resolution (both spatially and temporally) are required to quantify air quality at the scales which are present in the urban environment. We conclude that the instruments described here, and the low-cost/high-density measurement philosophy which underpins it, have the potential to provide a far more complete assessment of the high-granularity air quality structure generally observed in the urban environment, and could ultimately be used for quantification of human exposure as well as for monitoring and legislative purposes.

* Corresponding authors.
E-mail address: mim25@cam.ac.uk (M.I. Mead).

1352-2310/$ – see front matter © 2012 Elsevier Ltd. All rights reserved.
http://dx.doi.org/10.1016/j.atmosenv.2012.11.060

1. Introduction

1.1. Air quality and human health

Studies have shown that human health and urban air pollution, in the forms of both gas-phase species and particulate matter, are closely linked (e.g. World Health Organisation, 2000). In terms of gas-phase pollutants, nitrogen dioxide (NO_2) is identified as a key species that can affect quality of life and mortality rates (e.g. World Health Organisation, 2006). Both NO_2 and carbon monoxide (CO) are known to be respiratory sensitisers (e.g. McConnell et al., 2010) and both have a proportionally greater effect on those with existing respiratory or cardiovascular conditions (e.g. HEI, 2010). Long-term exposure to NO_2 also adversely affects lung function, whilst CO reduces the body's capacity to transport oxygen, thus affecting cognitive function at lower concentrations and being toxic at elevated concentrations (Lehr, 1970; Abelsohn et al., 2002). While seemingly not of primary importance for direct health impacts, nitric oxide (NO) rapidly interconverts to NO_2 (via reaction with ozone (O_3)) and, through its influence on the tropospheric O_3 budget, affects the oxidising potential of the troposphere. While clearly of obvious significance for health, legislation and atmospheric science, particulate matter is not discussed further here.

1.2. Existing measurement networks

In the UK, the largest network of sensors routinely monitoring gas-phase pollutants is the Automatic Urban and Rural Network (AURN) which is operated by the UK Department for Environment Food and Rural Affairs (Defra), with 132 monitoring sites currently in operation (Defra, 2011). The UK AURN is designed primarily to monitor NO_2, NO_x, CO, O_3, SO_2 and particulate matter (PM_{10} and $PM_{2.5}$).

Monitoring is also routinely undertaken in many parts of the world, including Europe and North America (e.g. the Environment Canada National Air Pollution Surveillance program which has 286 sites (Environment Canada, 2011)). In some areas of the world, however, information on air quality is either highly sparse (tending to be localised around a particular city or institute) or completely non-existent.

The costs of setting up fixed site monitoring stations using traditional technologies can be substantial, with individual instruments costing between £5000 and £60,000, and with significant additional resources required for maintenance and calibration (e.g. Ropkins and Colvile, 2000). Operation of such sites is also constrained by the need for significant infrastructure (secure enclosures, mains power etc.). The consequence is that, while well proven in terms of precision and accuracy of air quality measurements, most existing networks are sparse as higher network densities would be impractical as well as prohibitively expensive. There is, therefore, an urgent need to complement existing air quality monitoring methodologies with flexible and affordable alternatives, to improve monitoring capabilities for both scientific and legislative purposes, to allow source attribution and to improve understanding of health impacts of urban air quality.

Alternatives to existing high-cost sparse fixed-site monitoring stations have been discussed previously by several groups. For example Kamionka et al. (2006) discuss the potential of low cost sensors to increase measurement spatial resolution thereby complementing existing relatively sparse fixed sites. While they argued that measurements needed not necessarily to be at the accuracies or precision possible with traditional in situ instruments, they were not able to demonstrate suitable instrumentation. Low-cost alternatives for use at typical ambient concentrations have been investigated by for example De Vito et al. (2008) and Carotta et al. (2001), however these were primarily based on metal-oxide chemo-resistive sensors, as industrial electrochemical sensors had up to then not been developed with sufficient sensitivity for use in low-ppb regimes. The use of low cost sensors within networks has also been investigated (e.g. Tsujita et al., 2005), albeit with a lower spatial density and sensitivity than those described in this work. Collectively, these works highlight the difficulties in making measurements in the highly spatially variable and complex urban environment. The need for selectivity and stability in sensors for monitoring low concentrations in complex gas mixtures in the urban environment is illustrated in for example Pijolat et al. (1999) and Kamionka et al., with the potential for increasing measurement density in urban centres being also discussed by De Vito et al. (2008, 2009), based on the same sensor methodology as Kamionka et al. Although not discussed in this paper, both De Vito et al., and Tsujita et al., stressed the importance of calibration of urban air quality sensors in the reduction of measurement error, whilst Carotta et al., described the need for careful control of the sensor manufacturing process in ensuring sensor repeatability. This paper builds on elements of this previous work, demonstrating performance of state of the art electrochemical sensors at the parts-per-billion level.

While acknowledging the importance of particulate matter in air quality, this paper focuses on the capability of electrochemical sensors for gas-phase measurements (in this case NO, NO_2 and CO) and the demonstration of sensor networks utilising such techniques. The longer-term ambition is to extend the low-cost, high-density sensor network philosophy not only to other gas-phase species, but also to particulate matter and local micro-meteorology as suitable technologies become available.

2. Electrochemical sensors

2.1. Principle of operation

The electrochemical sensors used for these studies are low-power, robust and low-cost, and are based on widely understood amperometric sensor methodologies designed for sensing selected toxic gases at the parts-per-million-level in the industrial environment. Many detailed descriptions of amperometric sensing methodologies are available in the literature, and so only a brief overview is given here.

Each sensor contains a cell which incorporates three electrodes separated by so-called wetting filters. These filters are hydrophilic separators which enable ionic contact between the electrodes by allowing transport of the electrolyte via capillary action. The electrodes are termed the working, reference and counter electrodes (see Fig. 1). The working electrode is the site for either reduction or

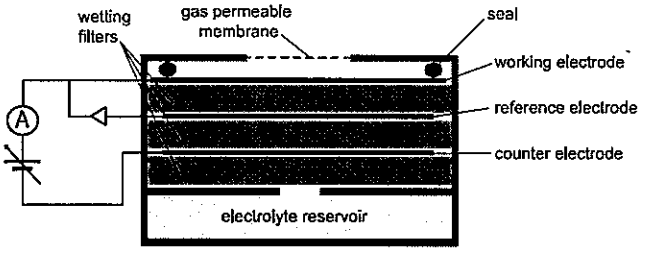

Fig. 1. Schematic of an electrochemical cell of the type used in this study. The gas diffusion barrier is a gas-permeable PTFE membrane used to prevent water and dust ingress to the cell. During operation the working and counter electrodes are maintained with a fixed voltage bias, and the current between them is the output of the sensor.

oxidation of the chosen gas species. It is generally coated with a catalyst selected to provide a high surface area and optimised to promote reaction with the gas-phase species of choice, which for these devices enters the sensor by diffusion. Electronic charge generated by the reaction at the surface of the working electrode is balanced by a reaction at the so-called counter electrode, thereby forming a redox pair of chemical reactions (where one species is reduced and one oxidised i.e. there is a transfer of electrons). Sensors are designed such that the rate of diffusion of the target gas to the sensor electrode is far slower than the rate of reaction of the target gas at the electrode. Consequently, the current output by the sensor is directly proportional to the concentration of the target gas (e.g. Stetter and Li, 2008).

During operation, the working electrode is maintained at a fixed potential while the potential of the counter electrode is allowed to float (i.e. it does not have a fixed potential). In clean (zero) air, the counter electrode has the same potential as the working electrode, but in the presence of the sensed gas, changes potential as it generates a balancing current to compensate for the current generated at the working electrode. The working electrode potential is maintained at a defined value during the operation using a third (internal reference) electrode, which is kept at a constant potential. Exploiting the three-electrode cell design means that the sensor sensitivity is stable thus ensuring sensor linearity over the range of use. The potential difference between the working and counter electrodes then generates an electric current which is the output signal of the sensor. The current generated by these types of electrochemical sensors is typically in the range 10s to 100s of nA per ppm of the sensed gas, and is measured using suitable electronics in a potentiostat configuration. Further extensive descriptions of the methodology and performance of electrochemical sensors can be found in e.g. Bard and Faulkner, 2001.

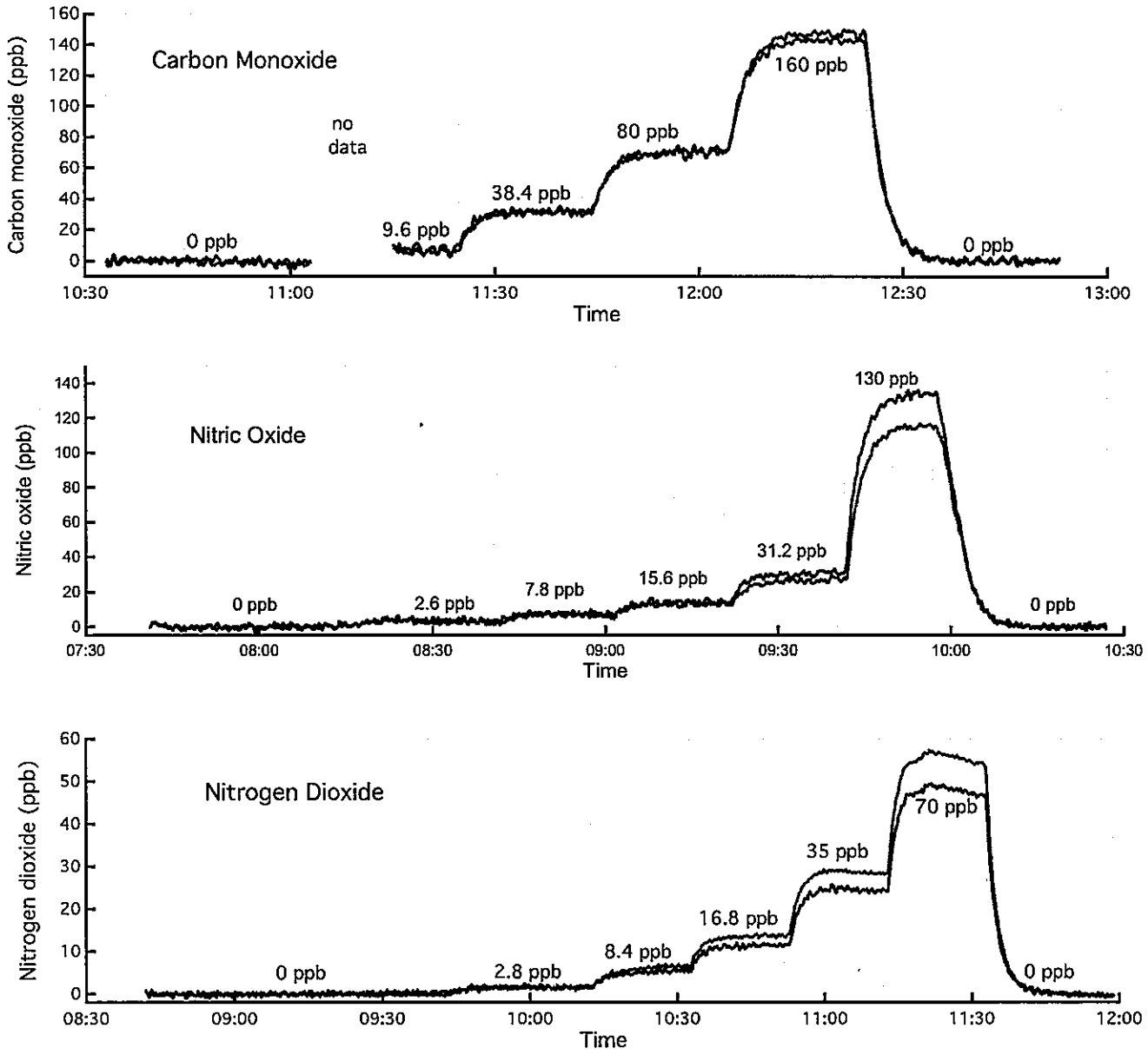

Fig. 2. Examples of responses of pairs of CO, NO and NO_2 sensors to step changes in the respective calibration gases. The sensor calibration parameters used were obtained during the sensor production process at the ppm level (see text). Also shown are the calibration gas mixing ratios at the different stages of the three experiments.

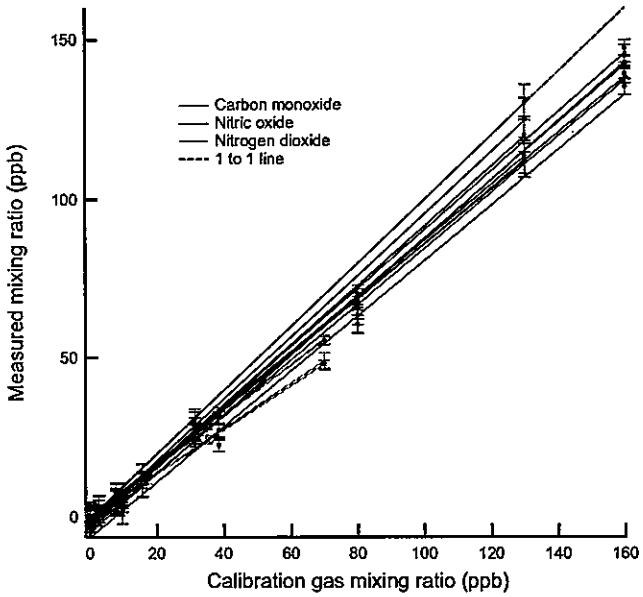

Fig. 3. Correlation plots of mixing ratios of CO, NO and NO_2 (in red, blue and green respectively) measured using electrochemical sensors described above for different calibrated gas mixing ratios. Error bars represent $\pm 1\sigma$. Linear regression lines and fit parameters are shown in each plot. In all cases the regression coefficients were 0.9996 or better; further details are given in the text.

2.2. Sensor performance at ppb levels

The sensors used in this project were variants of the CO-AF, NO_2-A1 and NO-A1 sensors for CO, NO_2 and NO respectively (Alphasense, UK). These variants were optimised for use at ppb mixing ratios by improvements in the sensor signal-to-noise ratio and sensitivity (related to improved techniques for electrode and sensor manufacture as well as careful design of the conditioning circuitry). Laboratory testing of sensor performance at ppb mixing ratios was carried out using gas standards and high-purity zero air (air with impurities removed). The zero air used was generated by taking in external ambient air and removing particles using a particulate filter before passing the air through a catalytic purification system (Whatman zero air generator, Model 76-818, USA). This system was used to provide the large amounts of high-purity zero air needed in the calibration process. To ensure that no artefacts from the zero air generator were present, the air was then passed through a second set of particulate filters before being dehydrated and then stored for subsequent use. Parts-per-billion mixing ratios of the selected gases were generated by blending calibration gases (Air Products Speciality Gases; CO 20.04 ppm (±1%), NO 21.00 ppm (±2%), NO_2 9.94 ppm (±2%)) with the zero air using mass flow controllers. For the purposes of these tests, the calibration (sensitivity) parameters used for the individual sensors were those determined as part of the routine manufacturing process (6–9 months previously), which was carried out at ppm mixing ratios rather than the ppb levels used here.

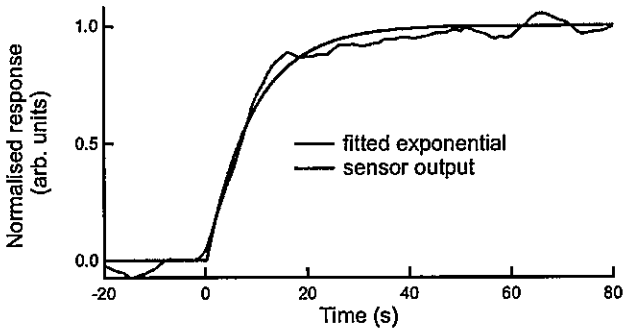

Fig. 5. Response of an NO_2 electrochemical sensor to step changes in target gas concentration. The data (red, grey in-print) are normalised signals obtained at 1 Hz, averaged over several step changes in calibration gas mixing ratio, with the fitted exponential relationship (blue, black in-print).

Calibration gases were injected into a perspex chamber containing a pair of sensor nodes (see Section 3), each measuring CO, NO and NO_2. Typical time series of measured mixing ratios derived using the ppm-level calibration parameters for the sensors are shown for each gas in Fig. 2. In each case a running average of measurements over 30 s is shown, which is derived from 1-s sampling times for CO and NO_2, and 5-s sampling times for NO; the difference is due to different control electronics for the different sensors used in this experiment. Calibration gas mixing ratios were typical of those expected to be present in the urban environment.

As can be seen, there is a close correspondence in the responses of the sensor pairs, although there are differences in absolute values which originate from the use of the ppm-level calibration parameters. It is also clear that there is sensitivity at the ppb level for all three gases.

Correlations between the calibration and measured gas mixing ratios, obtained by averaging appropriate periods of the calibration experiments, are shown in Fig. 3. Mean sensor responses (as fractions of the calibration gas mixing ratio) are 0.90 ± 0.025 for CO, 0.93 ± 0.06 for NO and 0.75 ± 0.06 for NO_2. As noted above, the sensor gains were determined from calibrations at ppm levels obtained during the manufacture process. The origins of the general low biases and the sensor-to-sensor variation in gain are unclear, however, provided there is sufficient long-term stability in sensor characteristics (see Section 2.4); such variations can be readily accounted for during operation. The figure (and in particular

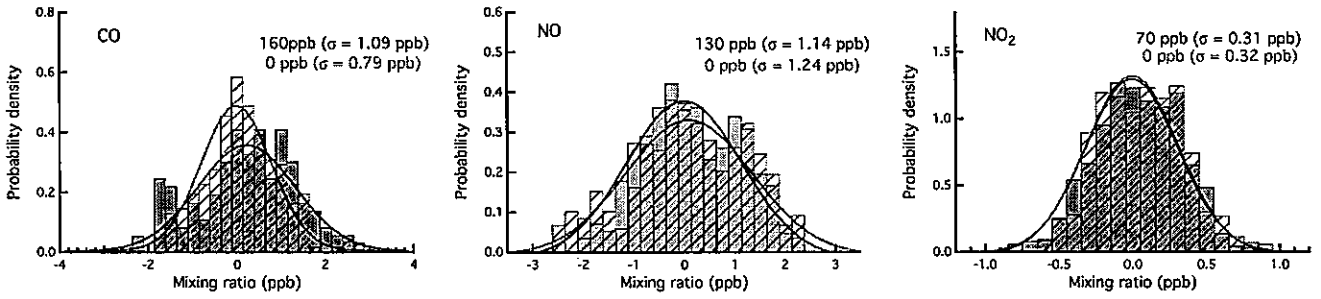

Fig. 4. Probability density plots of the CO, NO and NO_2 sensor responses in clean (zero) air (red) and at concentrations representative of those found in the urban environment (blue), with their respective Gaussian fits. Gas mixing ratios shown in the legends are those of the calibration gases.

Table 1
Cross sensitivities of CO-AF, NO-AF and NO_2-A1 electrochemical sensors to applied concentrations of CO, NO and NO_2 at typical ambient levels. Quoted errors are $\pm 1\sigma$, with the manufacturer's average cross sensitivities, derived from ppm-level measurements, shown in brackets.

Interferent gas	Electrochemical sensor		
	CO	NO	NO_2
CO	–	+0.10 ± 0.08% (0.1%)	−0.02 ± 0.03% (0.1%)
NO	+0.24 ± 0.05% (5%)	–	+1.2 ± 0.11% (0.5%)
NO_2	+0.20 ± 0.08% (0.1%)	+0.45 ± 0.2% (5%)	–

the fact that the regression coefficients are close to unity) confirms both the linearity of the sensors at the ppb level and the excellent noise performance (a combination of intrinsic sensor noise and noise associated with the electronic circuitry).

To illustrate further the intrinsic ppb-equivalent noise for the individual sensor types, probability density functions for CO, NO and NO_2 sensor outputs in zero air, and at mixing ratios representative of the ambient urban environment, are shown in Fig. 4, in all cases under laboratory conditions. The curves shown are derived from single-point data (in this case either 1 Hz or 0.2 Hz operation). The noise-equivalent detection limit of a sensor is defined as $\pm 1\sigma$ under these test conditions. Defining the instrumental detection limit (IDL) as a signal-to-noise ratio of 3, the IDL values (i.e. 3σ) were estimated to be <4 ppb, <4 ppb and <1 ppb for CO, NO and NO_2 sensors respectively, and were found to be largely independent of gas concentration.

The data in Fig. 2 reflect the exchange time for sample gas in the calibration chamber. The chamber volume was approximately 16 L, which, with a flow rate of 5 L min^{-1}, equates to an exchange time (1/e) of approximately 3 min. This corresponds to the response times seen in Fig. 2 of approximately 200–240 s. The intrinsic response time of an individual sensor is considerably shorter than this.

In Fig. 5 is shown the response of an NO_2 electrochemical sensor to step changes in calibration gas mixing ratios, in this case with a gas hood with a minimised dead volume of less than 0.02 L, was placed directly over the sensor. At the flow rates used, the reduced head volume corresponds to a gas exchange time of ~0.2 s, making the measurement effectively one of the sensor response time alone. The 1/e response time from the data in Fig. 5 is 9.16 s, which, neglecting the short chamber-exchange time, gives a sensor t_{90} (time to reach 90% of a step change) of 21 s, in line with the figure quoted by the sensor manufacturer (t_{90} < 40 s for NO_2). This response time is typical of the electrochemical sensors used for the studies described in this paper.

From the information shown above, it can be concluded that, correctly configured the electrochemical sensors respond at the ppb level in a highly linear fashion to the various gases. Instrumental precision is essentially independent of gas concentration but differs for the various gases being sensed. It is also clear that, at least on the basis of the laboratory studies, the intrinsic sensitivity and noise characteristics of the different sensors are compatible with their use in ambient air quality studies. Other sensor characteristics, particularly those arising from their use in the field environment, are discussed below.

2.3. Cross interferences for CO, NO and NO_2 electrochemical sensors

The use of multi-sensor nodes in the calibration process outlined above also enabled the cross interference of the different sensors to CO, NO and NO_2 to be derived directly (see Table 1). While several of the cross interferences are statistically significant, the sensor performances generally exceed the manufacturer's specifications in some cases substantially so. One exception is that of NO on NO_2 where a cross interference of 1.2% is seen. However, such small residual cross interferences can be readily accounted for during data analysis or data post processing.

Electrochemical sensors have other known cross-sensitivities (see for example Austin et al., 2006; Hamann et al., 2007) with, for this application, the most significant being for O_3, which is known to affect the NO_2 sensors used in these studies. Laboratory experiments conducted in conjunction with the sensor manufacturer show that the NO_2 sensors used here have an approximately 100% interference for O_3. This is discussed further in Section 3.3. The CO sensors used here are also known to demonstrate cross-sensitivity to molecular hydrogen which is present in the atmosphere at background mixing ratios of ~500 ppb, but which may also show short-term rises in an urban area due to

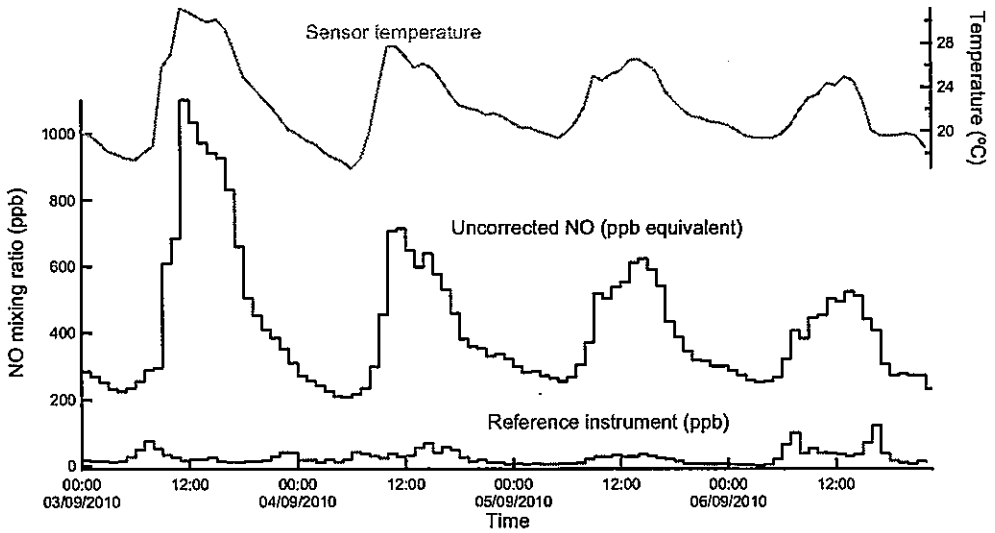

Fig. 6. Hourly averaged NO data from a roadside reference instrument (details) are shown in red (grey in-print) and uncorrected data from a type A1 NO electrochemical cell are shown as ppb equivalent in blue (black in-print). Also shown, in green (dashed in-print), is the instrument temperature. The data in the figure illustrate the importance of temperature effects on the performance of the sensor. See text for further details.

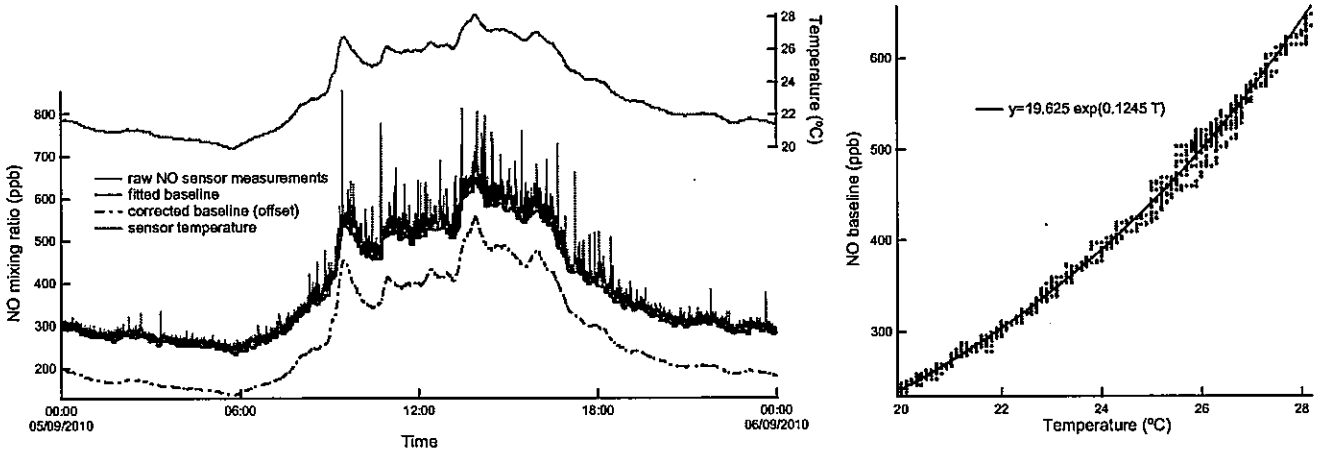

Fig. 7. Correction of baseline temperature effects for a type A1 NO sensor (see text for details) for the 24-h period shown shaded in Fig. 6. The left panel shows raw (0.2 Hz) NO data (red, grey in-print), with spikes associated with individual pollution events superposed on a strong diurnal baseline variation, and the fitted baseline (see text) (blue, black in-print). The right panel shows the exponential relationship between the fitted baseline and instrument temperature (see left panel, green, grey-dashed in-print). The temperature correction derived from this temperature-baseline correction is shown in the left panel (black, dashed line, dotted in-print), and is offset by 100 ppb for clarity.

emissions from transport and industry (Grant et al., 2010). While the high background interference is easily removed in post-processing of data, short-term peaks associated with local H_2 releases may not be correctly accounted for in this study. This approach can, of course, only correct for known interferent species.

2.4. Effects of ambient temperature and relative humidity

Changes in ambient temperature and relative humidity (RH) are known in principle to affect sensitivity and sensor gain to the sample gas and sensor baselines or zero offset (e.g. Hitchman et al., 1997). For measurements at the ppb level, the correction of sensor baselines (bias) for temperature or RH effects dominate with corrections of sensitivity (gain) being second order effects.

Generic data describing the relationship between sensor current response, temperature and relative humidity are available from the sensor manufacturer, allowing the generation of correction factors for these effects. However, while the data supplied by the manufacturer are sufficient for temperature and RH correction at ppm levels or for indoor gas alarm purposes, for sensor use in ambient conditions, where ppb sensitivities are required and where large temperature variations on both diurnal and seasonal timescales are often encountered, more sophisticated temperature correction procedures are required, as is described below in this case for a nitric oxide sensor (NO-A1).

It is clear from the data in Fig. 6 that there is little correspondence, either in absolute magnitude or diurnal pattern, between the NO mixing ratios measured by the reference instrument and the uncorrected electrochemical sensor data. However, it can be seen that there is a general correlation evident between the uncorrected NO electrochemical measurements and the instrument temperature (which broadly tracks ambient temperature), which is in fact due to the sensor baseline temperature dependence.

The temperature and RH correction procedure adopted for long-term data sets shown in this study was as follows: a sensor 'baseline' was defined for each measurement time t by applying a filter which obtained the minimum measurement encountered within a given time interval of $t \pm \delta t$. This process was carried out for a range of values for δt (between 50 and 1750 s) so that the optimal value (that which led to the best fit with temperature) could be

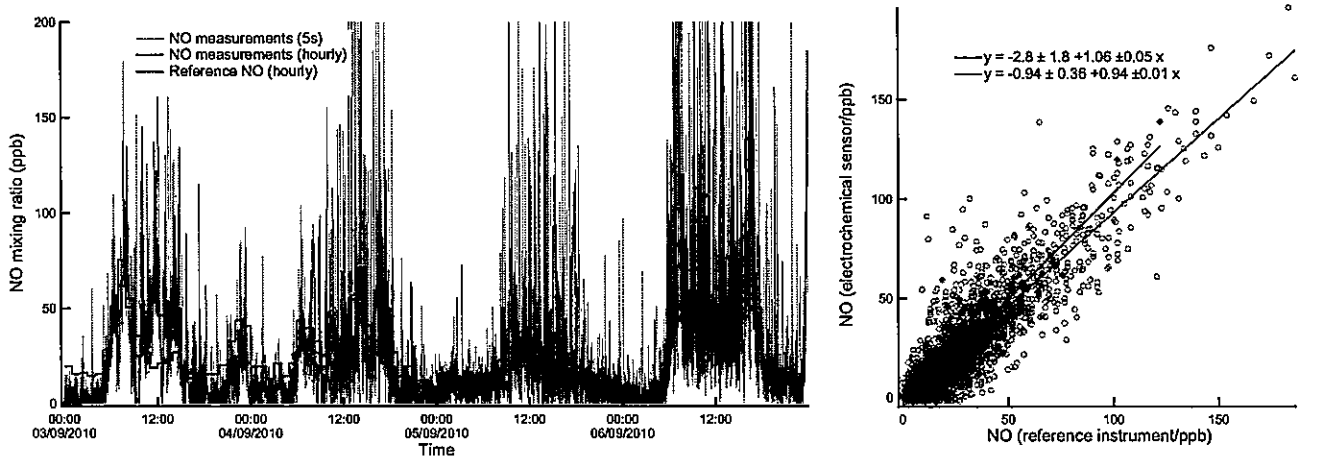

Fig. 8. Time series (left) and correlation plot (right) of hourly mean NO measurements from a ratified chemiluminescence instrument (red) and an electrochemical sensor corrected for temperature baseline effects (blue – hourly averages; green – 0.2 Hz data). Note the much larger variability evident in the 0.2 Hz data (which is truncated at 200 ppb for clarity). The correlation plot shows the hourly data for the period shown in Fig. 7 (blue) and the entire period (red), both showing excellent agreement with the reference instrument (see inset equations).

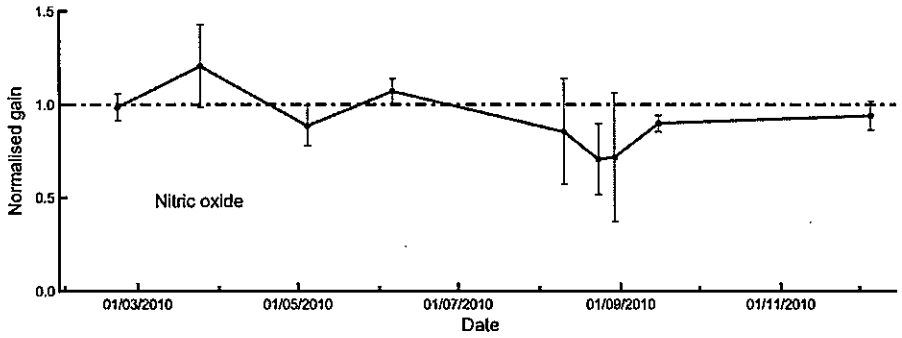

Fig. 9. Time series of sensor gain for 11 months of NO measurements, calculated by comparison to a reference instrument. The drift in sensitivity/gain is 13% ± 13% (1σ), showing that, within the experimental errors, the stability of the sensor has remained unchanged over the 11-month measurement period. Error bars in the figure represent ±3σ of the calculated gains for the different periods.

used to correct each day of data. Application of this filter process produced curves for each sensor type which reproduced the temperature or RH induce sensor baseline variations. This process, applied to the NO sensor shown in Fig. 6, is illustrated in Fig. 7.

During the temperature and humidity correction process, either a linear regression or exponential fit (depending on gas species) is obtained between an extracted baseline and the measured instrument temperature. In general over a 24-h period, atmospheric absolute humidity is found to be approximately constant. Consequently, as relative humidity (RH) changes are therefore largely determined by diurnal temperature changes, the correction process for instrument temperature variations also largely accounts for diurnal changes in RH. The correction process was therefore also adapted to account for absolute (rather than relative) humidity. For the case where the correction factors were linear, temperature and absolute humidity correction constants, corresponding to the baseline change per unit change in temperature (db/dT) and the baseline change per unit change in absolute humidity (db/dH), were derived. This process was repeated for each 24-h period of data. The data in Fig. 8 shows that, following this correction, there is excellent agreement between the NO sensor and a reference instrument. The temperature and humidity correction methodology is described in more detail in a paper in preparation (Popoola et al., in preparation).

2.5. Long-term sensor stability

The long-term stability of NO sensors can be illustrated using the same data which have been partially shown in Figs. 6–8. For each period of data collected over ~11 months, hourly averaged NO data measured by a single electrochemical sensor were compared with that from a ratified reference instrument with which it was co-located, allowing gain parameters for the electrochemical sensor to be derived. Assuming the reference instrument to have no instability itself, the sensor gain is stable to within ±13% (Fig. 9), i.e. not significant within the measured errors.

The data obtained during the 11-month period also permit other potential systematic errors to be evaluated. Table 2 shows correlations of the sensor gain, derived as described above, in this case with various meteorological parameters. As can be seen, after the temperature/RH correction has been applied as indicated above, there is no significant dependence of sensor gain on either parameter. Similarly, there is no significant dependence on atmospheric pressure (which is to be expected as the devices are intrinsically diffusion-limited (Stetter and Li, 2008)), although, intriguingly, there is a small apparent (negative) dependence on wind speed. The origin of the latter is unclear.

From the information shown in this section, it can be concluded that, when configured correctly, the electrochemical sensors discussed above respond in a highly linear fashion to ppb levels of their respective target gases. Detection limits are essentially independent of gas concentration but differ for the various gases being sensed. It is also clear, at least on the basis of the laboratory studies, that the intrinsic sensitivity and noise characteristics of the different sensors are compatible with their use in ambient air quality studies.

There are clear sensor offset (baseline) dependences on temperature and RH, which depend on sensor type. However, we have demonstrated that temperature/humidity effects on sensor baseline can be accounted for by suitable post-processing of data.

The following section is a description of sensor node design, after which results from a variety of field deployments are presented and discussed.

Table 2
Correlations of NO sensor gain with meteorological variables (see text). Errors shown are ±1σ.

Variable	Gain-change dependence
Ambient temperature	$-4.5 \times 10^{-3} \pm 5.2 \times 10^{-3}$/K
Pressure	$-4.4 \times 10^{-3} \pm 9.0 \times 10^{-3}$/hPa
RH	$-1.2 \times 10^{-3} \pm 5.2 \times 10^{-3}$/%RH
Wind speed	-0.12 ± 0.046/m s^{-1}

Table 3
Outline technical specifications for the mobile and static sensor nodes.

		Mobile	Static
Mass	Total	445 g	4260 g
	Excl batteries	333 g	1430 g
Dimensions		183 × 95 × 35 mm	260 × 177 × 135 mm
Power		4 × AA NiMH	Pb-acid batteries 6 V, 8 Ah, monobloc
Data storage		On board	On board
Transmission		GPRS (built in) to web server	GPRS (built in) to web server
PIC		PIC18F67J10, Microchip Technology Inc, USA	PIC18F67J10, Microchip Technology Inc, USA
Firmware		PIC chip (PIC18F67J10) programmed in C	PIC chip (PIC18F67J10) programmed in C
Sensor diameter (mm)		20.2	32.3
Temperature sensor		Pt1000 resistance thermometer	Pt1000 resistance thermometer
RH sensor		N/A	Honeywell 4000 series
GPS unit		Telit GM862-GPS	Telit GM862-GPS
Duration (single charge)		Approx. 14 h, sensing at 5 s intervals, 30 min send.	Approx. 3 months, sensing at 10 s, sending at 2 h intervals.

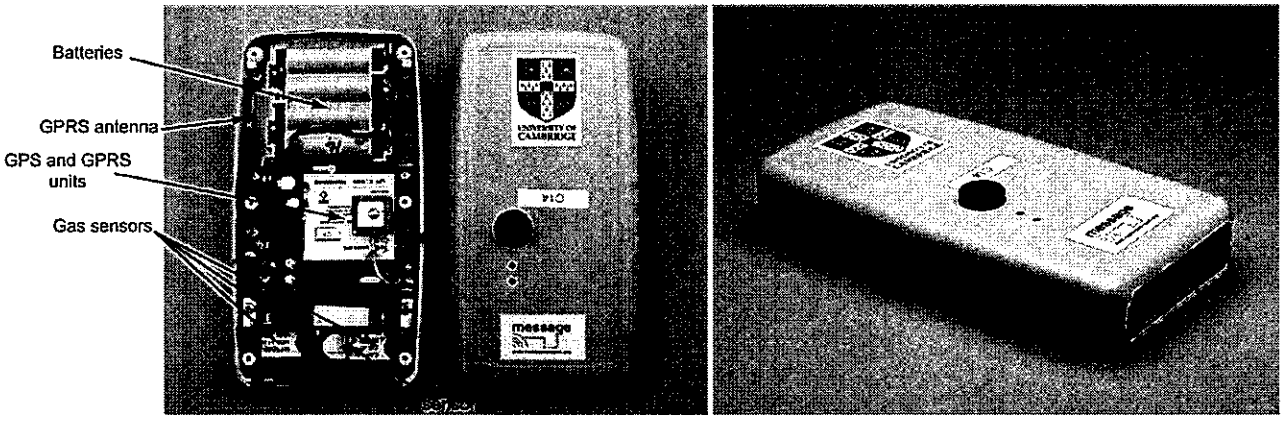

Fig. 10. Mobile sensor unit incorporating three electrochemical sensors (for CO, NO and NO_2 in this case). Various components (GPS/GPRS, batteries etc.) are identified in the left panel. For clarity, the unit is shown without its protective wire mesh, which, during operation, is located in front of the sensors.

3. Field measurements

3.1. Sensor node designs

The sensor nodes which were used in these studies are autonomous units incorporating multiple gas sensors, a GPS receiver and a GPRS transmitter, and have integral batteries allowing convenient deployment. The air quality data collected on the devices are firstly labelled by GPS location and time, and are then either stored in situ or transmitted to a central computer server for post-processing and on- or off-line analysis. Although several variants have been constructed, two basic types of sensor nodes were designed to allow both mobile and static deployments.

The mobile sensor nodes were designed to be highly compact and lightweight (see Table 3), and thus convenient to carry by volunteers. Electrochemical sensors (usually CO, NO and NO_2), along with a temperature sensor, were mounted behind a mesh opening at one end of the unit (see Fig. 10), which contained GPS/GPRS modules and batteries. Each node could be operated independently and autonomously, enabling networks to be scaled according to monitoring requirements. This flexibility allowed studies to be carried out in various types of environment, with minimal overheads relating to network design and infrastructure.

The static nodes developed for longer-term studies incorporated larger sensors, with larger electrolyte reservoirs for increased long-term baseline stability, and larger integral batteries allowing operation for in excess of 3 months without intervention. In this case sensors were sealed with rubber O-rings on the bottom of the enclosure behind a protective aluminium bracket (see Fig. 11) which was also used to mount the unit to lamp posts with suitable bands (see Section 4). Temperature and humidity sensors were mounted behind a gas-permeable, hydrophobic membrane on the side of each sensor node.

The main differences between the two generations of mobile nodes and the static node, along with other technical specifications, are summarised in Table 3.

3.2. Sensor reproducibility

Following the laboratory tests discussed in Section 2.2, a number of experiments to verify sensor performance in the field were carried out under typical urban conditions. One such experiment

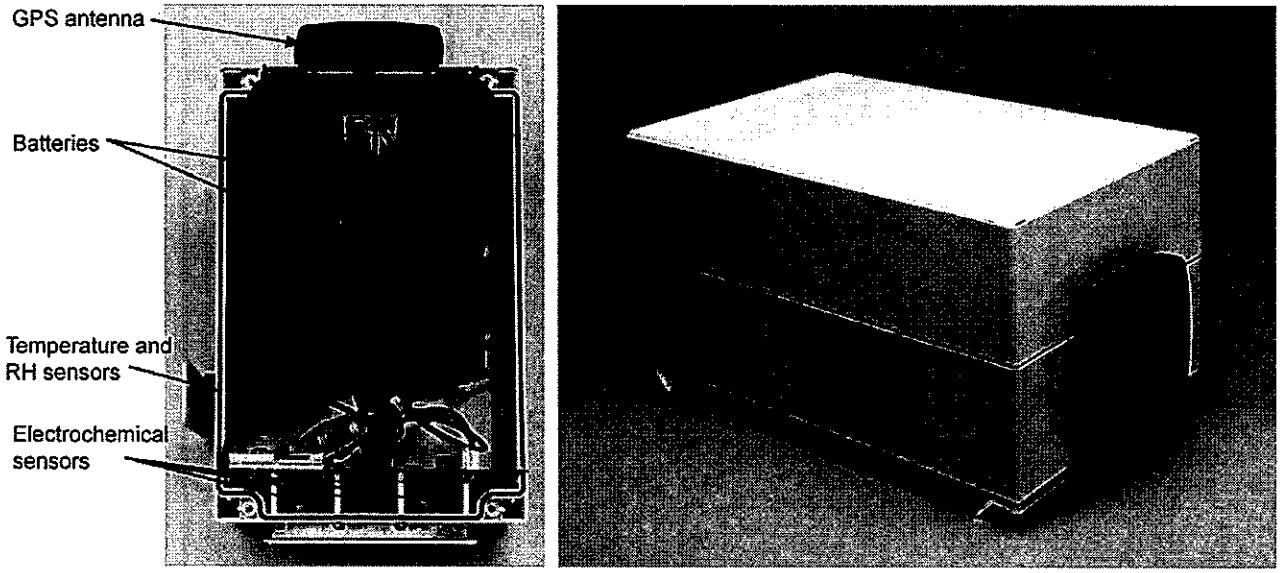

Fig. 11. Static sensor unit (or node) plus mounting baseplate. CO, NO, NO_2, temperature and relative humidity are recorded, along with GPS location and time. A view of the open sensor node is also shown (left).

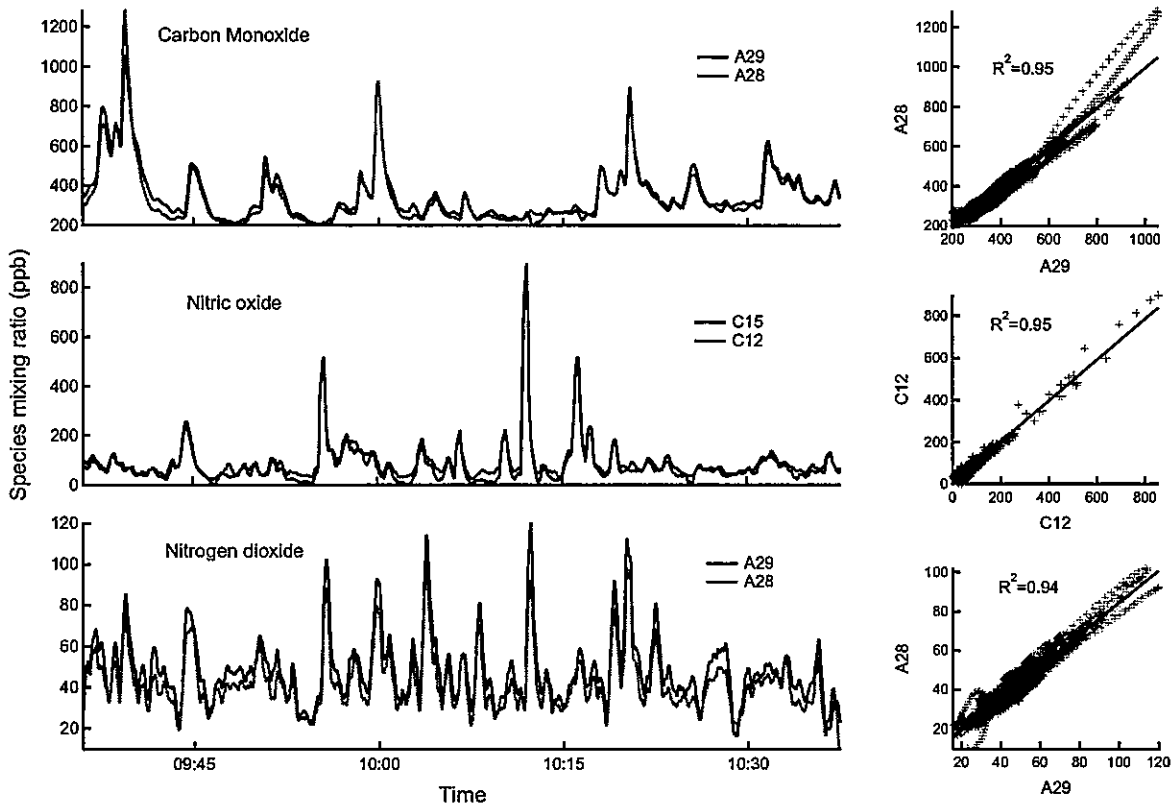

Fig. 12. (Left) Time series plots of CO, NO and NO_2 for sensor pairs co-located for the whole deployment period, and (right) corresponding scatter plots. Data used are a 30-s running average. NO_2 data are not corrected for cross interference with O_3 and the likely maximum bias is 24 ppb (equal to the nearest background AURN O_3 measurement (Wicken Fen, see Section 3.3)).

involved mobile sensor units being carried in pairs (2 pairs of sensors each for CO & NO, and NO_2) to confirm sensor reproducibility. This experiment took place over a one-hour period in central Cambridge (UK), during which two volunteers walked on different routes other than for short periods at the start and end of the experiment.

Fig. 12 shows time series data collected by one pair of sensor nodes co-located for the duration of the experiment. These illustrate the variability in the concentrations of the species measured over small spatial and temporal scales, and confirm that the sensors are responsive at the mixing ratios found in the urban environment. Scatter plots are also shown on the right-hand side, and from these it can be seen that sensor-to-sensor reproducibility is high (R^2 values of 0.95, 0.95 and 0.94 for CO, NO and NO_2 respectively). Performance is not as repeatable as that in Section 2.2 probably due to imperfect co-location of sensor nodes and local mixing effects so that, as a result, one sensor can potentially respond to a brief event slightly differently to its partner. An example of this is shown in the CO time series in Fig. 12, where at approximately 09.39 am there was a sharp, well defined event which was more evident in sensor A28 than its partner, either owing to its orientation (i.e. A28 was potentially nearer the source) or local micro-scale mixing. The R^2 correlation coefficient is biased accordingly; e.g. removal of data until 09.43 yields a slightly improved R^2 value of 0.96 for CO. Table 4 gives mean values of gradients and a range of R^2 values for linear fits generated between electrochemical sensors (two pairs for CO, NO and NO_2) sensors paired for the whole deployment period. These data show how well correlated the sensors are when taking local mixing into account. The Figure and tables were generated from 30-s (for CO and NO_2) and 10-s (for NO) running averages of that collected. Original data were collected at 1 Hz for CO and NO_2 and 0.2 Hz for NO.

Further illustration of the reproducibility of measurements is provided by Fig. 13, which shows some measurements of CO superimposed on a map of the area over which sensors were carried. Measurements by two volunteers along the same route are seen to differ when data are captured at different times (blue and yellow), but show a strong correlation when the volunteers were co-located (red and green).

The capability of the mobile devices is illustrated graphically in Fig. 13, in which three-dimensional plots of CO and NO_2 are superposed on a road map. Where the devices are co-located in both time and space, there is excellent correspondence between sensors (see, for example, Tables 4 and 5). However, when at the same location, but now separated in time by even a few tens of seconds, there is little correspondence in observed mixing ratios. This therefore also illustrates very effectively the importance of measurements at the appropriate spatial scales when considering personal exposure in the urban environment.

Table 4
Slopes and correlation coefficients for linear fitting equations generated for sensor pairs co-located for an hour-long walk in central Cambridge (UK).

Species	Gradient		R^2	
	Pair 1	Pair 2	Pair 1	Pair 2
CO	0.58	0.94	0.86	0.95
NO	0.89	0.91	0.97	0.84
NO_2	1.01	1.15	0.95	0.94

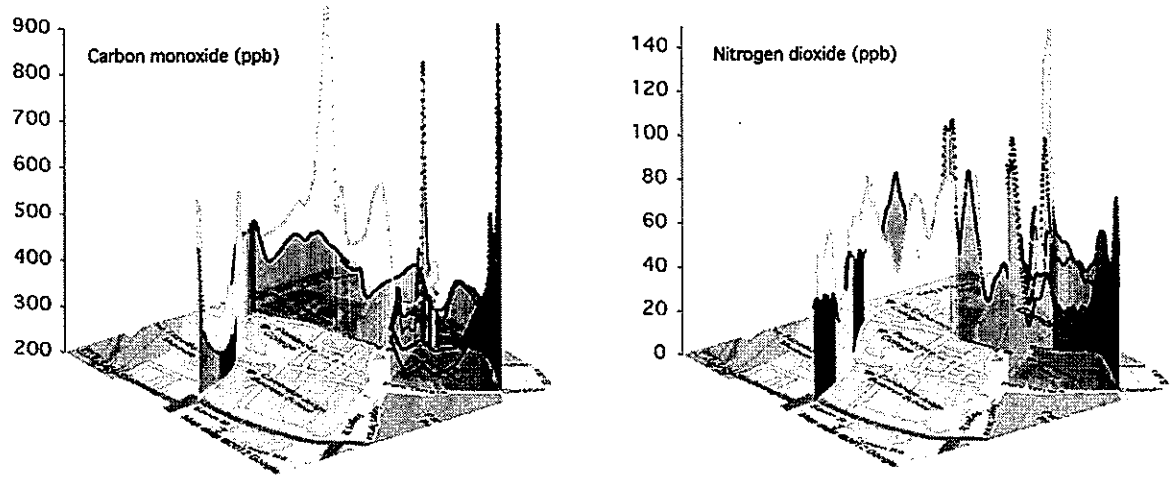

Fig. 13. Selected CO and NO_2 measurements from two sensor nodes in parts of central Cambridge superposed on a road map (map data© 2012 Google). Data from periods during which volunteers walked together are shown in red and green, and those from when they walked apart are shown in yellow and blue. NO_2 data not corrected for interference with O_3 (see Section 3.3).

3.3. Treatment of O_3 cross-interferences for NO_2 electrochemical sensors

Two sensor units (CO, NO, NO_2) were co-located with the Cambridge City Council (CCC) roadside AURN site to compare electrochemical sensor measurements of NO_x with a calibrated reference instrument. The reference instrument (Thermo Environmental Model 42C NO–NO_2–NO_x analyser) was located in the first-floor offices of the CCC building, with an inlet height of 4 m approximately 2.5 m horizontally from the kerbside above a busy urban road. Electrochemical sensors (in this case variants of the mobile nodes) were mounted inside a sealed chamber, through which external air was drawn via an inlet placed alongside that of the CCC instrument. As the sensors were indoors, they were exposed to minimal ambient temperature variations (less than ±0.5 °C). Fig. 14 shows time series data from midnight on the 23rd until 09.00 on the 26th of January for NO for the electrochemical and reference instruments. Similarly, data from NO_2 sensors over the same period are compared with the reference instrument in Fig. 15, before correction for interference with O_3.

Cross interference with O_3 is a significant issue for urban measurements made using the current NO_2 sensors, with cross sensitivity for this generation of sensors known to be 100%, making the data, in effect, a measurement of $[NO_2] + [O_3]$. At this stage there were no electrochemical measurements of O_3 available. However, O_3 measurements were available from the CCC AURN site, and these were therefore used to correct the NO_2 data presented in Fig. 15 as shown in Fig. 16. NO_2 measurements shown in other figures in the paper are not corrected for this effect.

Statistical relationships obtained between the NO and NO_2 electrochemical cell measurements and the reference instrument are shown in Table 5, showing a marked improvement in the agreement for the NO_2 measurements once corrected for the O_3 interference, although there is still a downward bias of ~20%.

Table 5
Statistics obtained from the inter-comparison of ECC NO and NO_2 sensors with reference measurements.

ECC sensor	NO gain	NO R^2	NO_2 gradient (uncorrected)	NO_2 gradient (corrected)	NO_2 R^2
1	0.97 ± 0.04	0.80	0.36 ± 0.02	0.81 ± 0.03	0.89
2	1.00 ± 0.06	0.95	0.38 ± 0.02	0.81 ± 0.03	0.92

The results of this experiment clearly show that the electrochemical sensors used to measure NO and NO_2 agree well with established reference techniques for these species, provided that known cross sensitivities are accounted for, although some biases remain for NO_2. Development work is in progress to develop NO_2 and O_3 electrochemical sensors with greater degrees of discrimination and selectivity, and this will be reported in future papers (Fig. 17).

3.4. Mobile sensor network results

Short-term, mobile sensor deployments can provide a representative picture of the rapidly changing and highly granular air quality in an urban area over a deployment period. However, they should not be expected to accurately represent the local air quality over longer timescales (despite collecting 10^5–10^6 measurements over periods of hours), where influences such as meteorology and source morphology become highly significant.

Despite this limitation, though, the "snap-shots" of pollution levels assembled from the data collected do illustrate the large degree of spatial and temporal variability in the concentrations of pollutant gases in different urban environments. The routine measurements currently made by fixed-site monitoring stations, which have intrinsically low spatial resolution when compared with the scales over which chemistry occurs, do not capture many aspects of real variability in urban air quality, as is illustrated below. A more detailed account of this will be given in a separate publication.

Mobile sensors have been used on numerous occasions across a range of different environments in Cambridge, London, Cranfield (all UK), Valencia (Spain), Kuala Lumpur (Malaysia) and Lagos (Nigeria). The largest-scale mobile sensor network deployment to date was in Cambridge and comprised 35 sensor nodes, of which 20 were mobile and measured CO/NO/NO_2 and temperature. Units were deployed using three transport modes (pedestrians, cyclists and drivers), and were also located alongside Cambridge City Council fixed-site monitoring stations. Spatial coverage extended over a 10 km-by-10 km area, but was weighted towards the heavily trafficked city centre.

Visual inspection of Fig. 18 enables a number of "hotspots" to be identified; these are usually located where traffic density is highest, for example around areas such as the central bus station, on major

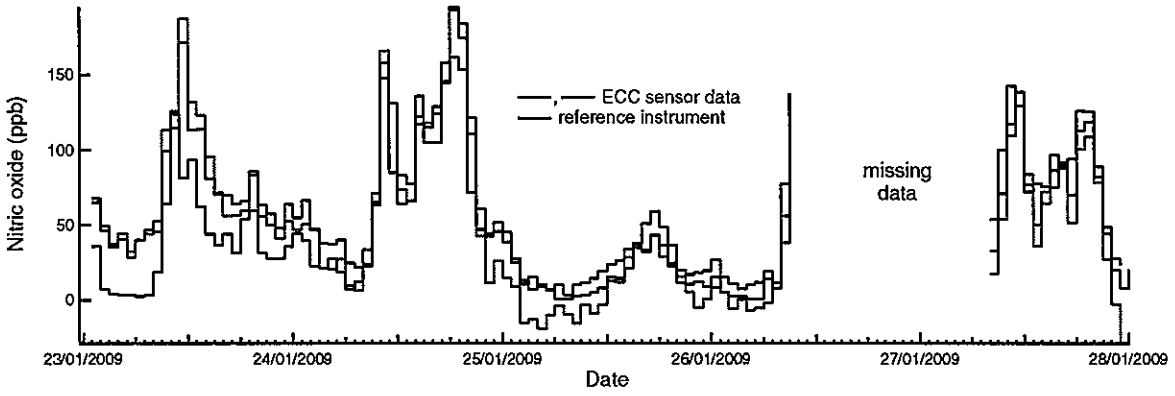

Fig. 14. Time series plot for electrochemical NO sensors co-located with a reference instrument at the CCC AURN site. The plots illustrate good agreement between the two techniques for this species.

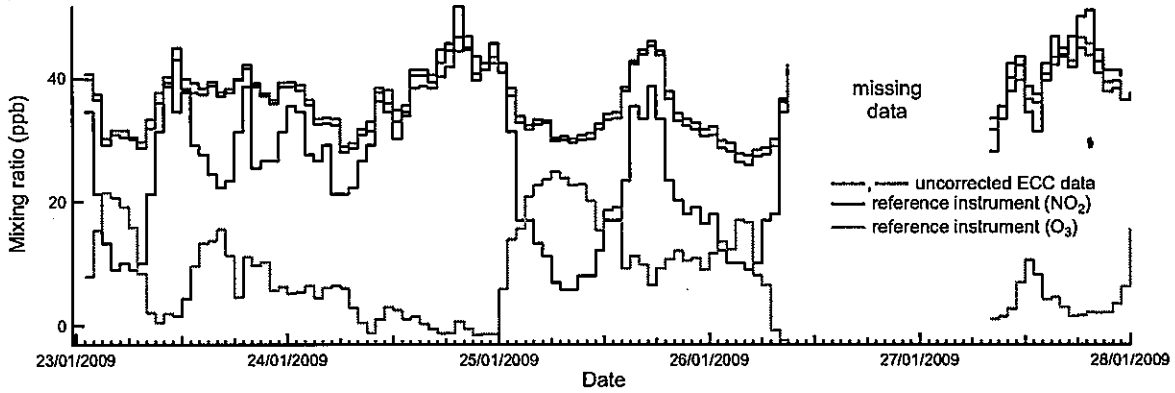

Fig. 15. Hourly averaged time series for the NO_2 sensors from the same study, uncorrected for the O_3 interference (see text). Also shown is the hourly average O_3 mixing ratio from a reference instrument. The two electrochemical sensors show excellent consistency with each other. However, there is a substantial discrepancy between the uncorrected NO_2 data and the reference instrument.

roads around Cambridge (the A14 and M11 specifically) and in areas where traffic is routinely static (e.g. traffic lights). However, as is discussed below, more sophisticated analysis methods allow more subtle exposure features to be extracted from the data. It should be noted, of course, that while this deployment is an important demonstration of the capabilities of the mobile sensor network philosophy, the fact that measurements were obtained over a short period means that specific features may not be representative of the longer-term environment.

3.4.1. *Examples of individual exposure*

As an illustration of individual exposure, data taken from one sensor node carried by a pedestrian in Cambridge at waist height are shown in Fig. 19. The mean mixing ratios calculated for this pedestrian sensor node were 515 ppb, 177 ppb and 68 ppb for CO, NO and NO_2 respectively. CO data were offset assuming a natural background mixing ratio of 200 ppb (in line with the initialisation mixing ratios used by Bright et al. (2011)). While the NO_2 measurements are strictly $[NO_2] + [O_3]$ in this case, as background O_3 is

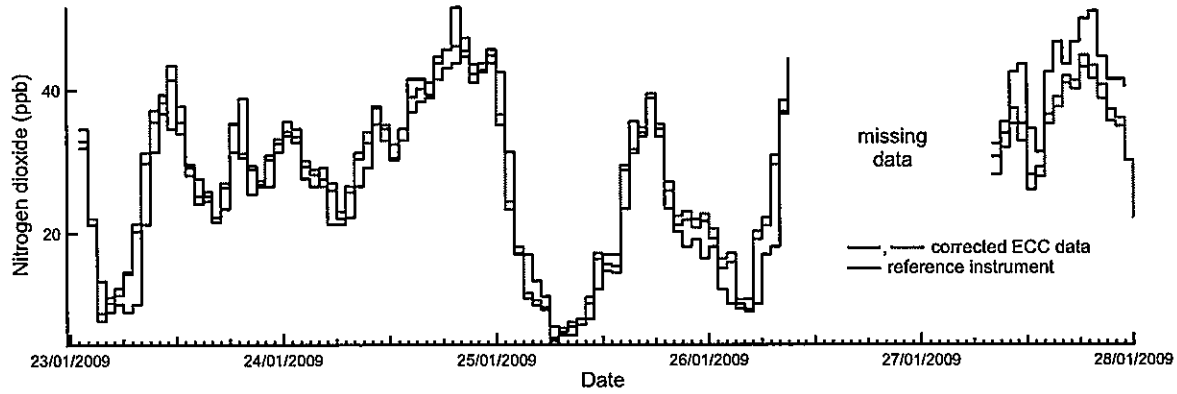

Fig. 16. Time series of NO_2 mixing ratios from a reference instrument and from electrochemical sensors, corrected based on the known O_3 cross interference. Agreement between the techniques, over the same period as Fig. 15, is significantly improved.

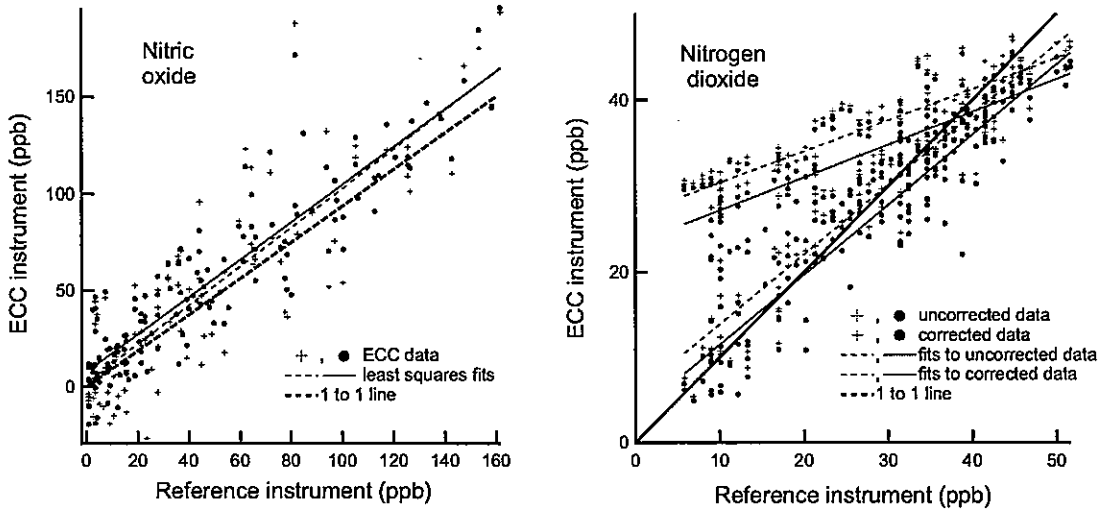

Fig. 17. Comparison of hourly averaged electrochemical measurements of NO and NO_2 (prior to and following correction of the sensors for the O_3 interference) against reference measurements.

Fig. 18. 3D plots (left to right respectively) of CO, NO and NO_2 mixing ratios giving overviews of measurements obtained during a large, mobile sensor deployment. The peak heights correspond to mixing ratio, with maximum values of 7 ppm, 4.5 ppm and 840 ppb for CO, NO and NO_2 respectively (map data© 2012 Google and© 2012 Infoterra Ltd & Bluesky).

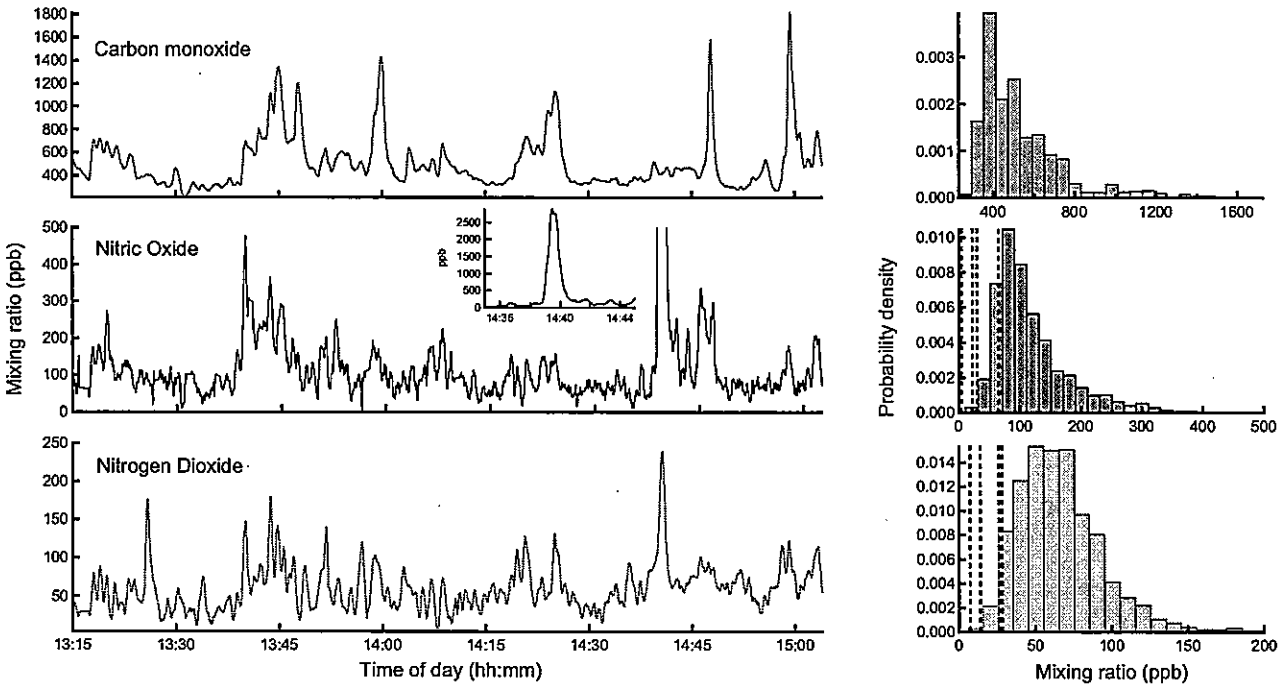

Fig. 19. Time series and histograms for a mobile sensor unit carried by a pedestrian as part of a mobile sensor deployment. NO_2 data are not corrected for interference with O_3 and therefore should be taken to be $[O_3] + [NO_2]$, i.e. there may be an additional baseline effect related to response to $[O_3]$. The inset NO figure shows that the peak at 14.40 exceeded 2.5 ppm. Histograms of the data for NO and NO_2 also show, in dotted lines, the average of two concurrent hourly mean values derived from each of the static sites maintained by the local authority in central Cambridge.

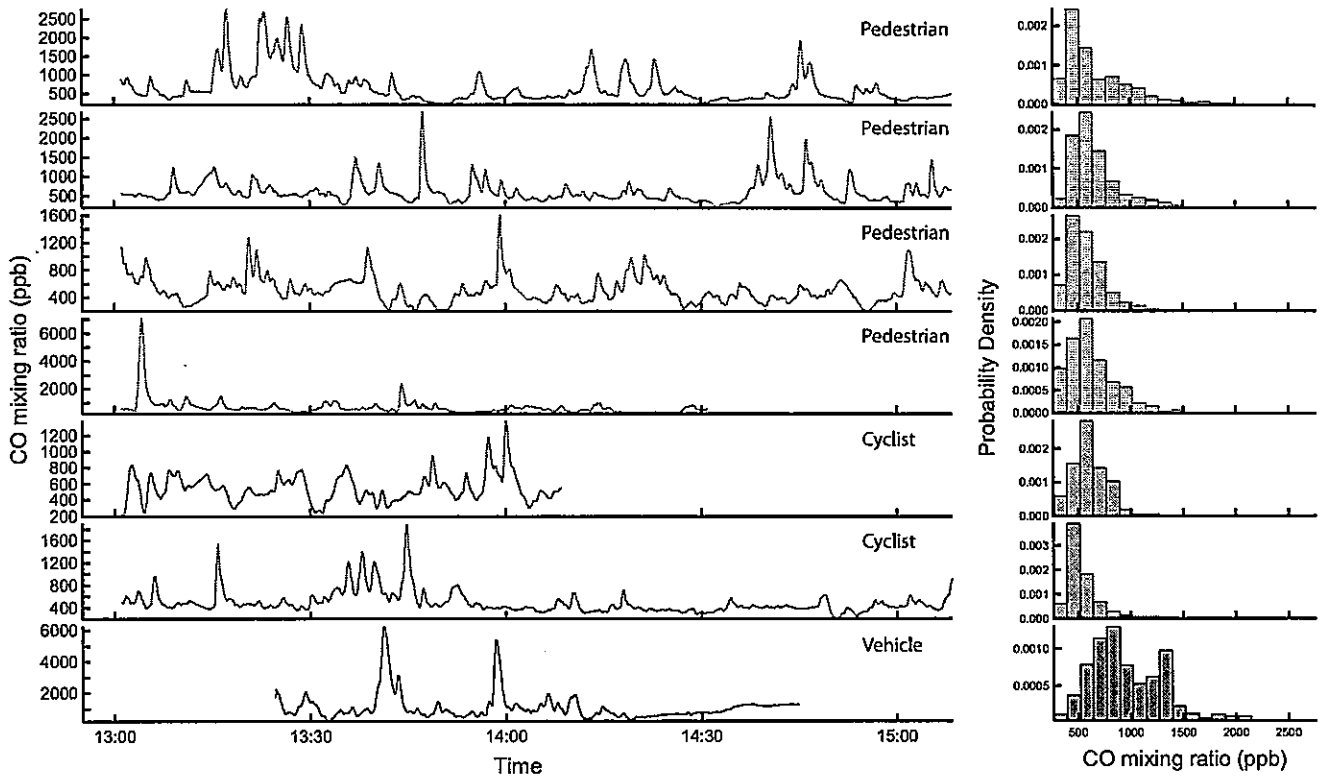

Fig. 20. Time series and measurement histograms of carbon monoxide, obtained from a number of sensor nodes deployed in central Cambridge (UK) as part of a large, mobile sensor network. Measurements made by pedestrians and cyclists are shown in green and red respectively, with in-vehicle measurements shown in blue (all traces in black in-print). For clarity, the abscissae of the histograms are on a single scale.

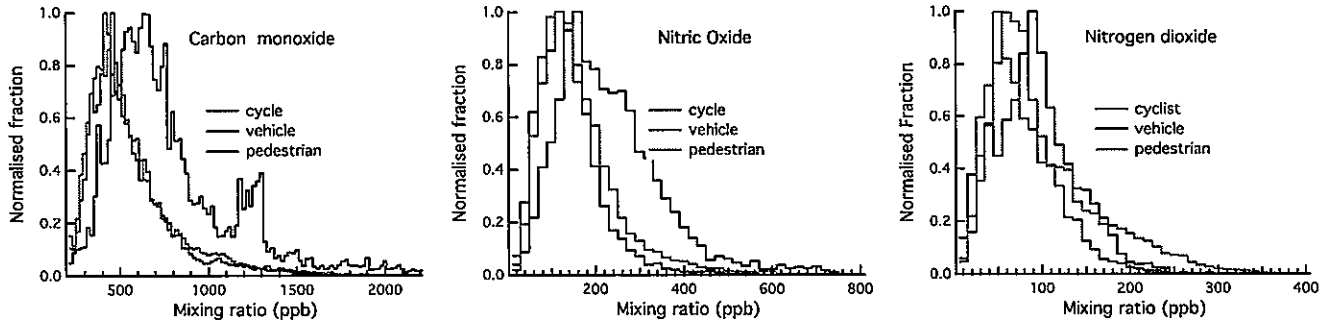

Fig. 21. Normalised probability distributions of CO, NO and NO_2 mixing ratios obtained during the Cambridge deployment, disaggregated by transport mode.

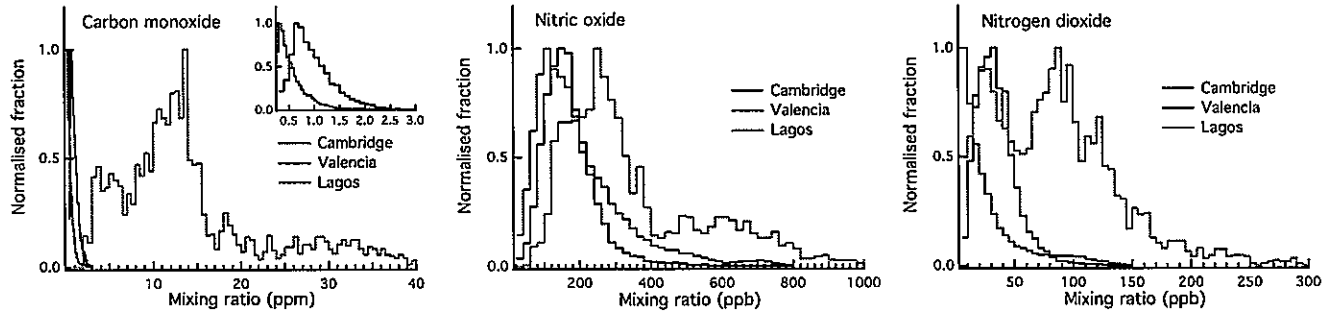

Fig. 22. Normalised fractional exposure obtained during short-term deployments in Cambridge (UK), Valencia (Spain) and Lagos (Nigeria) using the mobile sensor nodes discussed in Section 3.1.

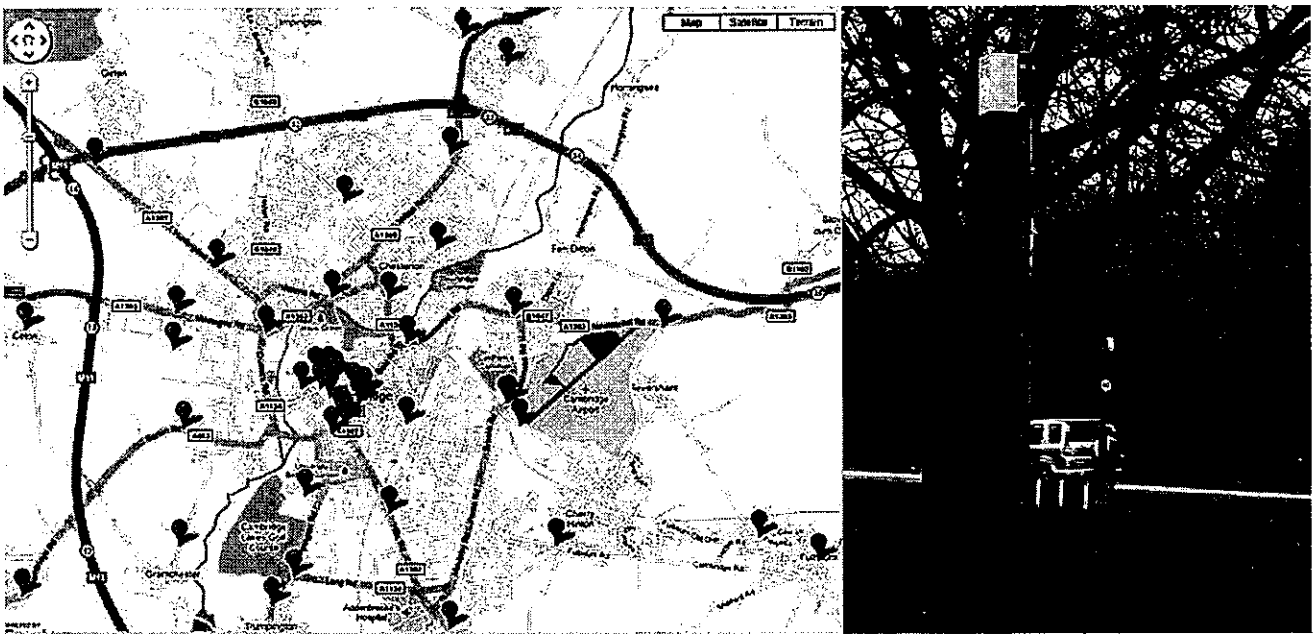

Fig. 23. Static sensor node locations used for the Cambridge static deployment (left), with typical lamppost mounting (photograph right) (Map data© 2012 Google).

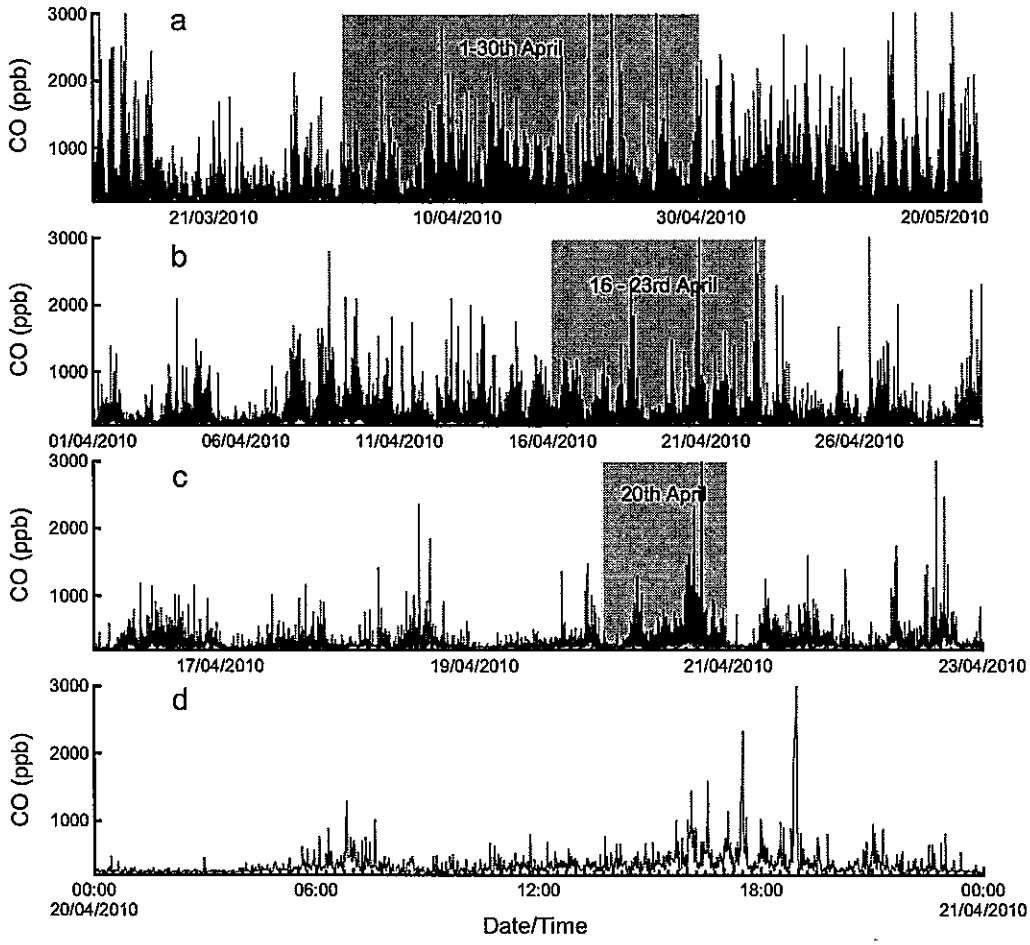

Fig. 24. Time series showing CO measurements from an inner-city electrochemical sensor node for the deployment duration a), together with subsets of one-month, one-week and one-day periods (b)–d) respectively) from a selected sensor node. All measurements are 30-s averages.

typically <40 ppb (Lee et al., 2006) it is clear that much of the structure observed is from primary NO_2 emissions.

There is a broad correlation between the different species (e.g. a minimum around 13.30 with elevated mixing ratios around 13.45 etc.), and clear correlations for some individual pollution events (e.g. most markedly for NO and NO_2 at ~14.40), although many pollution events, particularly for CO, are not well correlated with those of the other species. It is noticeable that, in this case, the observed NO_x values substantially exceed the average values measured by the neighbouring static sites (operated by the local authority) over the same period; this is one example of fixed monitoring sites not reproducing personal exposure to pollution events. In this case, the average NO_2 mixing ratio (68 ppb) was a substantial fraction of the hourly mean limit for AURN sites (200 $\mu g\ m^{-3}$ or ~100 ppb), while the average measured at the fixed sites was 16 ppb. The quantitative interpretation of these results is inevitably lessened by the fact that the NO_2 sensors were in fact also responding to O_3 as described in Section 3.3. The analysis method meant that this does not introduce a simple offset of the background O_3, but in fact is likely to slightly underestimate actual NO_2 amounts. For future studies, coupled measurements with NO_2 and O_3 sensors would resolve this uncertainty.

3.4.2. Air quality exposure by transport mode

The data shown in Fig. 18 can be disaggregated to describe exposure in a variety of different ways, including differences among individuals and across different transport modes. In Fig. 20 are shown time series and measurement histograms of carbon monoxide from several sensor nodes obtained in central Cambridge as part of the mobile sensor deployment. The data show the widely different air quality environments encountered by individuals, with a suggestion (see the histograms) that, for example, vehicle occupants are exposed to systematically higher values of carbon monoxide.

Fig. 21 shows probability distributions of CO, NO and NO_2 mixing ratios disaggregated by transport mode taken from the 3-h mobile deployment. Given the 'snapshot' nature of the study, some caution must be applied to their interpretation. However, at face value, it seems that vehicle occupants are exposed to significantly higher CO and NO concentrations than cyclists or pedestrians, while pedestrians appear to be exposed to a higher NO_2 tail in the distribution. The data on vehicle exposure are, however particularly limited owing to the fact that data from only 2 vehicles were used (c.f. 8 pedestrians, 10 cyclists). An additional factor to consider is that while the sensors provide information on exposure, they take no account of different levels of physical activity, leading to potentially differing dosages for similar exposures.

3.4.3. Air quality measurements in Cambridge, Valencia and Lagos

As a further illustration of the mobile sensor node capability, Fig. 22 shows normalised fractions obtained during short-term deployments in Cambridge (UK), Valencia (Spain) and Lagos (Nigeria). Subject to caveats about representativeness, there are clear indications of differences in all three species, most notably between Lagos and the European cities. The fact that these data may be gathered in such diverse locations with little to no infrastructure overheads illustrates the ease with which units may be deployed. A major implication of these studies is the potential

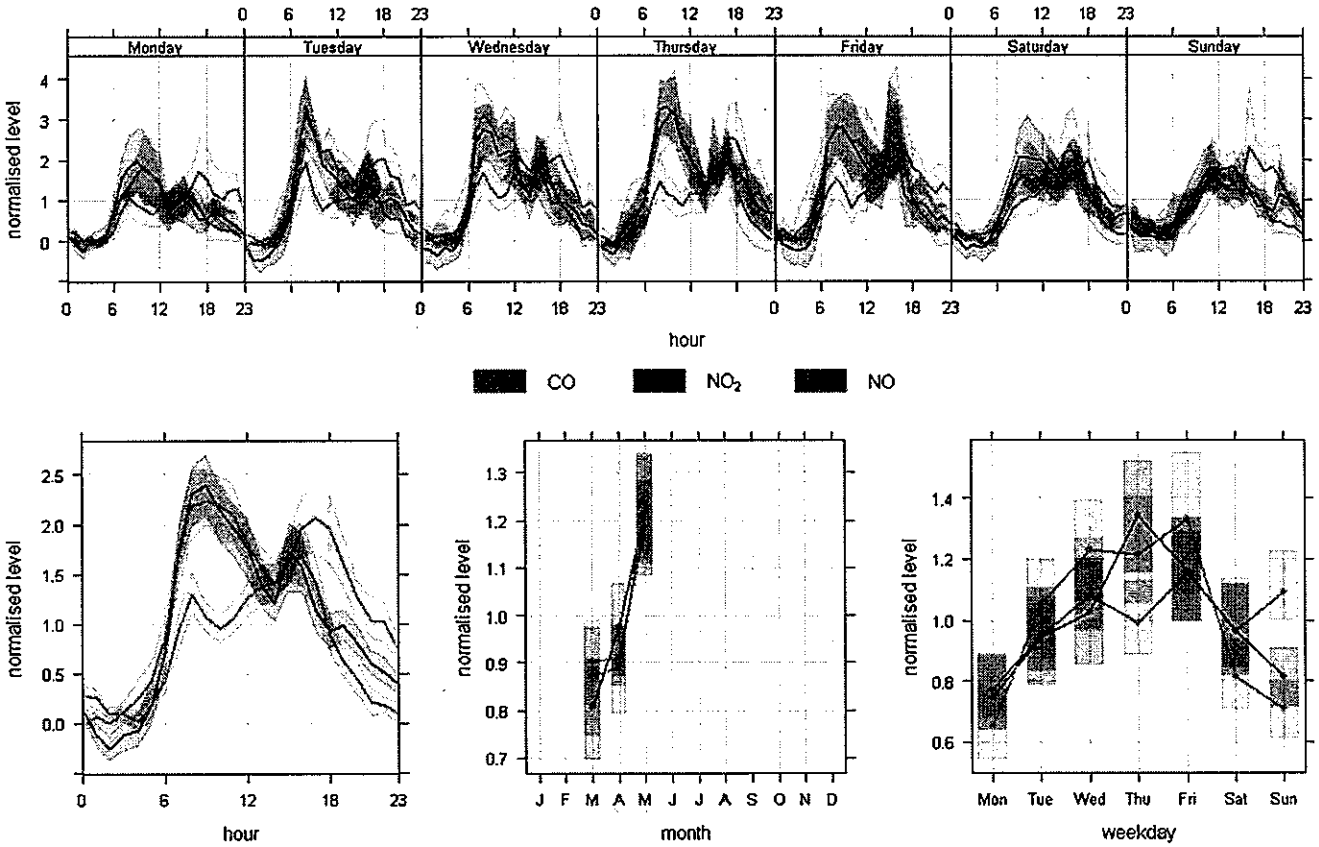

Fig. 25. Time series plots, averaged over different timescales, of hourly CO electrochemical sensor concentrations at the LAQN station in Gonville Place, Cambridge. The shading represents 95% confidence interval about the mean for each plot.

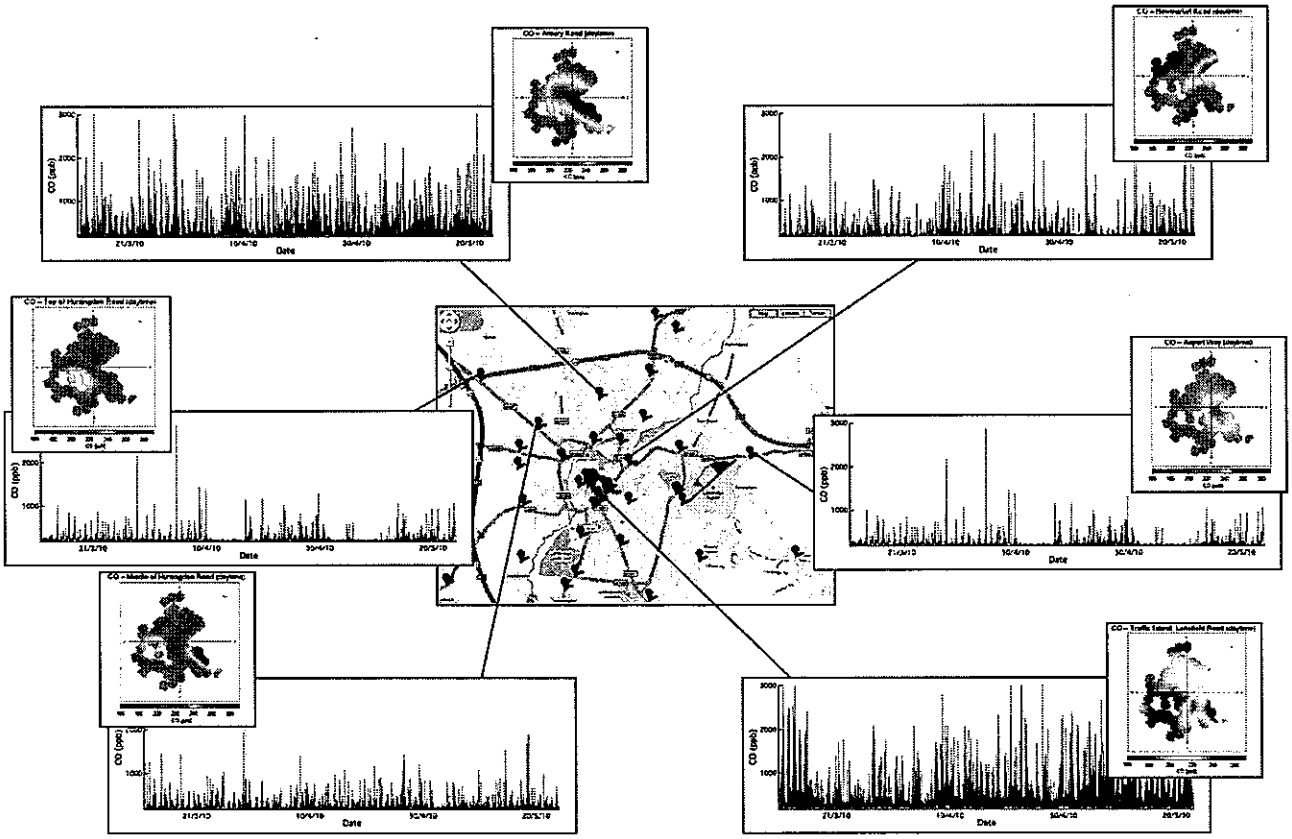

Fig. 26. Selected time series and bivariate polar plots for daytime carbon monoxide measurements obtained during a 2.5-month deployment of lamppost-mounted sensor nodes, as described in Section 4, in the Cambridge area, illustrating typical variability (see text for further discussion). Time series plots have identical ordinate scales. Bivariate plots are also on identical scales, with the exception of the central Cambridge site (bottom right) which, for clarity, has a different colour scale. Cambridge meteorological data is courtesy of the University of Cambridge Computer laboratory Digital Technology Group.

application of the mobile sensor nodes in studies involving exposure assessment for the purpose of providing the necessary pollution data for epidemiological studies.

4. Long-term, static networks

A network of static sensor nodes (see Section 3.1) was deployed in the Cambridge area for a period of approximately 2.5 months from 12th March to 26th May 2010. In total, 46 static sensor nodes were deployed, 21 of which were in central Cambridge. This is significantly denser than the existing infrastructure (five monitoring sites in Cambridge, one of which is a roadside AURN site monitoring NO_x) and the data gathered provide a far more detailed assessment of the local urban environment over the period of deployment. Each sensor node was installed at a height of 3 m on selected lamp-posts around Cambridge and South Cambridgeshire, with node locations as shown in Fig. 23.

This deployment generated a large number of measurements (excluding NO_2 measurements, over 90,000,000 measurements including CO, NO, RH and temperature) which will be discussed in detail in a number of subsequent papers. A subset of data from the deployment campaign is presented here to illustrate the capability of the sensor network approach. In Fig. 24 are shown several time series of CO mixing ratios obtained from a single, inner-city electrochemical sensor node during this campaign. The uppermost panel a) shows the complete 2.5-month time series, with a large number of individual pollution events superposed on a generally varying background. At this resolution any diurnal pattern is masked, although there are significant differences which are likely to be linked to synoptic weather patterns and, in particular, planetary boundary layer height and venting. Panel b) shows a single month (April) when again there is significant meteorologically linked variability, but where a diurnal periodicity is now beginning to be seen. Panel c) shows a single week (16–23rd April) where not only is the diurnal periodicity clearly apparent, but now subdiurnal features related to traffic flow are seen. Panel d) shows a single day (20th April) where individual pollution events are now apparent, superposed on the morning and evening traffic peak densities.

An example of the statistical information contained in these measurements is shown in Fig. 25 generated using the OpenAir open source air quality analysis tool (D.C. Carslaw and Ropkins, 2012; David Carslaw and Ropkins, 2012; R Development Core Team, 2012), where clear diurnal signatures in all species are now apparent, together with the longer time-series variability and the 'weekend' effect.

The capability of the high density fixed site network is illustrated by the data shown in Fig. 26, which shows time series and bivariate polar plots for daytime carbon monoxide obtained from a 2.5-month deployment of static sensor nodes (see Section 4) illustrating the range of conditions encountered in the urban and sub-urban areas associated with differing emission rates. Also apparent are increases associated with increased proximity to linear road sources (most notably in the top figures) where elevated concentrations occur when the wind direction is oriented parallel to the road. Although the details apparent are beyond the scope of this paper, the capability of the sensors for monitoring over extended periods as parts of dense networks is clear.

5. Discussion and conclusion

In this paper, we show that, operated suitably, CO, NO and NO_2 electrochemical sensors can provide parts-per-billion ($\sim\mu g\ m^{-3}$) level mixing ratio sensitivity with low noise and high linearity, making them suitable for urban air quality measurements. The sensors are generally highly selective, although there emerged from this work some cross-sensitivities e.g. between O_3 and NO_2 sensors; in future work, these will be catered for through the use of multiple sensors.

When operated in the field, the sensors show baseline (zero) signals which depend significantly (although differently for different sensor types) on ambient temperature and relative humidity. Of the sensor types investigated, this is most apparent for NO, and a post-processing procedure is presented which eliminates this effect, yielding excellent agreement with reference AURN instruments where measurements are available (NO and NO_2). Selected results also show that the sensors can be operated without significant gain attenuation over long periods (up to 12 months thus far), with the expectation of operable lifetimes of several years without replacement.

Air quality sensor nodes incorporating the electrochemical cells with GPS (for position) and GPRS (for data communication) have also been constructed for deployments as parts of mobile and static air quality sensor networks capable of sending real-time air quality data to a central server for processing and display.

Low-cost (~£100s) mobile and static networks of over 40 nodes have been successfully deployed, with results in the paper demonstrating the feasibility of high-density and scalable sensor networks for a variety of periods thus far up to 2.5-months. Results from these deployments shown in the paper have provided views of urban air quality segregated by, for example, transport mode and personal exposure. These data have a measurement density (in both space and time) which is unachievable using current standard measurement methods.

Overall, this work has demonstrated the potential of low-cost sensor network systems for air composition measurements in the urban environment, and to be capable of doing so at an appropriate granularity (and cost) to quantify airborne pollution levels on local scales. Such systems have been shown to be capable of producing high spatial and temporal resolution measures of pollution levels which could contribute to scientific understanding, as well as addressing economic, policy and regulatory issues spanning climate change, air quality and human exposure (and health) responses.

While it has been shown that post-processing and artefact removal are required to achieve results, the key conclusion is that low-cost miniature sensors previously considered at best indicative can, when suitably operated, be used for fully quantitative measurements of urban air quality. This work shows that low-cost air quality sensor networks are now feasible for widespread use for monitoring at ambient levels, complementing other measurement methodologies, and are now rapidly emerging as a feasible measurement technique for inclusion in air quality monitoring and regulation, source attribution and human exposure studies.

Improvements in sensor technologies are currently emerging and, for example, the inclusion of other gaseous species (e.g. O_3, SO_2), and suitable particulate monitors can only strengthen the case for their increasing use in assessing the scientific, health and legislative implications of urban air quality.

Acknowledgements

The authors would like to thank the following: Cambridge City Council for their cooperation in conducting these studies; O_2 for provision of hardware such as mobile phones and SIM cards used in the transmission of data; Brian Jones of the Digital Technology Group, University of Cambridge Computer Laboratory for meteorological data. The authors would also like to thank DfT and EPSRC for funding for the MESSAGE project.

References

Abelsohn, A., Sanborn, M.D., Jessiman, B.J., Weir, E., Jun 2002. Identifying and managing adverse environmental health effects: 6. Carbon monoxide poisoning. Can. Med. Assoc. J. 166 (13), 1685–1690.

Austin, C., Roberge, B., Goyer, N., 2006. Cross-sensitivities of electrochemical detectors used to monitor worker exposures to airborne contaminants: false positive responses in the absence of target analytes. J. Environ. Monit. 8, 161–166.

Bard, A.J., Faulkner, L.R., 2001. Electrochemical Method: Fundamentals and Application, second ed. John Wiley & Sons, New York.

Bright, V., Bloss, W., Cai, X., 2011. Modelling atmospheric composition in urban street canyons. Weather 66 (4), 106–110. http://dx.doi.org/10.1002/wea.781.

Carotta, M.C., Martinelli, G., Crema, L., Malagù, C., Merli, M., Ghiotti, G., Traversa, E., 2001. Nanostructured thick-film gas sensors for atmospheric pollutant monitoring: quantitative analysis on field tests. Sens. Actuators B 76, 336–343.

Carslaw, D.C., Ropkins, K., 2012. Openair — an R package for air quality data analysis. Environ. Model. Softw. 27-28, 52–61.

Carslaw, David, Ropkins, Karl, 2012. Openair: Open-source Tools for the Analysis of Air Pollution Data. R Package Version 2.15.0.

De Vito, S., Massera, E., Piga, M., Martinotto, L., Di Francia, G., 2008. On field calibration of an electronic nose for benzene estimation in an urban pollution monitoring scenario. Sens. Actuators B 129, 750–757.

De Vito, S., Piga, M., Martinotto, L., Di Francia, G., 2009. CO, NO_2 and NO_x urban pollution monitoring with on-field calibrated electronic nose by automatic Bayesian regularization. Sens. Actuators B 143, 182–191.

Defra, 2011. http://uk-air.defra.gov.uk/networks/network-info?view=aurn, Searched Nov 2011.

Environment Canada, 2011. http://www.ec.gc.ca/rnspa-naps/Default.asp?lang=En&n=5C0D33CF-1, Searched Nov 2011.

Grant, A., Stanley, K.F., Henshaw, S.J., Shallcross, D.E., O'Doherty, S., 2010. High-frequency urban measurements of molecular hydrogen and carbon monoxide in the United Kingdom. Atmos. Chem. Phys. 10, 4715–4724.

Hamann, C., Hamnett, A., Vielstich, W., 2007. Electrochemistry, second ed. Wiley-VCH, ISBN 978-3-527-31069-2.

Health Effects Institute, January 2010. Traffic-related Air Pollution: a Critical Review of the Literature on Emissions, Exposure, and Health Effects A Special Report of the HEI Panel on the Health Effects of Traffic-related Air Pollution. Special Report 17.

Hitchman, M.L., Cade, N.J., Gibbs, K.T., Hedley, N.J.M., 1997. Study of the factors affecting mass transport in electrochemical gas sensors. Analyst 122, 1411–1418. http://dx.doi.org/10.1039/A703644B.

Kamionka, M., Breuil, P., Pijolat, C., 2006. Calibration of a multivariate gas sensing device for atmospheric pollution measurement. Sens. Actuators B 118, 323–327.

Lee, J.D., Lewis, A.C., Monks, P.S., Jacob, M., Hamilton, J.F., Hopkins, J.R., Watson, N.M., Saxton, J.E., Ennis, C., Carpenter, L.J., Carslaw, N., Fleming, Z., Bandy, B.J., Oram, D.E., Penkett, S.A., Slemr, J., Norton, E., Rickard, A.R., Whalley, L.K., Heard, D.E., WJ, Gravestock, T., Smith, S.C., Stanton, J., Pilling, M.J., Jenkin, M.E., Dec 2006. Ozone photochemistry and elevated isoprene during the UK heatwave of august 2003. Atmos. Environ. 40, 7598–7613. http://dx.doi.org/10.1016/j.atmosenv.2006.06.057.

Lehr, E.L., Feb 1970. Carbon monoxide poisoning: a preventable environmental hazard. Am. J. Public Health Nation. Health 60 (2), 289–293.

McConnell, R., Islam, T., Shankardass, K., Jerrett, M., Lurmann, F., Gilliland, F., Gauderman, J., Avol, E., Kuenzli, N., Yao, L., Peters, J., Berhane, K., Jul 2010. Childhood incident asthma and traffic-related air pollution at home and school. Environ. Health Perspect. 118 (7), 1021–1026.

Pijolat, C., Pupier, C., Sauvan, M., Tournier, G., Lalauze, R., 1999. Gas detection for automotive pollution control. Sens. Actuators B 59, 195–202.

Popoola, O.A.M., Mead, M.I., Stewart, G.B., Jones, R.L. Development of baseline-temperature correction methodology for electrochemical sensors, and implications of this correction on long-term stability, in preparation.

R Development Core Team, 2012. R: a Language and Environment for Statistical Computing. R Foundation for Statistical Computing, Vienna, Austria, ISBN 3-900051-07-0. http://www.R-project.org/.

Ropkins, K., Colvile, R.N., November 2000. Critical Review of Air Quality Monitoring Technologies for Urban Traffic Management and Control (UTMC) Systems. Urban Traffic Management & Control (UK).

Stetter, J., Li, Jing, Feb 2008. Amperometric gas sensors — a review. Chem. Rev. 108 (2), 352–366. http://dx.doi.org/10.1021/cr0681039.

Tsujita, W., Yoshino, A., Ishida, H., Moriizumi, T., Oct 2005. Gas sensor network for air-pollution monitoring. Sens. Actuators B Chem. 110 (2), 304–311. http://dx.doi.org/10.1016/j.snb.2005.02.008.

World Health Organisation, 2000. Air Quality Guidelines for Europe, second ed. WHO Regional Publications No. 91, ISBN 92 890 1358 3.

World Health Organisation, 2006. Air Quality Guidelines for Particulate Matter, Ozone, Nitrogen Dioxide and Sulfur Dioxide. In: Global Update 2005. Summary of Risk Assessment. WHO/SDE/PHE/OEH/06.02.

European Network on New Sensing Technologies for Air Pollution Control and Environmental Sustainability - *EuNetAir*
COST Action TD1105

INTERNATIONAL WG1-WG4 MEETING on

New Sensing Technologies and Methods for Air-Pollution Monitoring
European Environment Agency - EEA
Copenhagen, Denmark, 3 - 4 October 2013

Action Start date: 01/07/2012 - Action End date: 30/06/2016 - Year 2: 2013-2014 (*Ongoing Action*)

WIRELESS SENSOR NETWORKS FOR AIR-POLLUTION MONITORING IN CITIES

UNIVERSITY OF CAMBRIDGE

Vivien Bright
SIG2 Member
University of Cambridge, Centre for Atmospheric Science, UK. vb323@cam.ac.uk.

COST is supported by the EU Framework Programme

ESF provides the COST Office through a European Commission contract

Scientific context and objectives

- Atmospheric composition within urban areas has a direct effect on the air quality of an environment in which a large majority of people live and work.
- Atmospheric pollutants including O_3, NO_2, VOCs and PM can have a significant effect on human health.
- Determine potential exposure of individuals and investigate processes that lead to the degradation of air quality within the urban environment.


Government issues Easter weekend smog alert
A smog warning has been issued for the Easter weekend amid fears that a combi of hot weather and pollution could cause health and breathing problems.

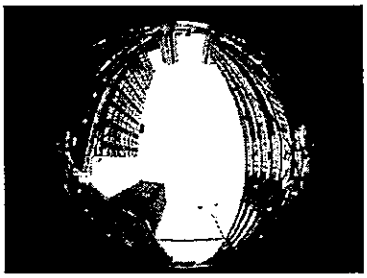

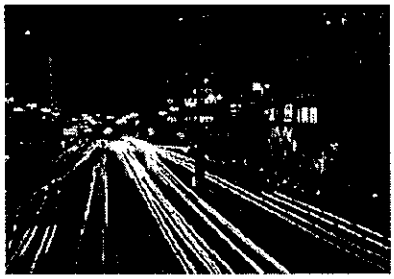

Scientific context and objectives

- Air quality within urban areas is highly heterogeneous in both time and space thus characterising air pollution is complex.
- Fixed site automated urban networks only provide low spatial resolution measurements.

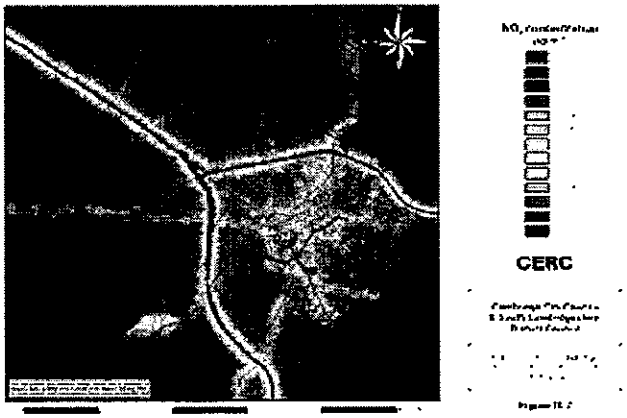

Street canyon effects

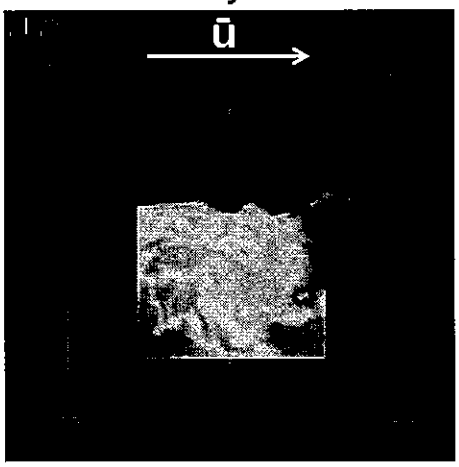

Bright *et al.*, 2013

Scientific context and objectives

- Deployment of a state-of-the art network of low-cost air pollution sensors.
- Provision of pollution data for science and policy applications.
- Comparison of data with emission inventories and pollution models.
- Source attribution.
- Creation of novel tools for data mining, network calibration, data visualisation and interpretation.
- Optimisation of sensor network for different environments.

Current activities of the Partner (1/2)

- Deployment of a state-of-the art network of low-cost air pollution sensors: The Sensor Networks for Air Quality at London Heathrow Airport (SNAQ-Heathrow) project.
- ~ 36 sensor nodes located in and around the airport.
- Web: http://www.snaq.org/

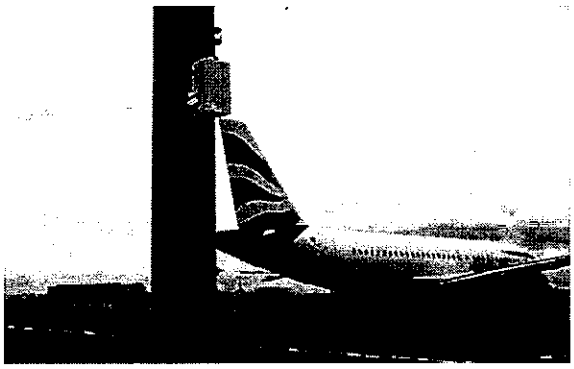

UNIVERSITY OF CAMBRIDGE

University of Hertfordshire

Alphasense THE SENSOR TECHNOLOGY COMPANY

MANCHESTER 1824

Heathrow

BRITISH AIRWAYS

NPL National Physical Laboratory

Imperial College London

Cambridge Environmental Research Consultants

Current activities of the Partner (2/2)

- High spatial and temporal resolution data provided.
- Demonstration of the utility of a high-density, low-cost sensor network.
- Source attribution for LHR airport.
- Network calibration.
- Investigation of pollutant variability on the local or micro-scale.

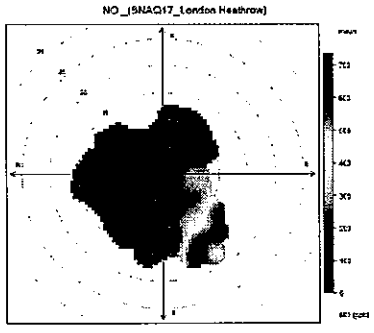

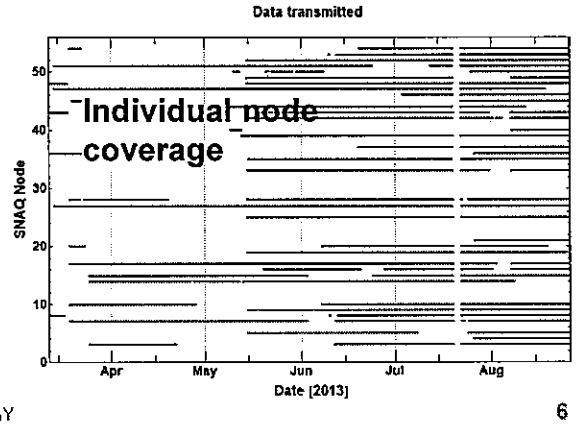

Facilities available for the Partner (1/2)

- **Instrumentation**

Chemical species:

- **(a)** Gas phase species: CO, NO, O_3, SO_2, NO_2 – (electrochemical sensors (EC) at 2 s)
- **(b)** CO_2 & total VOCs (optical at 10 s).
- **(c)** Size-speciated particulates 0.38 to 17.4 µm, optical (OPC) at 20 s

SNAQ sensor node

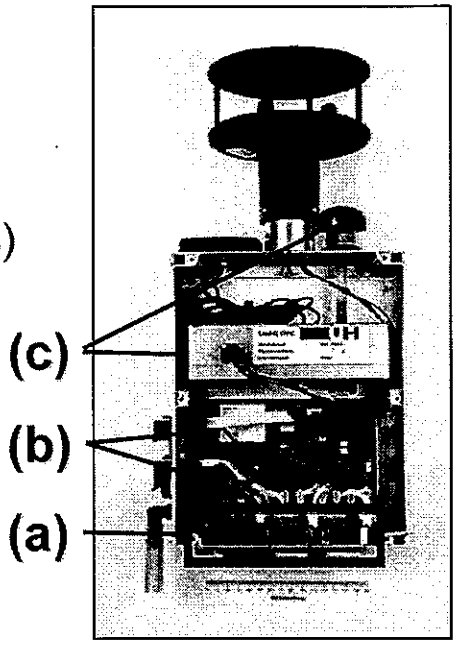

~49 x 22 x 16 cm. ~2.8 kg

Facilities available for the Partner (2/2)

- **Instrumentation**

Meteorology:

- **(d)** Wind speed and direction – Sonic anemometer.
- **(e)** Temperature and RH (probe).

Other:

- **(f)** GPS and GPRS (position and near-real time data transmission).

SNAQ sensor node

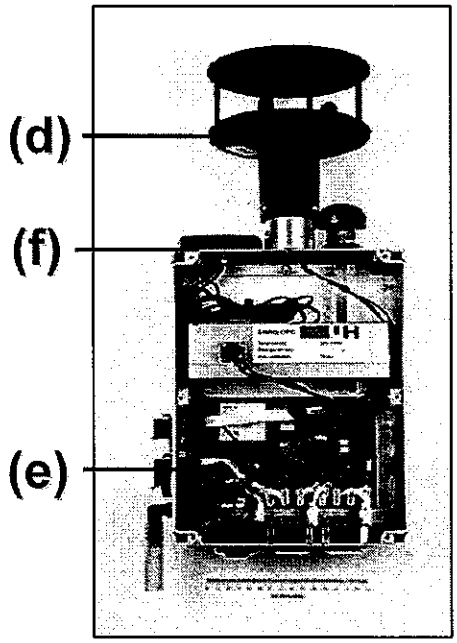

~49 x 22 x 16 cm. ~2.8 kg

Preliminary LHR results
- 1 month

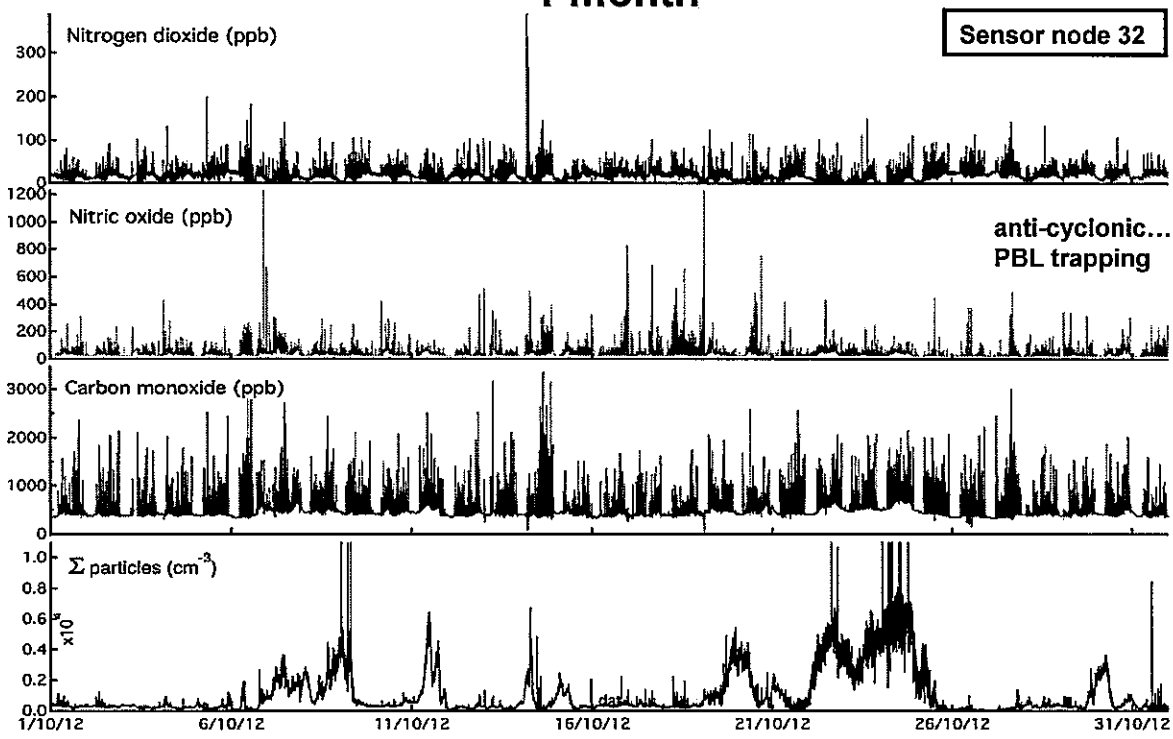

Preliminary LHR results
- 1 week

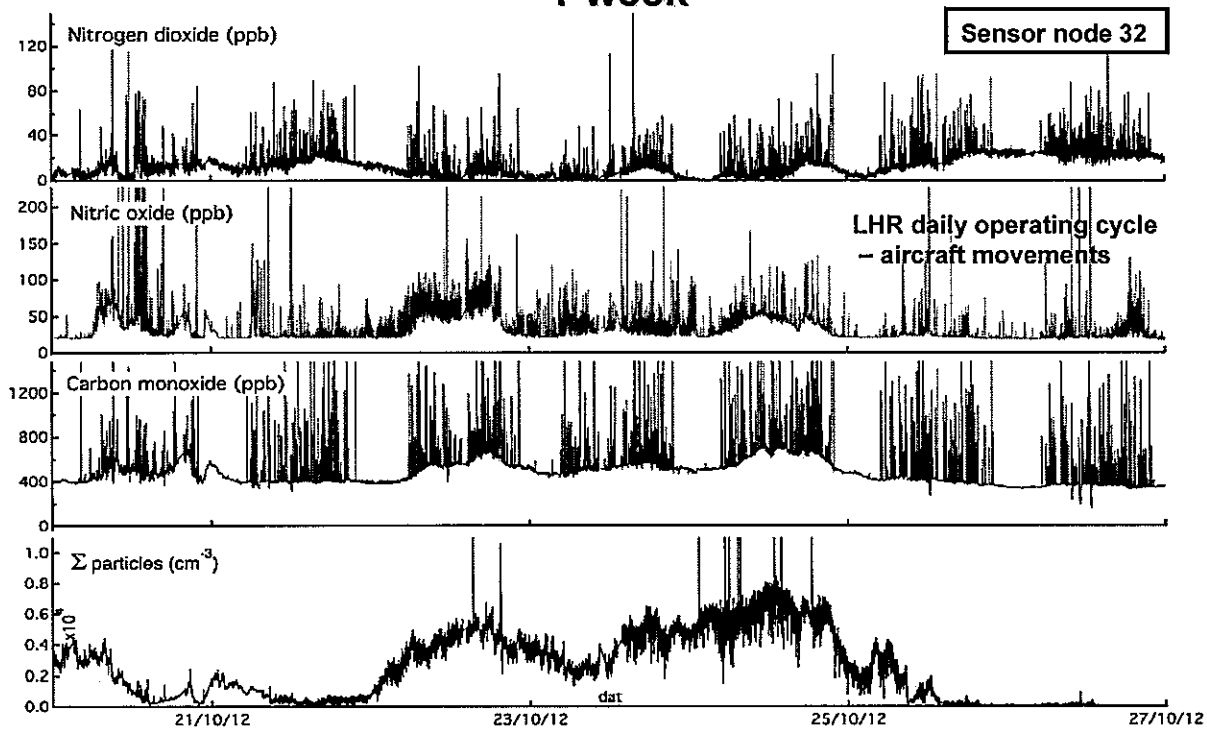

Illustrative results (LHR) – 1 month vs 1 week

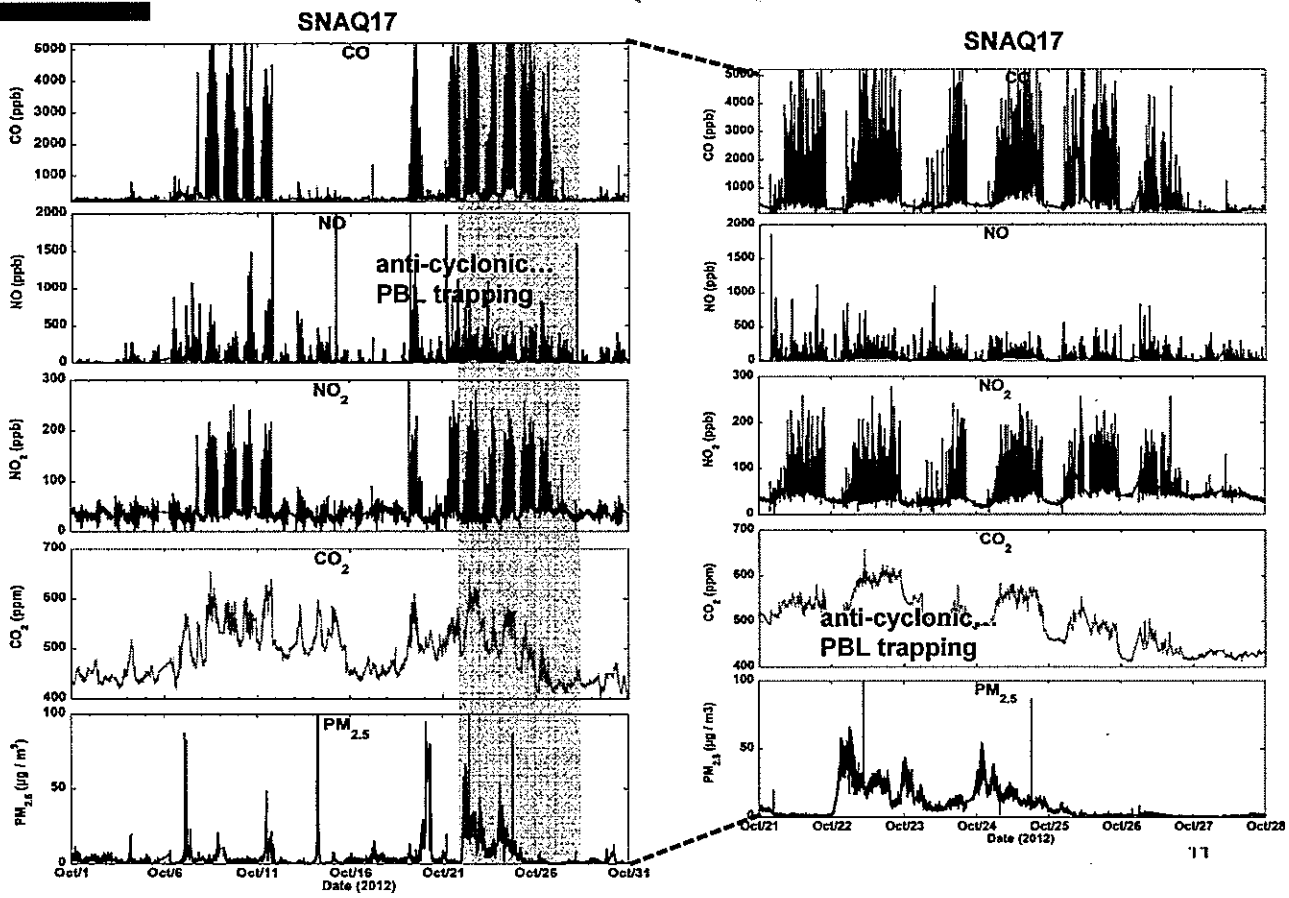

Source attribution –

Sensors at the west-end of southern runway (09R)

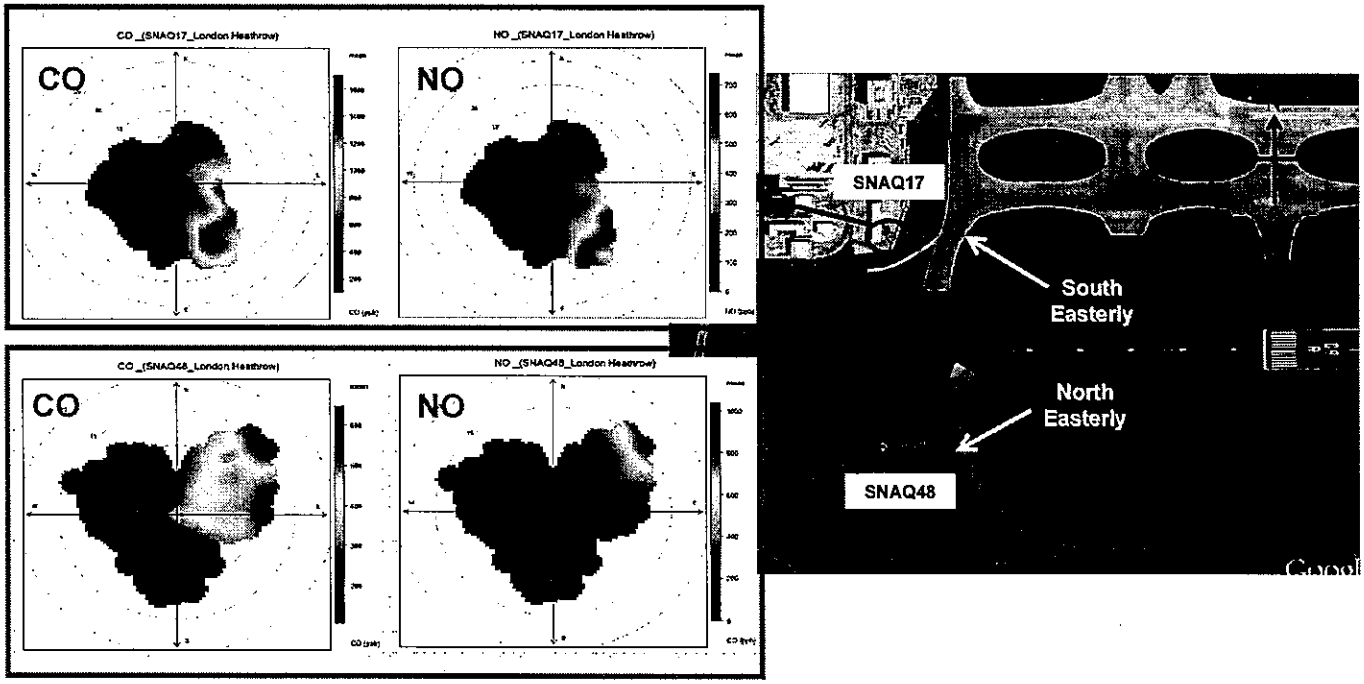

- Mirror image pollution mixing ratios observed
- High CO & NO mixing ratios (high wind speeds) indicate take-offs

Source attribution –

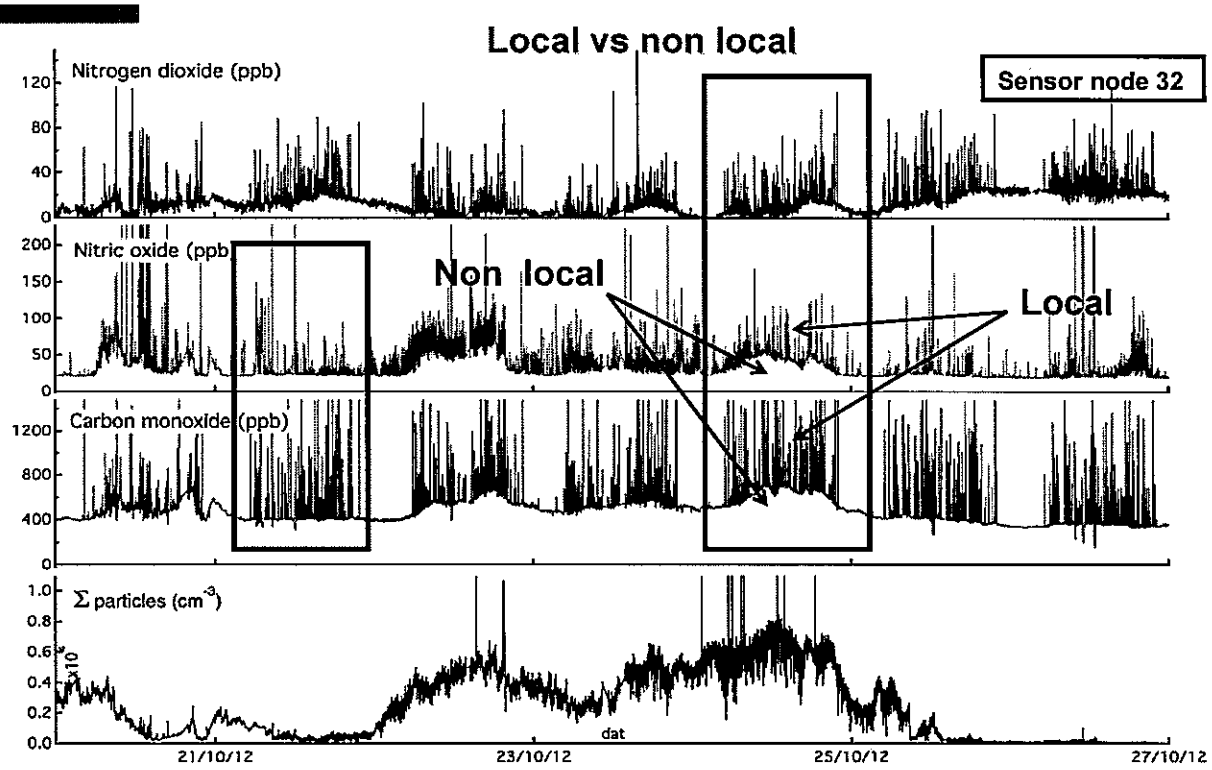

Network calibration *and* information

Network calibration

- Intermittency of emissions, *if measured at high time resolution*, allows determination of sensor 'baseline' – *local* vs *non local* sources.

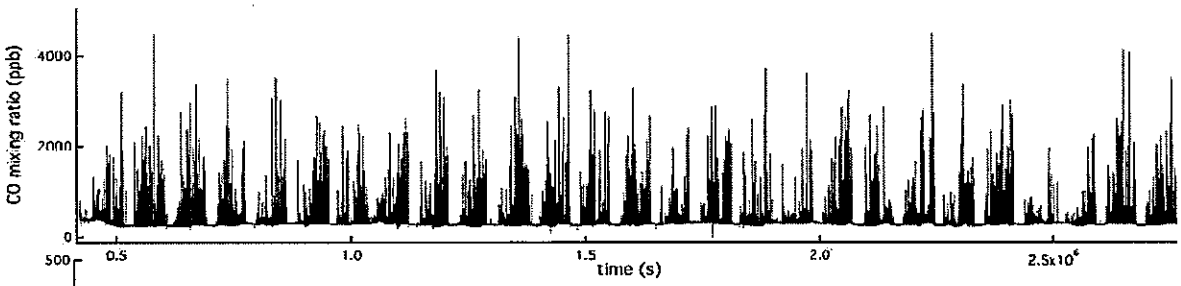

Sensor baseline: local emissions removed

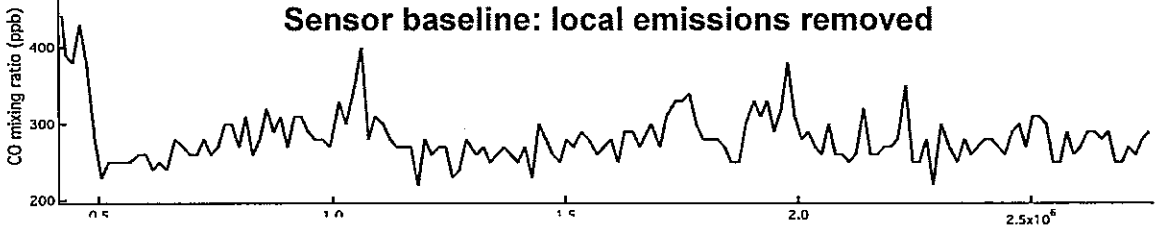

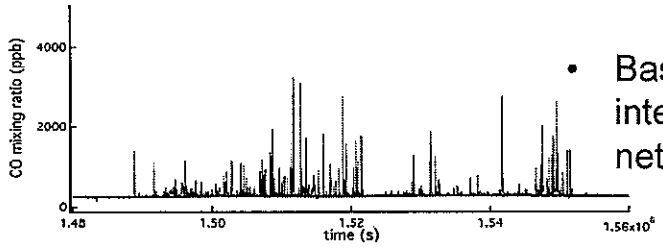

- Baselines replicated therefore method for inter-calibrating (and error checking) sensor networks.

Model optimisation -

Cambridge network, spring 2010

- 3 month static deployment in Cambridge: 45 low-cost electrochemical sensors
- High spatial and temporal (10 s) resolution data set of CO, NO and NO_2
- True variability in pollution levels across an urban area
- Representativeness of AURN sites in determining exposure

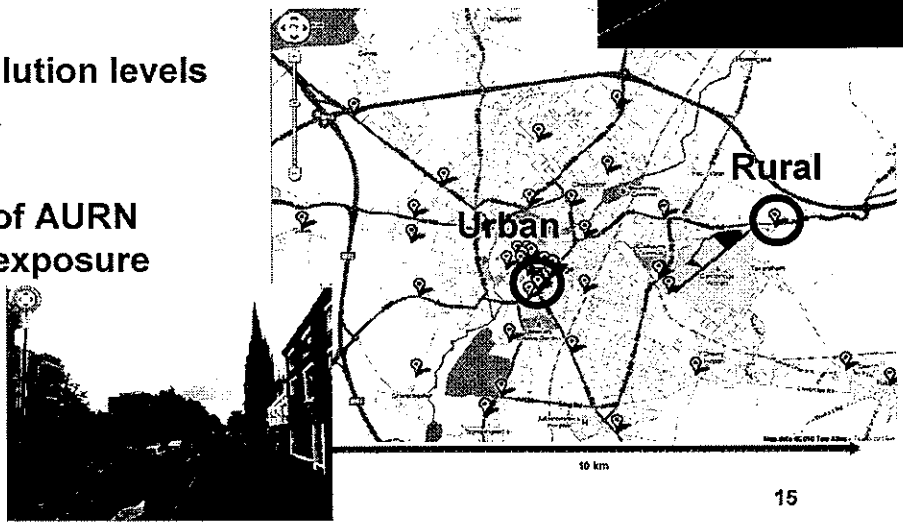

Model optimisation

- Measurements and ADMS-Urban model comparison
- CO adjustment of emissions to optimise model
- Removal of CO baselines to give local hourly

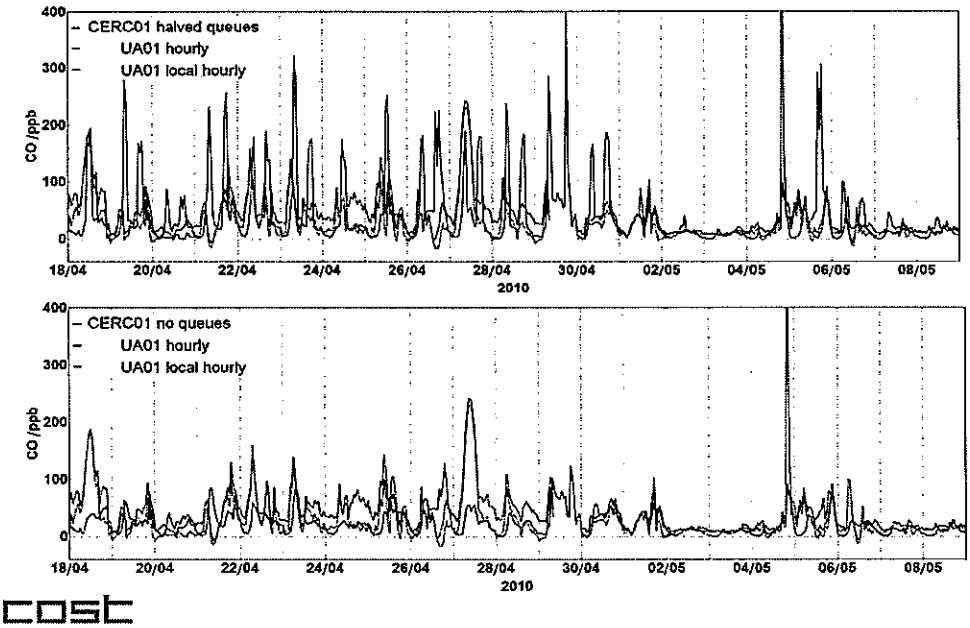

Street canyon effects

- Comparison of measurements made using a static AQ sensor unit and AURN site – Regent Street, Cambridge.
- Partial explanation of differences between ADMS model and observations?

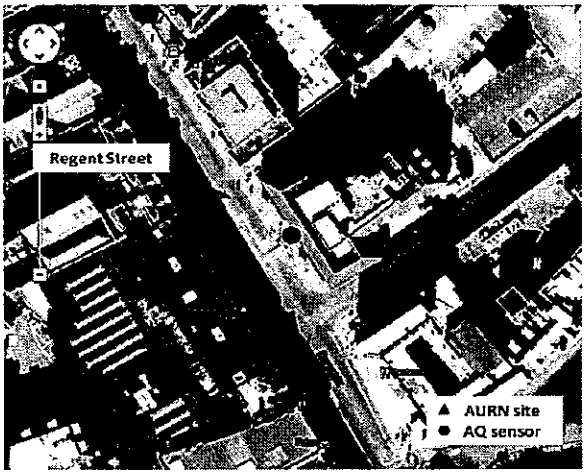

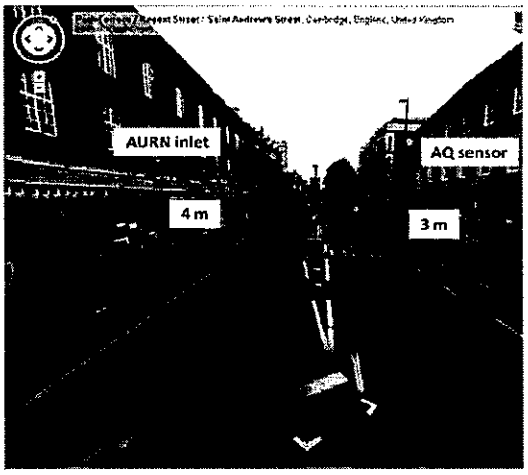

Street canyon effects

Wind direction approximately perpendicular to the canyon

Wind direction approximately parallel to the canyon

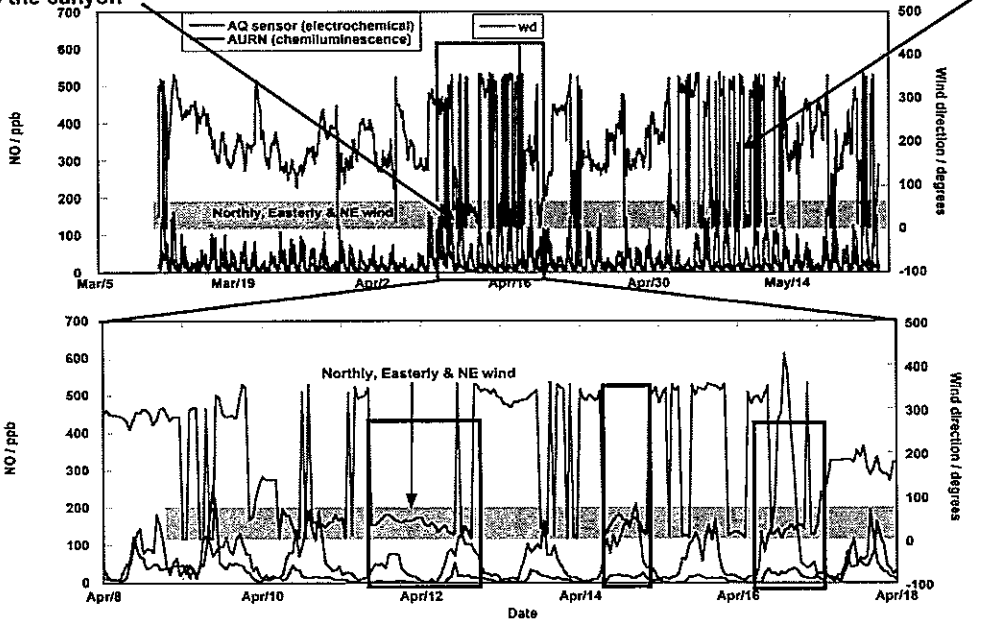

- Hourly mean wind direction and NO measurements from the AURN (chemiluminescence instrument) and AQ (electrochemical) sensor .

Within-canyon spatial variability

- Wind direction perpendicular relative to the street canyon axis (330°)

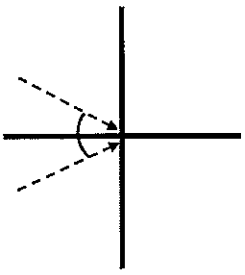

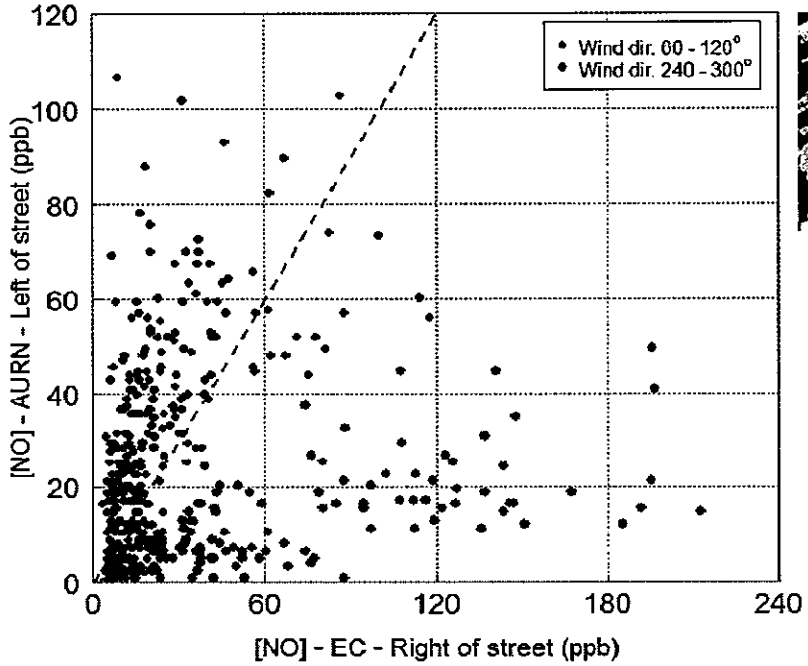

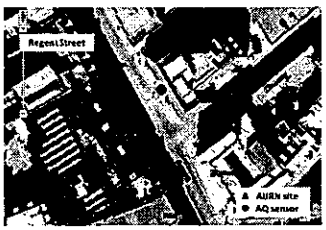

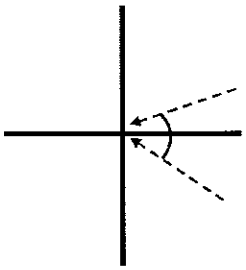

Channeling flow

- Wind direction parallel relative to the street canyon axis (330°)

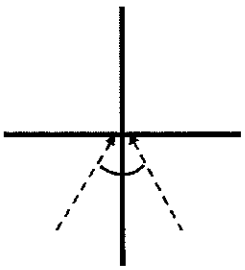

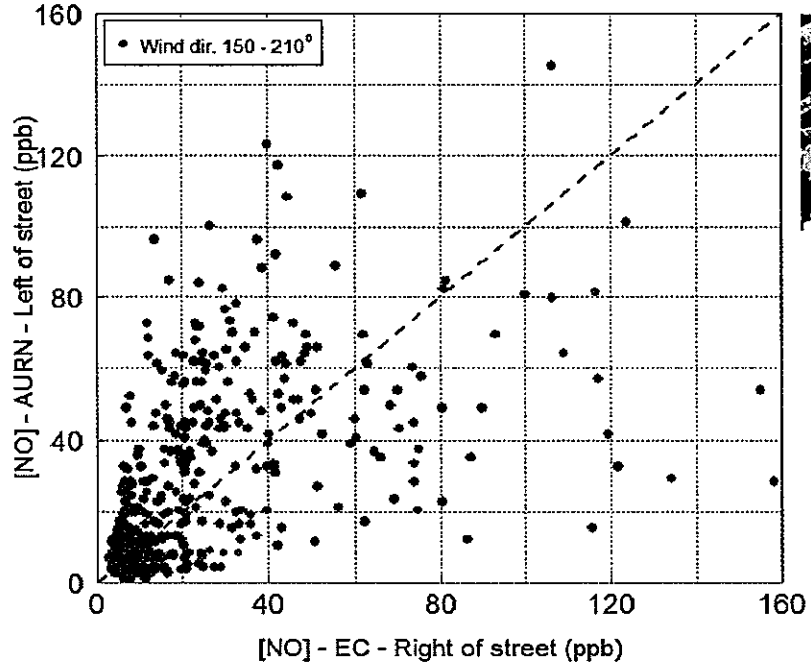

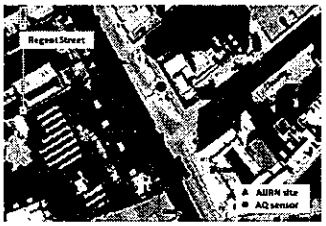

Within-canyon spatial variability

- Bivariate polar plots of NO measurements comparing measurements between the AURN station and the EC sensor.

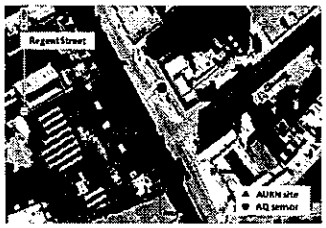

NO Chemiluminescence (AURN Regent Street)

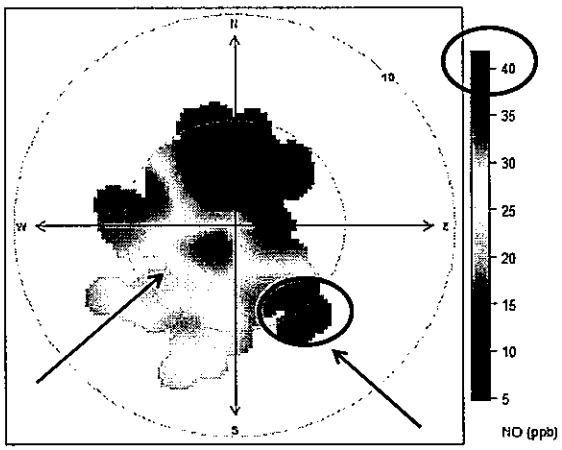

NO Electrochemical (Regent Str)

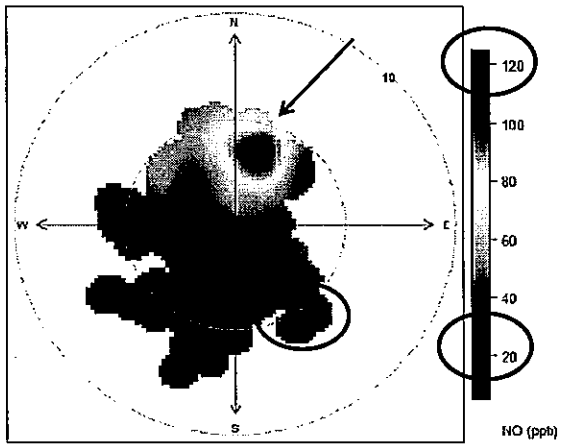

Future planned Activities

- Model verification through high (spatial and temporal) resolution observations.
- Model optimisation / source representation in models.
- Detailed analysis and source attribution – SNAQ-Heathrow
- Investigate personal exposure to pollutants.
- Citi-sense

CONCLUSIONS

- Low-cost sensor nodes equipped with GPS/GPRS – A.Q. measurements in near-real time, traditionally viewed as only achievable by costly and sparse fixed site monitoring stations.
- Demonstrated use of sensor nodes as part of static networks within urban environments - high spatial and temporal resolution data.
- Such measurements may be used to investigate personal exposure, regional changes in pollution levels, canyon effects and to perform model optimisation.
- Sensors require careful calibration (baseline levels, temperature and humidity effects).
- Sensor cross-sensitivity.

Acknowledgements

- **Cambridge Mobile Sensor Team:** Rod Jones, Lekan Popoola, Iq Mead, Gregor Stewart, Ines Heimann, Nahum Clements, Matt McLeod, Ray Freshwater, Mark Hayes, Shaun Hurst.
- **University of Hertfordshire:** Paul Kaye, Edwin Hirst, Warren Stanley.
- **University of Manchester:** Paul Williams.
- **Imperial College:** Robin North, Jeremy Cohen.
- **Alphasense:** John Saffell. Ronan Baron.

A Portable Low-Cost High Density Sensor Network for Air Quality at London Heathrow Airport

A31C-0059

Olalekan Popoola*(1), Iq Mead(1), Vivien Bright(1), Robin North(2), Gregor Stewart(1), Paul Kaye(3), and Roderic Jones‡(1)

(1) Department of Chemistry, University of Cambridge, UK
(2) Centre for Transport Studies, Imperial College London, UK
(3) Sensor & Technology Research Institute, University of Hertfordshire, UK

* oamp2@cam.ac.uk
‡ rlj1001@cam.ac.uk

1. SNAQ HEATHROW PROJECT

(a) Objective

- Deployment of state-of-the art network of pollution sensors (SNAQ sensor nodes) in and around LHR airport.
- Establishing pollution data for science and policy studies
- Comparing data with emission inventories and pollution models.
- Source attribution for LHR airport.
- Creation of novel tools for data mining, network calibration, data visualisations and interpretation.
- Optimisation of sensor network for different environments.

(b) Instrumentation

- Gas phase species:
  - ✓ CO, NO, O_3, SO_2, NO_2 (electrochemical (EC) at 2 s)
  - ✓ CO_2 and total VOCs (optical at 10 s).
- Size-speciated particulates (0.38 to 17.4 µm, optical (OPC) at 20 s)
- Meteorology:
  - ✓ wind speed and directions (sonic anemometer).
  - ✓ Temperature and relative humidity (RH)
- GPS and GPRS (position and real time data).
- Temperature and relative humidity (RH)

Figure 1: A typical SNAQ sensor node showing different components including gas sensors, particulate instrument, meteorology sensors and the GPS & GPRS module.

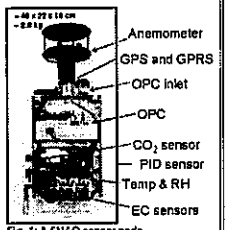

Fig. 1: A SNAQ sensor node

(c) Sensor network and data capture

- 36 sensor nodes deployed starting mid 2012.
- 31 nodes located within LHR covering all terminals, close to two runways and in proximity of the major roads within LHR
- 5 nodes are co-located with local monitoring stations outside LHR (all < 2 km from LHR)
- ~ 2×10^9 records (CO, NO, NO_2, O_3, SO_2, Σhydrocarbons, CO_2, size speciated PM, meteorology) transmitted (20 seconds data)
- 1-2 second data recorded on USB storage (~ 9×10^9 records)

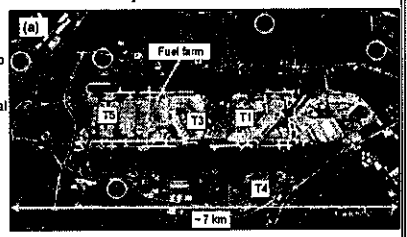

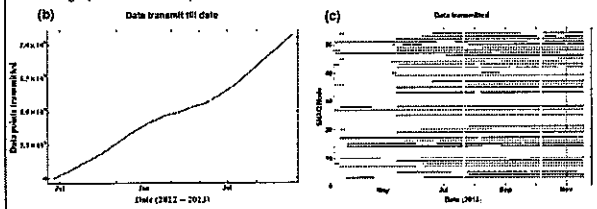

Figure 2: SNAQ network deployment (a) showing nodes within and outside LHR (orange circles) including the terminals (T1, T3,T4 & T5), data captured from the 35 nodes till date (b) and individual node coverage from Mar – Nov, 2013 (c).

2. CHARACTERISATION

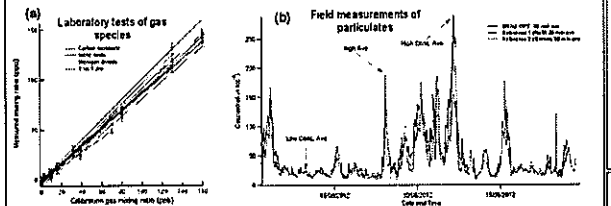

Figure 3: Laboratory calibration[1] (a) of CO, NO, NO_2 sensors against known gas mixing ratios and time series showing field measurement comparison between 30 minute average OPC measurements and two reference particle instruments.

- Excellent laboratory response at ppb mixing ratios[1] (fig. 3 (a)).
- Good instrumental performance against reference techniques under ambient conditions (fig. 3 (b)).

3. PRELIMINARY RESULTS AND DISCUSSION

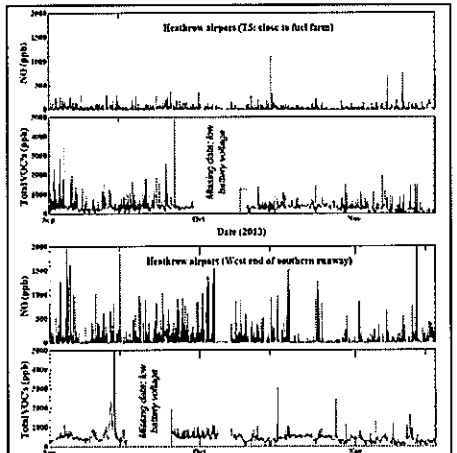

Figure 4: Time series of CO and total VOCs at two different location within the airport from Oct – Nov 2013.

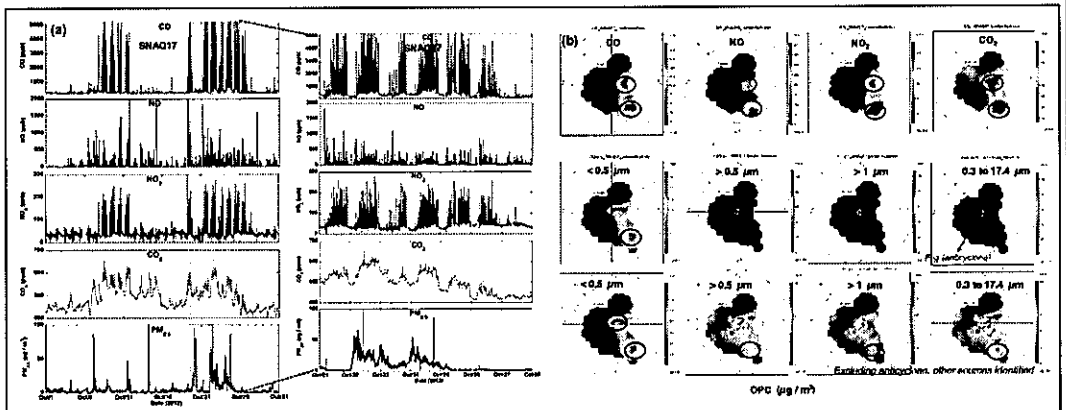

Figure 5: Time series (a) of CO, NO, NO_2 and $PM_{2.5}$ (equivalent) for Oct. 2012 and (b) the corresponding polar bivariate plots[2]. This sensor node is located at the west end of the southern runway.

- High spatial variability in gas species noticed across the SNAQ network in LHR (fig. 4). High VOCs and low NO (fuel farm close to terminal 5) compared to high NO and periodic high VOCs (close to end of runway)
- Increase in observed background concentrations associated with stable atmospheric condition (anticyclone) fig. 5 (a), while combining wind data with concentration measurements reveal potential pollution source(s) shown in black circles in fig. 5 (b).

Source attribution: northern and southern runways

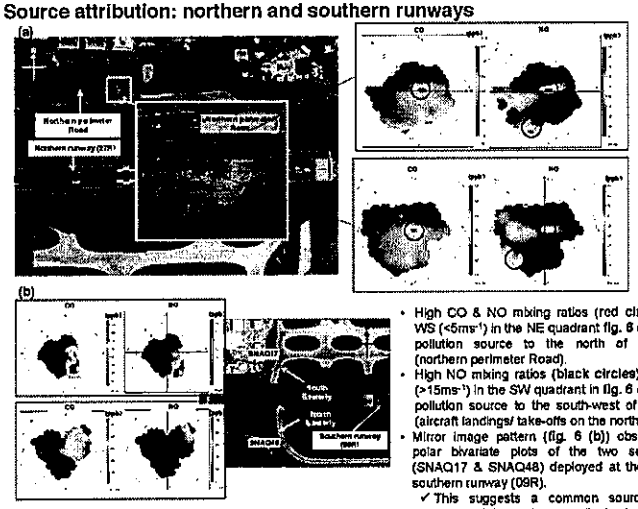

Figure 6: Bivariate polar plot of CO and NO (a) of two sensor nodes located to the north of the northern runway and a pair of sensor node located to the west-end of the southern runway (b).

- High CO & NO mixing ratios (red circles) at low WS (<5ms⁻¹) in the NE quadrant fig. 6 (a) suggest a pollution source to the north of the sensors (northern perimeter Road).
- High NO mixing ratios (black circles) at high WS (>15ms⁻¹) in the SW quadrant in fig. 6 (a) suggest a pollution source to the south-west of the sensors (aircraft landings/ take-offs on the northern runway)
- Mirror image pattern (fig. 6 (b)) observed in the polar bivariate plots of the two sensor nodes (SNAQ17 & SNAQ48) deployed at the end of the southern runway (09R).
  - ✓ This suggests a common source (southern runway) located perpendicular to the distance between the two sensors.
  - ✓ High CO & NO mixing ratios (at high wind speeds) suggests aircraft take-offs.

Source apportion study: southern runway

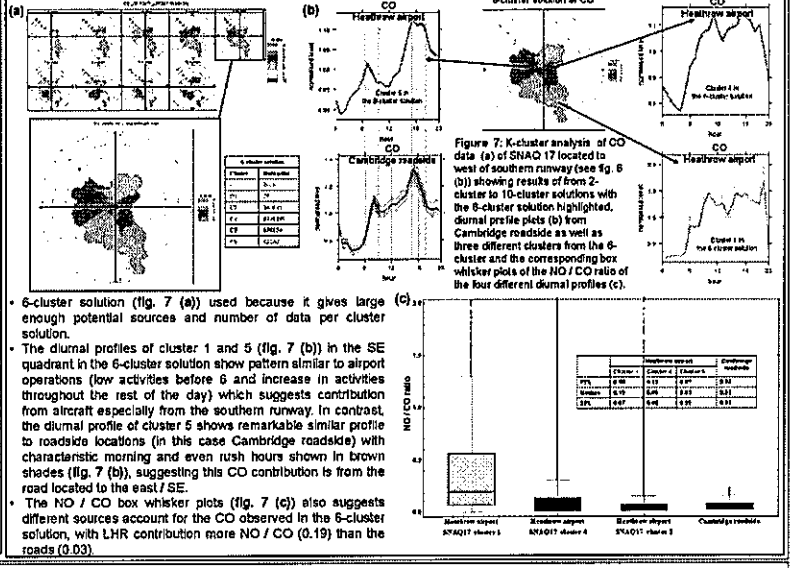

Figure 7: K-cluster analysis of CO data (a) of SNAQ 17 located to west of southern runway (see fig. 6 (b)) showing results of from 2-cluster to 10-cluster solutions with the 6-cluster solution highlighted, diurnal profile plots (b) from Cambridge roadside as well as three different clusters from the 6-cluster and the corresponding box whisker plots of the NO / CO ratio of the four different diurnal profiles (c).

- 6-cluster solution (fig. 7 (a)) used because it gives large enough potential sources and number of data per cluster solution.
- The diurnal profiles of cluster 1 and 5 (fig. 7 (b)) in the SE quadrant in the 6-cluster solution show pattern similar to airport operations (low activities before 6 and increase in activities throughout the rest of the day) which suggests contribution from aircraft especially from the southern runway. In contrast, the diurnal profile of cluster 5 shows remarkable similar profile to roadside locations (in this case Cambridge roadside) with characteristic morning and even rush hours shown in brown shades (fig. 7 (b)), suggesting this CO contribution is from the road located to the east / SE.
- The NO / CO box whisker plots (fig. 7 (c)) also suggests different sources account for the CO observed in the 6-cluster solution, with LHR contribution more NO / CO (0.19) than the roads (0.03).

4. CONCLUSIONS AND FUTURE WORK

- First, high-temporal and spatial, long-term deployment of pollution sensor networks in LHR airport measuring multiple gas species and particulates as well as meteorology.
- Exciting findings from preliminary results: 1.) Large temporal variations in mixing ratios of pollutants observed across the network. 2.) Anticyclone effect of pollution well captured. 3) Pollution source attribution and source apportion study within the airport.
- Future work includes deploying the remaining sensor nodes, comparing measurement data with dispersion models and emission inventories.
- Detailed analysis of data using information on airport operations to apportion pollution sources.
- Calibration of sensor network (baseline approach)

References and acknowledgements

1. Mead, M.I., Popoola, O.A.M., Stewart, G.B., Landshoff, P., Calleja, M., Hayes, M., Baldovi, J.J., Hodgson, T., McLeod, M., Dicks, J.,Lewis, A., Cohen, J., Baron, R., Saffell, J., Jones, R.L., *The use of electrochemical sensors for monitoring urban air quality in low-cost, high-density networks*. Atmospheric Environment. 2013, 70: p. 186-203.
2. David Carslaw and Karl Ropkins (2012). openair: Open-source tools for the analysis of air pollution data. R package version 0.7-0.

The authors will like to acknowledge Luke Cox, Spencer Thomas and David Vowles (BAA), NERC: High density network system for air quality studies at Heathrow airport (funded Oct , 2010), Alphasense Ltd, Ray Freshwater and Mark Heyes (University of Cambridge), Warren Stanley and Edwin Hirst (University of Hertfordshire).

New Technologies, New Opportunities for Odour Detection

Dr. John Saffell
Alphasense Ltd.
sensors@alphasense.com

Types of Gases
Sulphur compounds are the biggest problem

Organic
- sulphur compounds: H_2S, mercaptans/thiols
- amines
- aldehydes, ketones, alcohols
- methane

Inorganic
- NO_x, SO_x (acid gases)
- Ozone, chlorine/ bromine (disinfectants)
- Ammonia (nitrogenation)
- Hydrogen (used as surrogate for clean landfills)

Current Technologies
OK, but could do better

Organic
- Mass Spectrometry (MS) or GC/MS
- Long pathlength FTIR
- Photoionisation Detectors (PID)
- Electronic noses (sensor arrays)

Inorganic
- Electrochemical cells
- NIR laser spectrometry

New Technologies
Not there, yet

Organic
- NIR solid state spectrometry
- Nanomaterial sensor arrays (next generation electronic noses)
- Micro GC/MS (low cost, limited life detectors)
- Ion Mobility Spectroscopy (IMS/ FAIMS)

Inorganics
- Quantum Cascade Laser (QCL) spectroscopy
- Cavity Ring Down Spectroscopy (CRDS)
- Long wavelength NDIR
- Improved sensitivity electrochemicals

Quantum Cascade Lasers

- Solid state infrared lasers are now available at wavelengths to 20um

Resonant Cavity Laser Systems

- Bounce the light through the test cell hundreds, thousands of times to improve resolution
- Cavity Ring Down Spectroscopy (CRDS) is now commercially available for some gases

Resonant Cavity Diode Laser Absorption

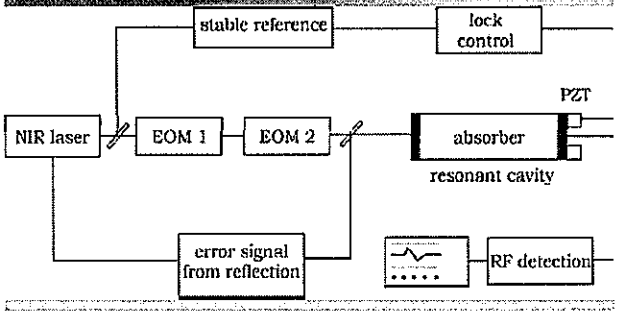

Near- Infrared spectroscopy has just become cheaper, better

- MEMS devices are replacing expensive optical wavelength selection systems

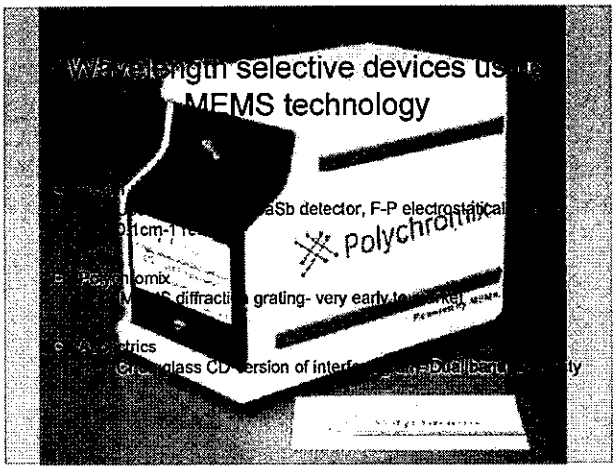

Electronic noses
Sensor arrays

- Based on polymer or semiconductor sensors
- Analysis of the measurements is difficult- keeps the programmers busy.
- Humidity, sensor drift, and array "training" are continuing problems. Hopefully, new sensor materials will rescue this technology.

Nanomaterials improve sensor performance

- Carbon nanotubes are in development as sensors for ammonia and hydrogen.
- Better organometallic sensing layers are more repeatable, thanks to organic LED (OLED) work for new TV, PC displays.

Carbon nanotubes

- Chemical resistors, or-
- Electrochemical replacements for graphite

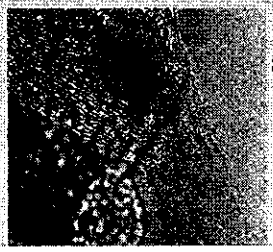

Single Wall CNT

Sensing layers: organometallic chemistry at its best

- Phthalocyanines
- Crown Ethers
- Dendrimers
- Hydro-, lipophyllic chains
- Chiral compounds
- Thiol on gold SAMs

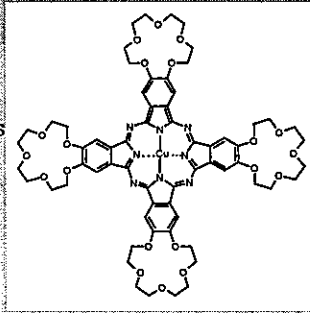

SPR Response to 130 ppb NO_2

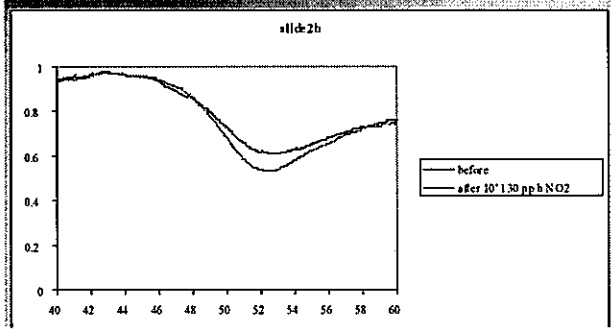

Amperometric Sensors

- Standard gas detection technology for H_2S, SO_x and NO_x continues to improve itself.

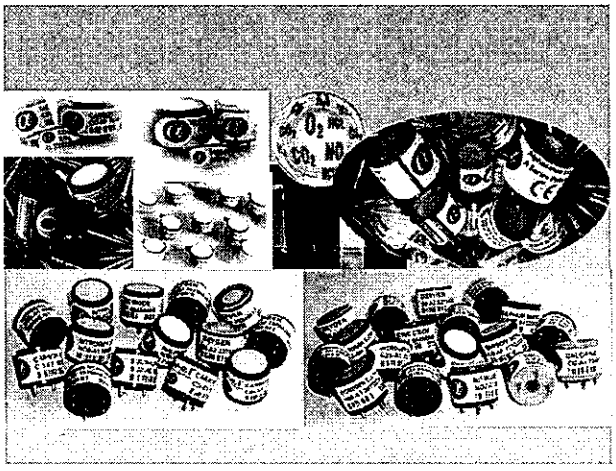

4 Amperometric Electrochemical

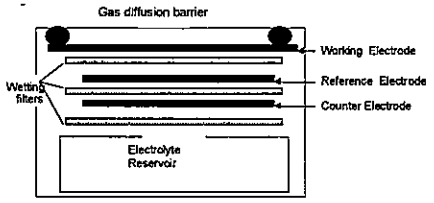

Electrochemical response to 1ppm NO_2

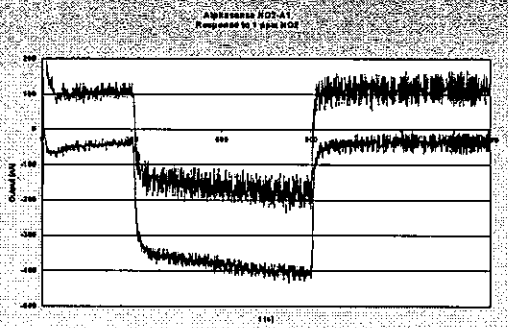

Electrochemicals give good response

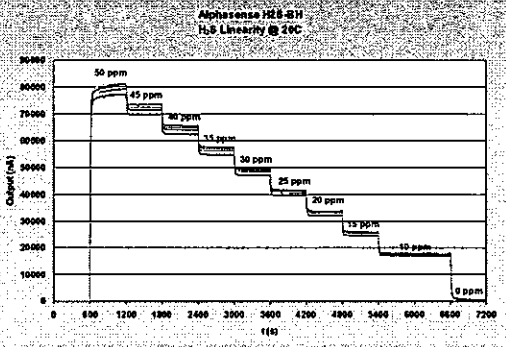

Gas Cameras

- The ultimate tool to measure odour dispersion in real time.
- But- a technical challenge still under development

Electronics and Computing come to the rescue

- ASICs and FPGAs give computing power at the sensor.
- Low power wireless ZigBee (IEEE 802.15.4) WiFi and GPS allow instant network systems without cables.
- Silicon MEMS permit low cost sensor arrays.

Conclusions

- VOC analysis using **spectroscopy** will become cheaper.
- H_2S and other inorganic gases will be cheaply measured at the 10-50ppb level with better **electrochemical sensors**.
- New **sensor materials**- they may be the hope for ammonia and mercaptans, but- still too early.
- Dioxins, PCBs will be analysed at the sub-ppb level inexpensively with the next step after PIDs: **Differential Mobility Spectrscopy**.
- **Research** is needed to determine how the hydrocarbons and hydrogen are useful surrogates for landfill monitoring.

What does the future offer us? When?

- These technologies are in development.
- But we are not there yet- products must be developed and supporting research is needed to ensure correct interpretation.

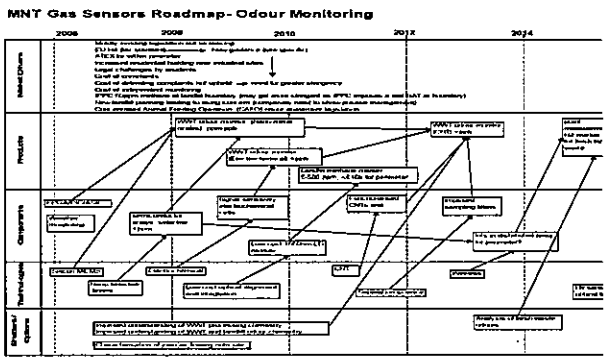

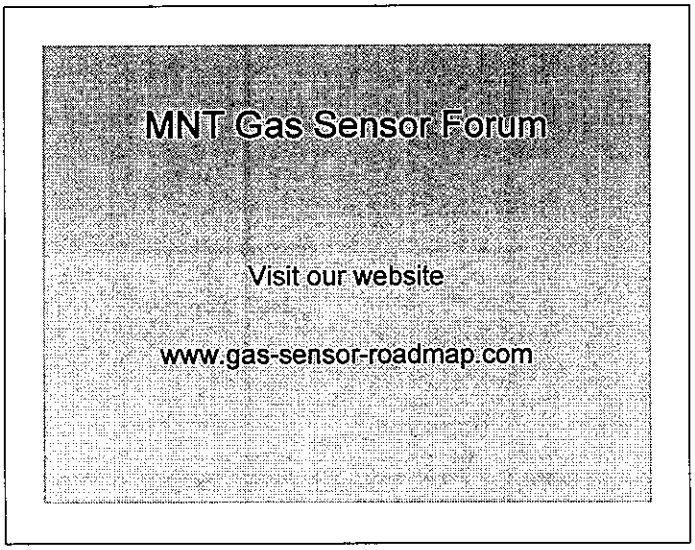
MNT Gas Sensor Forum
Visit our website
www.gas-sensor-roadmap.com

For Details, Contact:

Arthur Burnley
Email: awb@alphasense.com
Mobile :+44 0410 59 05 69
Webpage:www.alphasense.com

Alphasense Ltd
Oak Industrial Park
Great Dunmow
Essex CM6 1XN
Tel: + 44 (0) 1371 87 80 48
Fax: + 44 (0) 1371 87 80 66

αlphasense Product News Release

ATAV ensures High Quality Standards for Alphasense

The Alphasense Automatic Test And Validation System (ATAV) is an automated, computer-controlled system for performance testing Gas Sensors. The ATAV is the result of years of experience gained from Gas Sensor and Gas Detection instrument manufactures.

All sensors pass through this system and are subjected to a series of tests that can be specified by the customer. A customised sensor performance report can then be provided. This reinforces the high quality, sensor performance Alphasense customers have come to rely on.

The ATAV can accommodate a wide range of customised data, specific to each customer's needs. This can include such parameters as humidity and temperature. Additional features of ATAV include continuous monitoring of each sensor during the initial stabilisation period after manufacture. Many quality problems in electrochemical gas sensors are caused by not allowing sufficient stabilisation time. Performance tests are only carried out after the zero signal has definitely stabilised and the sensor is showing steady, repeatable performance. Each Sensor has a unique barcode that is used to access Sensor performance data from a purpose designed database for its' warranted life. The ATAV also allows the accumulation of batch data from more detailed tests over large numbers of production batches allowing a greater understanding of sensor performance.

Alphasense ATAV system provides full traceability for every sensor despatched and together with ISO 9001:2000 procedures, ensures the high quality standards customers have come to expect from the Alphasense range of gas sensors.

Please contact Arthur Burnley for further information

For Immediate Release

New 'hyperlocal' sensor network to create world's most sophisticated air monitoring system across London's streets

London Mayor Sadiq Khan launches new, street-by-street monitoring system to improve air quality.

Sensors will be attached to lampposts, buildings and in dedicated Google Street View cars.

London, UK (21 June 2018) — The Mayor of London, Sadiq Khan, and C40 – a network of cities committed to bold action on climate change – have launched a cutting-edge new project to better understand Londoners' exposure to air pollution around the city. Sensors will measure harmful pollution in tens of thousands of locations, making London's new air quality monitoring network the most sophisticated in the world.

Air pollution is threatening the health of Londoners, with most areas of the capital regularly breaking limits for safe levels of air pollution. Scientists estimate[12] that thousands of Londoners' lives end sooner than they should each year because of unclean air. And that the yearly cost of that dirty air to London's economy is £3.7 billion.

London already has one of the best networks of air quality monitors of any city. Despite this, the network still does not cover enough of London. More sensors and more data are needed to say for sure which actions to tackle air pollution are working best. More sensors will also help explain how air quality changes not just because of the amount of traffic, but also because of other factors such as weather and road layout.

From July, new fixed and mobile sensors will be rolled out across London's streets. 100 fixed sensors will be fitted to lampposts and buildings in the worst affected areas and sensitive locations, and two dedicated Google Street View cars will be driving across the city, mapping air pollution at an unprecedented level of detail. The two Google Street View cars assigned to this project will take air quality readings every 30 metres, building up a picture over the course of a year, and identifying pollution "hotspots" that the existing network of fixed monitors might miss.

With this new 'hyperlocal' data, the Mayor will be able to track what actions are making the biggest difference to people's health. Whether that's more electric vehicles, or improvements to public transport, robust science means we will know more than ever about what works and what doesn't when it comes to cleaning up our air.

Online maps showing data in real time will give Londoners information on just how dirty the air they breathe really is as they move around the city. These new tools will help the capital take action to tackle the most dangerous environmental threat to people's health. The study will improve the accuracy of air pollution forecasts for the coming three days, making it possible for people to plan and respond to high pollution warnings.

The project will be run by a team of air quality experts led by the charity Environmental Defense Fund Europe, in partnership with Air Monitors Ltd., Google Earth Outreach, Cambridge Environmental Research Consultants, University of Cambridge, National Physical Laboratory, and the Environmental Defense Fund team in the United States. King's College London will also be undertaking a linked study focused on schools that will form part of the year long project.

The project is the result of a partnership between the Greater London Authority and C40 Cities.

The results from this initiative will be shared with the 96 members of the C40 Cities network, with the ambition of improving air quality for hundreds of millions of people living in cities around the world.

The announcement comes just a day after the Mayor brought together city leaders from across England and Wales for a national air quality summit, and unveiled that London will have the largest pure electric double-deck bus fleet in Europe.

The Mayor of London and C40 Vice Chair, Sadiq Khan, said: "London's toxic air is leading to the premature deaths of thousands of Londoners every year so I am pleased that we are embracing the very latest smart technology to monitor hot-spots and demonstrate how effective our policies to combat this global issue are.

"I'm doing everything in my power to tackle London's lethal air including cleaning up our bus and taxi fleets, introducing the Toxicity Charge for the oldest polluting vehicles in central London and bringing forward the introduction of the world's first Ultra-Low Emission Zone to start in April 2019. "I am delighted to be joining up with C40, the Environmental Defense Fund, Google and the rest of the team on this exciting project that will provide a treasure trove of new data and information to improve air quality here in London, and deliver an approach that can be replicated across the world."

"This project will provide a step change in data collection and analysis that will enable London to evaluate the impact of both air quality and climate change policies and develop responsive interventions," **said Executive Director for Environmental Defense Fund Europe, Baroness Bryony Worthington.** "A clear output of the project will be a revolutionary air monitoring model and intervention approach that can be replicated cost-effectively across other UK cities and globally, with a focus on C40 cities."

Mark Watts, C40, Executive Director said: "Almost every major city in the world is dealing with the threat of toxic air pollution, which is taking an incredible toll on the health of citizens, public finances, quality of life and contributing to climate change. London is already a world leader in responding to this global threat and with this initiative it will set a new global standard for how street level air quality monitoring can inform strategic policy making. Cities across the C40 network and around the world will be watching closely to understand how this street level air quality monitoring can deliver cleaner air for their citizens."

-Ends-

Notes for editor

For more information, contact:

C40 Cities: Josh Harris, Head of Media, C40, jharris@c40.org; +44 (0) 7739 021000

EDF: Anneliese Allen-Norris, aallennorris@edf.org +44 (020) 33105915

Earlier this month, the Mayor published Smarter London Together – his roadmap for how he will realise his ambition to make London the world's smartest city. In it the Mayor sets out how he will help the city's public services use tech and data to improve the lives of all Londoners.

The roadmap includes plans to supporting the commission of a new generation of smart technology, a bold new approach to connectivity and the promotion of greater data sharing among public services through the London Office of Data Analytics.

###

About Environmental Defense Fund
Environmental Defense Fund Europe is a registered charity (1164661) in England and Wales. A recently established affiliate of leading international non-profit Environmental Defense Fund (EDF), the organisation links science, economics, law, and innovative private-sector partnerships to create transformational solutions to the most serious environmental problems. Connect with us at edf.org/europe, on *Twitter* and on our *EDF Voices*, *EDF+Business* and *Energy Exchange* blogs.

About Air Monitors Limited
Air Monitors is the UK's leading air quality monitoring company, supplying and supporting instrumentation to central government, local authorities, research and industry. Based in Tewkesbury in Gloucestershire and Glasgow in Scotland the company leads the field in new small-sensor technologies with its AQMesh range and will also provide and maintain the equipment within the Google Street View cars in the project.

About Cambridge Environmental Research Consultants
Cambridge Environmental Research Consultants (CERC) are world leading developers of air quality modelling software. Their renowned ADMS-Urban model will be used together with the sensor data to generate hyper-local air quality mapping both for nowcasts and forecasts, and for policy studies.

About Google Earth Outreach
Google Earth Outreach is a program from Google designed specifically to help non-profit and public benefit organisations around the world leverage the power of Google Maps and Cloud technology to help address the world's most pressing social and environmental problems.

About the National Physical Laboratory (NPL)
NPL is the UK's National Measurement Institute, providing the measurement capability that underpins the UK's prosperity and quality of life. Every day our science, engineering and technology makes a difference to some of the biggest national and international challenges, including addressing air quality issues. http://www.npl.co.uk/about/what-is-npl/

About University of Cambridge Department of Chemistry
The University of Cambridge Department of Chemistry is a world leading research and teaching institution. At Cambridge, the Centre for Atmospheric Science has played a primary role in the development of low-cost sensors for air quality monitoring and in the development of techniques for analysing and interpreting measurements from sensor networks.

About the C40 Cities Climate Leadership Group

Around the world, C40 Cities connects 96 of the world's greatest cities to take bold climate action, leading the way towards a healthier and more sustainable future. Representing 700+ million citizens and one quarter of the global economy, mayors of the C40 cities are committed to delivering on the most ambitious goals of the Paris Agreement at the local level, as well as to cleaning the air we breathe. The current chair of C40 is Mayor of Paris Anne Hidalgo; and three-term Mayor of New York City Michael R. Bloomberg serves as President of the Board. C40's work is made possible by our three strategic funders: Bloomberg Philanthropies, Children's Investment Fund Foundation (CIFF), and Realdania.

---

[1] In 2015 a study by King's College London, 'Understanding the Health Impacts of Air Pollution in London', commissioned by Transport for London, showed that air pollution in London could be causing thousands of premature deaths a year.
https://www.kcl.ac.uk/lsm/research/divisions/aes/research/ERG/research-projects/HIAinLondonKingsReport14072015final.pdf

https://www.london.gov.uk/what-we-do/environment/pollution-and-air-quality/health-and-exposure-pollution

[2] Researchers from the University of Oxford and the University of Bath produced 'The health costs of air pollution from cars and vans' in 2018, which showed that health impacts from air pollution from internal combustion engine vehicles costs tens of billions of pounds each year.
https://www.cleanairday.org.uk/Handlers/Download.ashx?IDMF=7eb71636-7d06-49cf-bb3e-76f105e2c631